ระยะปลายสำหรับแผ่นพลาสติกเสริมเส้นใยคาร์บอนที่ยึดประสานกับคานเหล็ก

นายอัครวัชร เล่นวารี

วิทยานิพนธ์นี้เป็นส่วนหนึ่งของการศึกษาตามหลักสูตรปริญญาวิศวกรรมศาสตรดุษฎีบัณฑิต
สาขาวิชาวิศวกรรมโยธา ภาควิชาวิศวกรรมโยธา
คณะวิศวกรรมศาสตร์ จุฬาลงกรณ์มหาวิทยาลัย
ปีการศึกษา 2545
ISBN 974-17-1669-9

TERMINAL DISTANCES FOR CFRP PLATES ADHESIVELY BONDED TO STEEL GIRDERS

Mr. Akhrawat Lenwari

A Dissertation Submitted in Partial Fulfillment of the Requirements
for the Degree of Doctor of Philosophy in Civil Engineering
Department of Civil Engineering
Faculty of Engineering
Chulalongkorn University
Academic year 2002

ISBN 974-17-1669-9

Thesis Title	Terminal Distances for CFRP Plates Adhesively Bonded to Steel Girders
By	Akhrawat Lenwari
Field of Study	Civil Engineering
Thesis Advisor	Prof. Dr. Thaksin Thepchatri

Accepted by the Faculty of Engineering, Chulalongkorn University in Partial Fulfillment of the Requirements for the Doctor's Degree

..... Dean of Faculty of Engineering
(Professor Somsak Panyakeow, D.Eng.)

THESIS COMMITTEE

..... Chairman
(Professor Ekasit Limsuwan, Ph.D.)

..... Thesis Advisor
(Professor Thaksin Thepchatri, Ph.D.)

..... Member
(Assistant Professor Kaukeart Boonchukusol, Dr.Ing.)

..... Member
(Assistant Professor Tospol Pinkaew, D.Eng.)

..... Member
(Dr. Suphasit Sirisak, Ph.D.)

อัครวัชร เล่นวารี : ระยะปลายสำหรับแผ่นพลาสติกเสริมเส้นใยคาร์บอนที่ยึดประสานกับคานเหล็ก (TERMINAL DISTANCES FOR CFRP PLATES ADHESIVELY BONDED TO STEEL GIRDERS) อ.ที่ปรึกษา : ศ.ดร.ทักษิณ เทพชาตรี : 135 หน้า. ISBN 974-17-1669-9.

งานวิจัยนี้ทำการศึกษาพฤติกรรมของคานเหล็กที่เสริมกำลังบางส่วนด้วยแผ่นพลาสติกเสริมเส้นใยคาร์บอนภายใต้แรงสถิตย์และแรงกระทำซ้ำซากเพื่อกำหนดระยะปลายของแผ่นที่ต้องเผื่อออกไปจากจุดหยุดแผ่นที่กำหนดจากความต้องการด้านกำลัง พฤติกรรม 3 แบบที่ใช้กำหนดระยะปลายของแผ่นเสริมกำลังนี้ได้แก่ 1) การวิบัติแบบเกิดการหลุดฉับพลันของแผ่นภายใต้แรงสถิตย์ 2) การเกิดความเป็นคอมโพสิต (Composite) ของหน้าตัดโดยแผ่นมีหน่วยแรงดึงสอดคล้องกับหน่วยแรงจากการวิเคราะห์หน้าตัดคาน และ 3) การเกิดการหลุดร่อนที่ปลายแผ่นภายใต้แรงกระทำซ้ำซาก โดยระยะที่มากที่สุดจากการพิจารณาทั้ง 3 กรณีนี้จะเป็นระยะปลายของแผ่นที่ต้องการ

ในงานวิจัยนี้พบว่าผลลัพธ์ที่ได้จากการทดสอบกำลังของรอยต่อชนิดแผ่นเหล็กปะกับคู่แบบสมมาตร (Double-strap joint) ร่วมกับหลักการของกลศาสตร์การแตกหักเชิงเส้น สามารถนำไปใช้ในการอธิบายพฤติกรรมแบบที่ 1 ได้อย่างดี สำหรับพฤติกรรมแบบที่ 2 พบว่าการวิเคราะห์เชียร์แลก (Shear lag analysis) สามารถนำมาใช้ประเมินระยะที่แผ่นต้องการเพื่อพัฒนาหน่วยแรงดึงจนเกิดความเป็นคอมโพสิตของหน้าตัดได้ สำหรับพฤติกรรมแบบที่ 3 พบว่าช่วงความเข้มของความเค้น (Stress intensity factor range) มีความเหมาะสมที่จะใช้ในการทำนายอายุที่เริ่มเกิดการหลุดร่อนที่ปลายแผ่น จากผลการทดสอบคานที่มีแผ่นพลาสติกเสริมเส้นใยคาร์บอนภายใต้แรงกระทำซ้ำซากที่อัตราส่วนความเค้น 0.2 ความถี่ประมาณ 2 รอบต่อวินาที ซึ่งในทุกชิ้นงานที่ทำการทดสอบไม่พบรอยร้าวที่ปีกคานซึ่งเป็นข้อดีของการใช้วัสดุประสาน จากการศึกษาพบว่าคุณสมบัติการยึดเหนี่ยวระหว่างผิวเหล็กและวัสดุประสานเป็นสิ่งสำคัญที่มีผลต่อพฤติกรรมแบบที่ 1 และแบบที่ 3

จากการศึกษาผลของตัวแปรต่างๆที่มีผลต่อระยะปลายของแผ่นอันได้แก่ ความหนาของแผ่นที่ใช้เสริมกำลัง, ความหนาของชั้นวัสดุประสาน, โมดูลัสของแผ่นที่ใช้เสริมกำลังและโมดูลัสของวัสดุประสานพบว่าเมื่อพิจารณาพฤติกรรมที่ 1 และ 3 ระยะที่แผ่นต้องการจะเพิ่มขึ้นตามทุกตัวแปร ยกเว้นกรณีที่ชั้นวัสดุประสานหนาขึ้นระยะที่แผ่นต้องการจะลดลง สำหรับพฤติกรรมที่ 2 ระยะที่แผ่นต้องการจะเพิ่มขึ้นตามทุกตัวแปร ยกเว้นกรณีที่โมดูลัสของวัสดุประสานเพิ่มขึ้นระยะที่แผ่นต้องการจะลดลง

ภาควิชา วิศวกรรมโยธา ลายมือชื่อนิสิต _____

สาขาวิชา วิศวกรรมโยธา ลายมือชื่ออาจารย์ที่ปรึกษา _____

ปีการศึกษา 2545 ลายมือชื่ออาจารย์ที่ปรึกษาร่วม -

##4171813821 : MAJOR CIVIL ENGINEERING
KEY WORDS : STRESS SINGULARITY/CFRP/STRENGTHENING/STEEL BEAMS/BI-MATERIAL WEDGE

AKHRAWAT LENWARI : TERMINAL DISTANCES FOR CFRP PLATES ADHESIVELY BONDED TO STEEL GIRDERS, THESIS ADVISOR : PROF.DR.THAKSIN THEPCHATRI, 135 pp., ISBN 974-17-1669-9.

This research studies the flexural behaviors of steel beams strengthened with partial-length adhesive-bonded CFRP plates under static and constant amplitude fatigue loadings. Three main behaviors related to the determination of a terminal distance, a distance between the theoretical plate's cut-off point and the actual plate's cut-off point for the strengthening purposes, are : 1) the premature plate separation failure mode, which is an unfavorable local failure mode, under static loading 2) the development of tensile stresses in the bonded plate to conform to the conventional beam theory, and 3) the occurrence of debond cracks at the end of the bonded plate under fatigue loading. The terminal distance is the maximum distance from the consideration of these three behaviors.

To predict the first behavior, a fracture criterion is proposed using results from the double strap joint testing. The fracture criterion is based on linear elastic fracture mechanics concepts. To study the second behavior, tensile stresses in bonded CFRP plates were measured during the static test. It is found that a shear lag analysis provides reasonable agreements with the test data. So it may be used for determining a distance that the bonded plate should extend beyond the theoretical cut-off point to achieve flexural conformance. The third behavior, on the other hand, is investigated by conducting fatigue tests at a stress ratio of 0.2 and frequency 2 Hz. From the fatigue study, the stress intensity factor range is found to be suitable for evaluating debond initiation life. One advantage found from all such composite beams tested is that no fatigue crack occurred in the flanges of the beams. From the study, interface characteristics of an adhesive/steel bi-material are the important factors affecting the first and the third behaviors.

Finally, effects of the plate thickness, the adhesive layer thickness, the modulus of the plate, and the modulus of the adhesive on the terminal distance are discussed. From a parametric study, a longer plate is required when all parameters, except the adhesive thickness, increase regarding the first and the third behaviors. For the second behavior, a distance that the plate requires to achieve the flexural conformance increases when all parameters, except the adhesive modulus, increase.

Department Civil Engineering Student's signature _____
Field of study Civil Engineering Advisor's signature _____
Academic year 2002 Co-advisor's signature -

ACKNOWLEDGEMENTS

I would like to express my deep gratitude to my dissertation advisor, Professor Dr. Thaksin Thepchatri, for his fruitful advice, support and strong encouragement. Sincere thanks to Professor Dr. Eiichi Watanabe at Kyoto University for his valuable suggestions on the work. I am also grateful to other members of the dissertation committee for their time and advice. They are Professor Dr. Ekasit Limsuwan, Assist. Prof. Dr. Kaukeart Boonchukusol, Assist. Prof. Dr. Tospol Pinkaew, and Dr. Suphasit Sirisak.

Thanks to Dr. Pairod Singhatanadgid and Dr. Jirapong Kasivitamnuay for many interesting discussions and information on the composite materials and the fatigue experiments.

I also want to express my thanks to all technicians of the Civil Engineering Department and Mr. Chanwat Gairuitanasom from Sika's technical service division for their assistance during the experiments. Also thanks to undergraduate students Mr. Sorawut Paointara, Mr. Supat Suwannakarn, and Mr. Suthit Yuvaves for their help during the experiments. Thanks to all my fellow graduate students for their supports. My appreciation also goes to a good friend, Chawalit Machimdamrong, for his helpful discussion.

Financial support for this study is provided by the Thailand Research Fund. Acknowledgment is also due to Sika (Thailand), Ltd. for supplying composite materials and fabricating the test specimens. The experiments could not have been completed without good collaboration on specimen fabrication.

This dissertation is dedicated to my parents, my sister, and my brother, who give me love, support, and encouragement.

TABLE OF CONTENTS

Page

TABLE OF CONTENTS (Cont.)

Page

LIST OF TABLES

Page

LIST OF FIGURES

Page

LIST OF FIGURES (Cont.)

Page

LIST OF FIGURES (Cont.)

Page

CHAPTER 1

INTRODUCTION

1.1 PROBLEM STATEMENT

On the verge of a new century, the need for repair and strengthening of deteriorated, damaged, and substandard infrastructure has become one of the most important challenges confronting the repair and rehabilitation industries worldwide (Buyukozturk, 1999). Development of effective, durable, and cost-effective repair/retrofit materials and methodologies is, thus, important.

One of the most common methods of strengthening beams and girders is by adding cover plates to the top and bottom flanges near the midspan (Ghosh, 2000). Although cover plates often have different end geometries, the most frequently used details are square-ended and tapered (Hassan and Bowman, 1995). While cover plates could be riveted, bolted, or welded to a beam member, welding has been widely used due to fabrication simplicity and ease. However, the cover-plate end is the most severe of all details and represents a lower bound on the fatigue strength of bridge details. Researches examining the fatigue life of the end-welded detail and ways of improving it were summarized in Albrecht *et al* (1983), and in Hassan and Bowman (1995). From the available test data, AASHTO (1996) classified the details used in bridge construction into five general categories. Category E in this classification was intended to represent the most severe details with respect to fatigue strength, including beams with welded partial-length cover plates. The plain welded beams represent an upper bound for the fatigue strength of welded beams.

Progressive crack extension by fatigue is a major cause of failure of steel highway bridges (Albrecht *et al,* 1982). Fatigue may be defined as the initiation and propagation of microscopic cracks by the repeated application of load. The crack growth rate increases exponentially with crack size. This is aggravated by a continuous decrease in cross sectional area. Eventually, the crack grows to a size where either the remaining area is insufficient to carry the applied load or the fracture toughness is reached.

One efficient way of connecting two structural parts is by the use of adhesive bonding. In the aircraft industry, bonding is an established technique (Groth, 1987: 7). Adhesive bonding is more appealing than welding in view of fatigue because of lower stress concentration and no fretting problems (Hoskin and Baker, 1986: 116).

Fiber reinforced plastic (FRP) composites have experienced significant cost reductions in the last two decades that now allow consideration for use in infrastructure applications. Total project costs can be achieved due to low transportation costs, easy handling, and rapid application of repair. FRP's properties are affected by the types of fiber and binder, the volume of the fibers, the cross-sectional configuration, and the fiber orientations etc. However, there are some properties that all FRP composites have in common including light weight, high tensile strength, elastic behavior up to tensile failure, high resistance to corrosion, non-magnetic property and high fatigue resistance (Demers, 1998).

In recent years, FRP systems externally bonded to reinforced concrete structures as a means for repair and strengthening have gained popularity worldwide. Although numerous research studies (e.g. Ritchi *et al* (1991), Saadatmanesh and Ehsani (1991), Sharif *et al* (1994) Meier (1995), Quantrill *et al* (1995), Swamy and Muskhopadhyaya (1995), Chaallal *et al* (1998), Spadea *et al* (1998), Shahawy and Beitelman (1999)) have revealed that FRP composite systems bonded to various structural concrete members can significantly increase their stiffness and load carrying capacity, a few works on steel members have been reported (Sen *et al*, 1995, 2001; Messick, 1996).

In the application of bonded composite repair to steel structure, the design and analysis of bonded patch repair is a challenging task. Moreover, the possible failure modes that can occur should be studied (Lenwari and Thepchatri, 2001). To the author's knowledge, no previous work has been reported on the proper length of a bonded plate in the bonded composite repair.

If linear elasticity is assumed, stress singularity is present at a bi-material wedge, which is a condition at the plate cut-off point. So any stress or strain criterion may be unsuitable for evaluating the "premature" separation of a bonded plate due to

fracture at the plate ends. Under cyclic loadings, very high stresses at the plate end are also the main factors affecting the service life of the strengthened systems due to debond crack initiation. From literature review, studies on fatigue performance of steel beams adhesively bonded with FRP materials have been limited (Messick, 1996; Demers and Abdelgadir, 1999). Since the plate's cut-off point usually locates in a low stress region (it is usually extended near the supports), theory of linear elasticity seems to be applicable for this problem provided that nonlinear material responses are minimal.

Three problems are studied in this work: 1) the fracture problem leading to separation of a bonded plate from a steel beam, 2) the development of tensile stresses in a bonded plate, and 3) the debond problem at the plate end under cyclic loading. Flexural behaviors of steel beams strengthened with partial-length adhesive-bonded CFRP plates are investigated. The terminal distance, a distance that the partial-length bonded plate shall extend beyond the theoretical cut-off point for strengthening purposes, should be the maximum distance from the consideration of these three behaviors.

1.2 OBJECTIVES

The objectives of this study may be itemized as follows:

1. To develop a test protocol for evaluating the fracture leading to separation of a bonded plate from the steel beam.

2. To verify the proposed test protocol and a failure criterion with the experimental results from static test on steel beams strengthened with different lengths of partial-length bonded CFRP plates.

3. To apply the Reciprocal Work Contour Integral Method for evaluating the value of a stress intensity factor at a bi-material wedge corner.

4. To numerically investigate the geometrical and mechanical effects of the plate and the adhesive on both the stress singularity parameters and the distance for the

bonded plate to develop the flexural conformance, i.e. develop the tensile strain to conform to conventional beam theory.

5. To investigate the flexural behaviors under static loading of the strengthened systems, including the strengthening and stiffening effects.

6. To study the debond behaviors under constant amplitude fatigue loading. Debond crack initiation life is obtained from a visual inspection with the help of a crack detection technique developed in the study.

7. To construct a fatigue initiation criterion for the evaluation of debond initiation life of structure. The criterion is based on linear elasticity theory.

8. To provide suggestions for designing the terminal distances of partial-length adhesive-bonded CFRP plates.

1.3 SCOPE

Environmental effects and long term behaviors are beyond the scope of this work.

1.4 ORGANIZATION OF THE DISSERTATION WORK

Chapter 1 gives the introduction to the research work followed by the objectives and scope of the study.

Chapter 2 provides a literature review. Past researches on fatigue problems in steel beams with welded steel cover plates, on the applications of advanced composite materials for structural members, and on the analysis of the singularity problems in linear elasticity are summarized.

Chapter 3 describes the complex variable method, the reciprocal theorem, the reciprocal work contour integral method (RWCIM) for a bi-material system, and the shear lag analysis modified for the strengthened beam.

Chapter 4 develops a double strap joint specimen. The proposed test specimen and the fracture criterion are described.

Chapter 5 evaluates the stress intensity factors by the use of finite element analysis. Results from the submodeling technique and the RWCIM are discussed.

Chapter 6 describes the static test and the fatigue test on steel beams with partial-length adhesive-bonded CFRP laminates. Main objectives of the static test are to evaluate the accuracy of the proposed method in evaluating the fracture leading to premature separation of a bonded plate from the steel beam and to investigate the flexural responses of the strengthened beams. Main objectives of the fatigue test are to observe the growth behaviors of debond fatigue cracks and to determine the fatigue strength of the partial-length adhesive-bonded end detail with regard to the debond initiation life. The fatigue test was conducted under constant amplitude fatigue loading.

Chapter 7 discusses the results from the static and fatigue tests.

Chapter 8 studies the geometrical and mechanical effects of a bonded plate and an adhesive layer on both the stress singularity parameters and the distance for a bonded plate to develop the flexural conformance. The stress singularity parameters, which govern both a premature plate separation failure mode and debond fatigue life of the strengthened beams as well as the distance for a bonded plate to develop the flexural conformance are the main factors determining the terminal distance of a bonded plate.

Chapter 9 summarizes the findings of this study and gives recommendations for further research.

CHAPTER 2

LITERATURE REVIEW

2.1 OVERVIEW

For bridge structure, fatigue is an important limit state. Steel beams with partial-length welded steel cover plates are classified in the category having the lowest fatigue strength in many design provisions and recommendations such as AASHTO (1996) and JSSC (1995). From this point, adhesive bonding is more appealing than welding. In addition, the use of lightweight composites is easy and minimally disrupts traffic. From past researches, strengthening of steel beams or girders with the partial-length adhesive-bonded composite plates seems to be a viable method. However, one possible failure mode of the steel beams strengthened with adhesive-bonded plates is the premature separation of the plates. This failure mode is unfavorable and greatly reduces the effectiveness of the strengthening scheme. Moreover, the occurrence of debond at the plate's cut-off point under fatigue loading can reduce the service life of the strengthened structures. As a result, they should be prevented. Based on some analytical models such as a shear lag analysis, the plate end is a critical location since very high stresses are present. Specifically, if linear elasticity is assumed, there are stress and strain singularities at the plate end due to material and geometric discontinuities.

In this chapter, previous works related to the main objectives of this study are reviewed.

2.2 FATIGUE PROBLEMS IN STEEL BEAMS STRENGTHENED WITH WELDED STEEL COVER PLATES

Fatigue is the phenomenon of material failure by repeated applications of loads which, when induced only a single time or infrequently, would cause no undesirable effects or failure. In general, welded bridge details are more susceptible to fatigue failure than riveted or bolted ones. Fatigue cracks, if not controlled, can lead to serious reduction of member area or to sudden fracture of the member. From a

preliminary fatigue test on a steel beam with partial-length, tapered, welded steel cover plate, fatigue failure of the specimen is shown in Fig. 2.1.

Test data on welded details since 1960s (Fisher *et al* 1970, 1974, 1983, 1987, 1993) have demonstrated that all fatigue cracks commence at some initial discontinuities in the weldment or at the weld periphery and grow perpendicularly to the cyclic tensile stresses. Discontinuities are always present to some degree, regardless of the welding processes and techniques used during fabrication. Attachments including cover plates always introduce a transverse weld toe perpendicular to the live-load stress, causing a stress concentration. This results in fatigue cracking that starts from small sharp discontinuities at the weld toe. High-tensile residual stresses caused by all welding processes were also found by the measurement along the weld toe of cover plates (Fisher, 1997: 6). Tensile residual stresses maybe near the yield point. The stress ratio, $R = S_{\min} / S_{\max}$, does not play a significant role in defining the fatigue strength of the welded details under cyclic loads because the maximum stress, $S_{\max}$, and the minimum stress, $S_{\min}$, at the point of fatigue crack initiation and growth, i.e. the location in the weld or at the weld toe, are almost always in tension due to the very high tensile residual stresses at this point. It was found that the stress range has a significant influence on the fatigue strength (Fisher, 1997: 7).

From the available test data, AASHTO (1996) classified the details used in bridge construction according to the fatigue strength into five general categories, as shown in Fig 2.2(a). Category E in this classification was intended to represent the most severe details with respect to fatigue strength, including beams with partial-length welded cover plates. Later, a lower category E' was added to account for the reduction in fatigue strength of thick sections. For each category the straight line was found to be a good estimate of the relation $\log S_r$ vs. $\log N$, where S_r is the stress range during a loading cycle and N is the number of such cycles to failure. Another classification of fatigue strength can be found in JSSC (1995), in which the structural details are classified into category A to H for joints subjected to normal stress, as shown in Fig. 2.2(b). In this classification, as-welded cover plate end details with the plate length more than 30 cm are classified into category G.

Figure 2.1 Typical fatigue failure from welded cover plate details

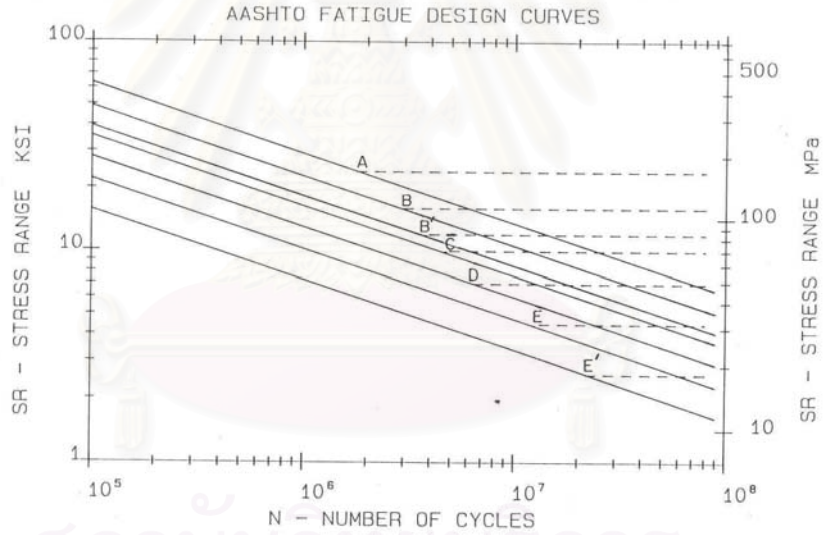

(a)

Figure 2.2 Fatigue strength categories for structural details (a) AASHTO (1996) (b) JSSC (1995)

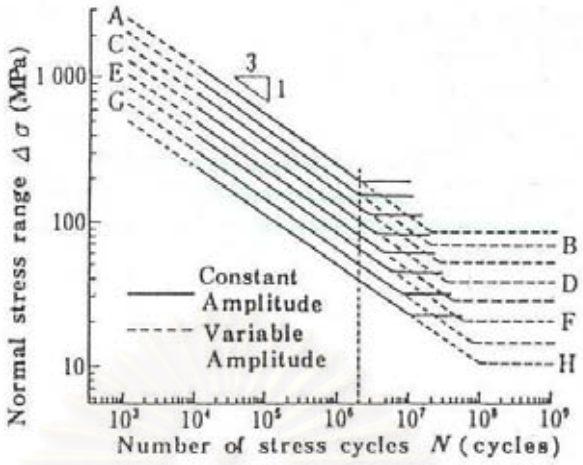

Fig.4.1 Fatigue design curves for joints subjected to normal stress

(b)

Figure 2.2 Fatigue strength categories for structural details: a) AASHTO (1996) b) JSSC (1995) (Continued)

Sahli *et al* (1984) conducted experiments to determine the fatigue strength of cover plate ends, repaired with splice plates and high strength bolts in friction. The flanges at the cover plate end were noncracked simulating a condition after rehabilitation, half-precracked, or fully-precracked prior to the repair. It was found that the mean fatigue life of the repaired noncracked cover plates exceeded the AASHTO category B mean and was 18.2 times longer than the category E mean. In noncracked ends, crack initiation was found in the tension flange at the bolt holes or at the transverse weld toe which connects the cover plate to the flange.

Wattar *et al* (1985) found that welding a cover plate to a rolled steel beam and bolting the plate end by high-strength bolts with a friction-type connection increased the fatigue strength from category E for end-welded cover plates to category B. Crack initiation was found in the flange of specimens near the bolt holes under fatigue loading. Most cracks led to failure of specimen.

Albrecht (1987) examined the fatigue strength of steel beams with adhesively-bonded steel plates. The adhesive in the study was Versilok 201 and Hysol EA 9309. Increase of fatigue life by 20 times over that of welded cover plates, from category E to B, was reported. Gradual debonding during stress cycling was found at six cover

plate ends that were bonded but not bolted to the tension flange. So, all cover plate ends were bonded and bolted prior to stress cycling for the remaining specimens. Cracks were found near the bolt-holes in the tension flange or at the flange surface due to fretting which is caused by the friction between the bolt head and the flange. No fatigue crack initiated in the cover plate, nor did flange cracks propagated across the bond line and into the cover plate.

Kagawa *et al* (1999) proposed an improved welded cover plate end detail. The thickness and width were tapered, therefore reducing the stress concentration at the transverse end weld. Fatigue tests of six full-scale cover plated beams with and without improved cover plate end details were conducted. Conventional end conditions in the test were the square plate end and the plate end specified in JRA specification. It was concluded that the end shape tapered in width and thickness with round end could improve fatigue strength up to JSSC category D. It was suggested that the fillet weld toes be ground smooth around the round end. In the test, cracks were found to propagate independently since the planes of the cracks were not the same. Since there was no coalition of cracks, the fatigue life of the proposed detail was longer than any other end detail used in their investigation.

2.3 CURRENT APPLICATIONS OF ADVANCED COMPOSITE MATERIALS

In general, a composite material can be defined as a material that consists of two (or more) identifiable distinct constituent materials. “Fiber composites” (or, sometimes, “fiber reinforced plastics”) originally used in for aircraft structures comprise continuous fibers embedded in a resin (or “plastic”) matrix. Fibers provide a composite with its key structural properties. Matrix serves mainly to bond the fibers into a structural entity and protect the fibers from environment (Hoskin and Baker, 1986: 1&47).

Regarding engineering properties, high-performance composites generally exhibit high strength and stiffness, low density, and good resistance to fatigue and corrosion. (Hoskin and Baker, 1986: 62)

Recent advances in adhesive bonding and fiber-reinforced composite materials suggest the application of bonded composite repair technology for repairing cracks and corrosion damage. In the aircraft industry, widespread fatigue damage, multi-site damage, and corrosion are all examples of common issues that affect large areas of aging fleets. Not only are the repairs technically more efficient and more effective than riveted repairs at preventing crack growth, they are also frequently more cost effective to install.

Several investigators have studied the behaviors of cracked plates repaired with composite patches under both static loading (e.g. analytical works of Rose (1981, 1982), Chien-Chang Lin *et al* (1993)) and fatigue loading (e.g. Denney and Mall (1997), Naboulsi and Mall (1997), Kam *et al* (1998), Wang *et al* (1998), Schubbe and Mall (1999 a, 1999 b)). Due to much merit of composites, repair of cracked or aging structures with bonded composite patches has shown great promise to become a viable method for life extension of such structures (Kam *et al*, 1998: 645). A number of works (e.g. Rose (1981, 1982) and Chien-Chang Lin *et al* (1993)) have proposed different methods for stress analysis and the subsequent derivation of stress intensity factor of cracked aluminum structures after repair. Recently, An investigation on the applicability of the adhesively bonded composite patch repair technique to riveted steel bridges damaged by fatigue was conducted (Bassetti *et al*, 1998, 2000a, 2000b, 2000c). It was reported that the application of CFRP strip and the introduction of a compressive stress by pretension of CFRP strips prior to bonding produce a significant increment of the remaining fatigue life of riveted members.

Fiber reinforced polymer (FRP) composites are currently viewed by structural engineers as “new” and highly promising materials in the construction industry. Composites have found their ways as strengthening materials for reinforced concrete elements (beams, slabs, columns, etc.) in thousands of applications worldwide, where conventional strengthening techniques may be problematic. For example, replacing epoxy-bonded steel plates with FRP strips provides satisfactory solutions to several problems, including the corrosion of the steel plates which bring about the bond deterioration, the difficulty in manipulating heavy steel plates in tight construction sites, the need for scaffolding, and the limitation in available plate lengths for flexural

strengthening of long girders, which results in the need for joints. Also, replacing the conventional steel jackets (shells) with FRP fabrics or strips wrapped around RC elements provides substantial increase in strength (axial, flexural, shear, torsion) and ductility without much affecting the stiffness (Gdoutos *et al*, 2000: 408).

Numerous works on the use of fiber reinforced polymer as strengthening materials for reinforced concrete structure were reported (e.g. Richti *et al* (1991), Saadatmanesh and Ehsani (1991), Sharif *et al* (1994), Spadea *et al* (1998), Buyukozturk and Hearing (1998), Chaallal *et al* (1998), Shahawy and Beitelman (1999)). Most works were related to flexural strengthening of beams, slabs or columns, shear strengthening of beams or columns, and confinement of columns or column-type elements (e.g. chimney). Firstly, flexural strengthening was provided by bonding FRP strips or fabrics in the tension zones of reinforced concrete elements. The failure analysis of such elements follows well-established procedures for reinforced concrete structures, provided that the contribution of external FRP reinforcement is taken into account properly, and that special consideration is given to the failure modes associated with bond failure at the FRP-concrete interface. Separation of the bonded steel or FRP plates from the strengthened RC beams was reported in some works (Jones *et al*, 1988; Oehlers and Moran, 1990; Richti *et al*, 1991). This failure mode was investigated in more details by some researchers (Ziraba *et al*, 1994; Malek *et al*, 1998; Maalej and Bian, 2001). Secondly, shear strengthening can be achieved by applying FRP strips or fabrics either covering partially or wrapped around reinforced concrete elements. The failure analysis of shear-strengthened elements is based on the well-known truss model for reinforced concrete, properly modified to account for premature FRP failure due to debonding (Gdoutos *et al*, 2000: 445). Finally, confinement effect provided by external FRP jackets wrapped around columns may be taken into account through proper modeling of the constitutive laws for concrete. Bond behaviors and transfer length were investigated by Chajes *et al* (1996), Maeda *et al* (1997), and Volnyy and Pantelides (1999), Bizindavyi and Neale (1999).

Common methods that have been used to repair or rehabilitate steel bridges are a) Repair of critical members, b) Introduction of new member to the system, c)

Reduction of dead loads, and d) Modification of structural system. In some cases, a combination of the schemes mentioned may be employed to achieve the needs. One of the most common methods of strengthening beams and girders is by adding steel cover plates to the top and bottom flanges near the midspan (Ghosh, 2000: 100). However, it has been found that the fatigue strength of bridge girders with weldments is governed by the cover-plate end. It is the most severe of all details and sets a lower bound on the fatigue strength of welded girders (Albrecht *et al*, 1982: 4). From a survey on fatigue of steel bridges conducted by Hassan and Bowman (1995) throughout the United States, most of the states reported that the steel cover plate detail was used primarily in the past. The current trend in design is either to avoid the use of cover plates or to use full-length cover plates to avoid fatigue problems associated with the partial-length cover plate end details.

Sen *et al* (1995, 2001) investigated the use of carbon fiber reinforced plastic (CFRP) plates for strengthening steel composite bridge members. In the study, six steel composite specimens were strengthened using CFRP plates and then loaded to failure. The specimens were first loaded in flexure past yield of the tension flange of the beams. Then, the tension flanges were bonded with CFRP laminates. Laminate thickness of 2 mm and 5 mm were selected and the length of the CFRP plate was about three-fifth the span length. The repaired specimens were then tested to failure. No separation of the CFRP plate was found in specimens strengthened with 2-mm plates when no additional load could be applied. Specimens strengthened with 5-mm plates attached to the steel flange using fasteners failed when bolt sheared through the plates. One specimen that was strengthened with 5-mm plate without bolts failed without any warning due to separation of the plate. Estimated ultimate strength gains ranging from 11% to 50% were reported. The stiffening effects of CFRP plates were primarily limited to the post-yield range of the plain steel composite specimen. The stiffening in the elastic region was more modest. The study suggested that it is feasible to strengthen steel composite members using CFRP laminates.

Messick (1996) investigated the effects of environments on the durability of the strengthening systems with adhesive-bonded CFRP plates. Static test and constant amplitude fatigue loading test were conducted. Debond cracks were found at the plate

end of one specimen during the fatigue test. The cause of debond was thought to be due to improper fabrication of the specimen, i.e. the uneven pressure applied to the CFRP plate by the wood surface during the specimen fabrication. From the study, isopropyl alcohol was suggested for cleaning steel surface instead of acetone for better resistance to environmental attacks.

Demers and Abdelgadir (1999) studied the fatigue strength at the end of carbon fiber sheet (CFS) bonded to the bottom flange of the steel beam. No crack was found in the flange of the steel beam. Also, no debond was observed at the sheet end when the test was terminated at 1.13 million cycles. A review of existing fatigue data, which had been generated in the context of aerospace, marine, and mechanical applications for a wide range of composite material systems under various loading conditions, was previously reported by Demers (1998). The selected data revealed that the fatigue life of unidirectional CFRP composites could be represented by AASHTO category A detail under tension-tension fatigue loading with frequency 20 Hz or less and without environmental concerns. Fatigue life is also dependent on the R ratio. Specimen shape and loading waveform appear not to affect the fatigue life. Also, the existence of a fatigue limit can not be clearly defined.

2.4 STRESS AND STRAIN SINGULARITIES IN LINEAR ELASTICITY

According to the classical elasticity theory, certain discontinuities in boundary geometry and prescribed boundary data lead to singular states of stress and strain. Any applied load, regardless of the magnitude, will cause the prediction of arbitrarily large stresses in the vicinity of the singular points. (Hong and Stern, 1978: 21)

In a two-dimensional problem, the singular stress states are more easily described in a local system of polar coordinates with origin located at the singular point. In such a system, a typical component of stress near the singular point is characterized by an expression of the form

$$\sigma = Kr^{-\alpha} f(\theta) \qquad (2.1)$$

where r, θ are the local polar coordinates, $f(\theta)$ is an angular function, and α is the strength or order of the singularity having the value between zero and one. The value of the generalized stress intensity factor, K, depends on overall geometry and loading of the body.

Although not explicitly shown in Eq. (2.1), there are certain special combinations of elastic properties, wedge angles (e.g. bi-material wedges), and loadings that can also generate logarithmic singularities (Bogy, 1971; Dempsey and Sinclair, 1981; Yang, 1998).

There have been many studies on the order of singularity as well as the stress and displacement fields around singular points such as the interface corner, the wedge or notch apex, and the interfacial crack tip. Some important contributions are summarized as follows.

William (1952, 1959) was one of the first investigators to examine plate configurations with cracks of finite opening. His work concerned obtaining the order of singularity for the finite crack problem formulated as an eigenvalue problem. Eigenvector approach for determining the eigenvalues for general opening notches in one material was also used by England (1971 a). He (1959) found that appearance of flaws or cracks on the bond between two dissimilar materials can reduce the strength of the structure dramatically. He also discovered that the significant stresses are inversely proportional to the square root of the radial distance from the crack tip, and has an oscillatory character which itself becomes singular near the crack tip.

Bogy (1968, 1971) investigated the problem of two dissimilar materials with arbitrary notch angles subjected to surface tractions on the boundary of the configuration. Later, Bogy and Wang (1971) studied on the problem of the interface corner. The emphasis was to determine how the order of singularity in the stress field depends on the notch angles and material constants.

Dundur (1969) proposed new parameters, which significantly reduces the algebraic complexity in Bogy (1968). He pointed out that for the bodies consisting of two isotropic, elastic materials in plane stress or plane strain loaded by prescribed

surface tractions, the stress induced in the bodies depends on only two combinations of elastic constants.

Hein and Erdogan (1971) calculated the first several eigenvalues. They showed that the lowest or dominant eigenvalue may be either real or complex depending on the values of the elastic constants of the materials considered.

Dempsey and Sinclair (1981) provided analytical information on the stresses which can occur in the neighborhood of the vertex of a two-dimensional bi-material wedge for a wide range of boundary and interface conditions.

2.5 ANALYSIS FOR FRACTURE MECHANICS PARAMETERS

The works in the previous section studied the order of singularity and the nature of stress field around the singular point. Both a configuration of the same material and that of dissimilar materials with general opening notch or wedge were investigated. However, they did not give a computational procedure for determining the coefficient associated with the first or dominant eigenvector, which is related to the stress intensity factor.

Due to complex geometry and boundary conditions, computational methods such as the finite element method and the boundary element method are usually employed to singularity problems. However, their applications are not an easy task because of the singular nature. A conventional finite element analysis will yield a finite stress, even at the singular point.

Finite element analysis has been one of the most popular methods for calculating the value of the stress intensity factor since a closed-form analytical solution for stresses and strains is possible in limited cases (Anderson, 1991: 660). For the configuration of dissimilar materials with general opening notch, a very fine mesh was used near the singular point to capture rapidly varying stress field in many works (Reedy, 1990; Munz and Yang, 1992; Liu *et al*, 1999; Wang and Rose, 2000).

Gradin and Groth (1984) and Groth (1985) used a collocation type procedure for calculating the stress intensity factor. A fine mesh near the singular point was required in order to evaluate the proper value.

Tan and Meguid (1997) developed a special singular finite element. This element facilitated the determination of the stress intensity factor at a bi-material wedge vertex. The problem of a bi-material plate containing a central interfacial crack was analyzed using a combination of the proposed singular element and conventional two-dimensional elements. In the singular element, two singular terms and the constant stress terms were included in the shape functions. The calculated stress intensity values were closed to those from the analytical solution.

Chen and Sze (2001) developed a novel hybrid finite element model, in which the asymptotic displacement fields used for the wedge-tip element were obtained numerically from the finite element method-based eigenanalysis. After the eigensolutions, especially the eigenvectors, were obtained, general expressions for the stress and displacement fields were used to create a wedge-tip element. Three types of the bi-material wedge problems were examined. Good agreement between the associated generalized stress intensity factor obtained from a hybrid finite element analysis and the reference solutions was reported.

One factor that is common to all joining techniques is that the failure usually initiates at the point of high stresses. A fracture criterion based on the stress intensity factor has been successfully applied to evaluate the static strength of electronic devices (Hattori *et al*, 1988) and many types of adhesive joints. Single lap joints were investigated by Groth (1985, 1987, 1988 a, 1988 b), Groth and Jangblad (1987), and Hattori (1991), while butt joints were studied in Reedy and Guess (1993, 1996, 1997). Another common approach for estimating the strength of these bodies is to assume that a preexisting crack emanates from the discontinuity, and then use linear elastic fracture mechanics to determine the load to propagate the crack (Kinloch, 1987). The length of the crack used in the LEFM analysis might be based on a detectable limit in a flaw tolerance assessment, or might possibly be based on a representative population of flaws introduced during fabrication.

Groth (1988 b) tested single-lap joints with a spew fillet condition for a range of overlap length. He used an interface corner stress intensity factor to predict the failure of the joints. No preexisting crack was assumed. The agreement between test and analysis was good for large overlap lengths, but poor for smaller overlaps.

Hattori *et al* (1988) proposed a method using two parameters, which were the stress intensity factor and the strength of singularity, for evaluating adhesive strength of various kinds of bonding edges found in plastic encapsulated LSI device. These parameters were calculated based on the interfacial shear stress, σ_{xy}, distributions near the singular point. Later, Hattori (1991) applied this method to single lap joints. By using this method, the shearing strength of adhesive single-lap joints was evaluated. The influence of lap length, adhesive layer thickness, adherend thickness, and bonding edge angle on the joint strength were also studied.

Reedy (1993) conducted elastic-plastic finite element analyses of a thin adhesive layer subjected to tensile loading. Properties of the adhesive are representative of high strength epoxy. It was found that the region dominated by the interface corner stress singularity was reasonably large relative to layer thickness, and that the interface corner plastic yield zone was contained within the asymptotic field at nominal failure load. These calculated results suggested that it might be possible to characterize butt tensile joint failure in terms of a critical value of the stress intensity factor.

Reedy and Guess (1993) conducted an experiment on cylindrical butt joints with steel adherends to find the tensile strength of the joints for a wide range of bond thickness from 0.25 to 2.0 mm. These data were then compared with the prediction based on the stress intensity factor. Good agreement was found in their study on the bond thickness effect. The adhesive was unfilled epoxy adhesive (a mix of Shell Epon 828epoxy resin and Texaco T-403 hardener) and was cured at room temperature for more than seven days. To be useful as a failure criterion, the singular stress field characterized by the stress intensity factor must dominate a region around the interface corner that is significantly larger than the fracture process zone, intrinsic flaw size, and the plastic yield zone.

Reedy and Guess (1996) studied the interfacial peeling stresses, σ_{yy}, in the butt joints under tensile loading. The adhesive used was a tough, room temperature curable, paste adhesive (Dexter Corporation's Hysol EA 9394). It was an amine-cured epoxy, and contained aluminum powder as a filler. Like many toughened adhesives, this adhesive displayed significant material nonlinearity before yield. Three adhesive models in the study were linear elastic, power law hardening, and perfectly plastic. It was found that a small scale yielding condition existed for the model with 70 MPa perfectly plastic yield strength. The perfectly plastic asymptotic stress field was embedded within the filed dominated by the power law stress singularity, which was in turn embedded within the field dominated by the elastic stress singularity. However, for an elastic-perfectly plastic with a 40 MPa yield strength, the small scale yielding conditions no longer apply and the elastic interface corner stress intensity factor could not characterize the fracture process zone.

Reedy and Guess (1997) reported the test results of butt joints with aluminum adherends. The results from Reedy and Guess (1993) on steel adherends were also compared to study the effects of adherend stiffness and bond thickness on joint strength. It was found that the bond thickness dependency was accurately predicted by an analysis assuming that failure occurs at a critical value of the interface corner stress intensity factor. Also, the measured strength of joints with steel adherends varied as the inverse cube root of the bond thickness, while the strength of the joints with aluminum adherends varied as the inverse fourth root of the bond thickness.

Mohammed and Liechti (2000) formulated a crack nucleation criterion that can apply to all corners and not just one particular corner angle. The interface was modeled as a separate constitutive entity by incorporating a cohesive zone model in the numerical analysis. Displacements near the singular point were measured using moire interferometry. Calibration of the cohesive zone model was conducted at the specific corner angle (e.g zero corner angle) by comparing the numerical results with the measured displacements in order to give values of the parameters in the model. Based on the failure load of a bi-material with zero corner angle, failure loads of bi-materials with different corner angles were predicted.

Studies on the fatigue strength of bonded joints and bonded bodies were conducted by some researchers (Imanaka *et al*, 1995, 1999; Imanaka and Iwata, 1996; Ishii *et al*, 1998, 1999; Lefebvre and Dillard, 1999 a, 1999 b). Fatigue failure was defined by either the failure of specimens or the initiation of debond cracks.

Imanaka and Iwata (1996) conducted cyclic tensile fatigue test on adhesively bonded butt, scarf, and butterfly type joints, where the stress multiaxiality in the adhesive layer was varied in a wide range. In general, stress multiaxiality affects the ductility of most polymeric material. The principal stress ratio, σ_2 / σ_1 or σ_3 / σ_1, was used to define stress multiaxiality in the adhesive layer. Stress ratio and loading frequency was controlled to be 0.1 and 30 Hz, respectively. From the test results, it was found that the endurance limits decreased with increasing σ_3 / σ_1, irrespective of the adhesive layer thickness. Also, the endurance limit defined by the maximum principal stress, σ_1, was little affected by σ_3 / σ_1 compared with those defined by Mises equivalent stress and maximum shear stress in the uniform stress region away from the singular point. So the maximum principal stress was considered to be a suitable stress parameter for evaluating the strength of the joints where there were rather uniform multiaxial stress distributions in the adhesive layer.

In contrast to Imanaka and Iwata (1996), Imanaka *et al* (1999) proposed apparent singularity parameters K_{app} and λ_{app} for evaluating the fatigue strength of adhesive joints, which were 1) single lap joint 2) cracked single lap joints and 3) single step double lap joints, where the singularity governs the fatigue strength. For different types of singular nature associated with each joint type, a characteristic range was defined as the medium region between the region governed by a singular point and that governed by global geometry. Based on Imanaka and Iwata (1996), K_{app} and λ_{app} were calculated from the maximum principal stress distribution in a characteristic range, since it was less sensitive to the stress multiaxiality than other kinds of stress components. The endurance limit was defined from the upper limit of load range, under which specimens did not fail in the 10 million cycles. From the analysis and test data, the range of characteristic range was found to be from 0.05 to 0.5 mm away from the singular point.

Lefebvre and Dillard (1999 a, 1999 b) conducted a fatigue test of an epoxy wedge on a flat aluminum substrate. A fatigue initiation criterion, characteristic of the bi-material interface, was then constructed from the fatigue data. This criterion was a 3-D surface with the ordinate representing the stress intensity factor and the two horizontal axes representing the number of cycles to crack initiation and the order of singularity, respectively. The stress intensity factor was calculated from the distribution of interfacial peel stresses, σ_{yy}, using FEM with a very fine mesh.

The Reciprocal Work Contour Integral Method (RWCIM), which is based on the concept of Betti's law, involves using a classical solution in the region encompassing the stress singularity in conjunction with a finite element solution in the region away from the singular point. It has the advantage that special elements are not required, relatively coarse finite element meshes can be used, and complex external boundaries and loading conditions can be handled.

Stern *et al* (1976) developed this method to compute stress intensity values near the crack tip in a two-dimensional cracked body. This method, similar to J-integral method, used data removed from the crack tip, so there was no need for accurate data in the vicinity of the crack. It also yielded directly the independent values of stress intensity factors in opening mode and shearing mode.

Hong and Stern (1978) extended the RWCIM to treat the problem of two bonded dissimilar materials with a crack along the bond. By this way, the stress intensity factor at the crack tip was calculated in terms of an integral involving tractions and displacements of a contour remote from the crack tip.

Carpenter (1984 a, 1984 b) adapted the method developed by Stern *et al* (1976) to a general opening crack problem. For plate configuration containing a crack with a finite opening angle, it was shown that there are two eigenvectors that give stress singularity at the crack tip. By this method, the coefficients associated with these two eigenvectors can be calculated. These coefficients are related to the stress intensity factors.

Carpenter and Byers (1987) also extended the RWCIM to the problem of a V-notched crack in a bi-material. They formulated the eigenvalue problem using the complex potential method of England (1971 b). Subsequently, coefficient associated with the dominant eigenvector for the configuration can be calculated.

CHAPTER 3

THEORETICAL BACKGROUND

In this chapter, concepts of linear elastic fracture mechanics are first reviewed. Next, the complex potential method for a bi-material wedge configuration is presented. The reciprocal theorem and the reciprocal work contour integral (RWCIM) are then described. Finally, one-dimensional analyses of adhesive shear stresses, tensile stresses in a bonded plate, and peel stresses are presented.

3.1 LINEAR ELASTIC FRACTURE MECHANICS CONCEPTS

In linear elasticity, stress solutions involving singular stresses and strains appear close to material or geometrical discontinuities. The stress singularity at the tip of a crack is well known and is widely used for the prediction of fracture and fatigue crack growth in materials. There are also other local geometries and material combinations that yield singular stress field, such as configurations of the same material with general opening V notches, bi-material wedges, and interface corners. These configurations have received lesser attention for failure prediction purposes. (Groth, 1987: 11)

Microscopic events that lead to fracture in various materials generally occur within the plastic zone (or damage zone, to use more generic term). General important assumption is that if the size of plastic zone is small compared with the singularity-dominated zone, the stress intensity factor can be used as a failure criterion. The concept of “Similitude”, which implies that the crack tip conditions are uniquely defined by a single loading parameter, provides the theoretical basis for crack problems (Anderson, 1991: 598). Different structures loaded to the same stress intensity factor value have identical crack tip conditions. Even though the actual stress distribution in the plastic zone is not known, boundary conditions of the singularity dominated zone, which covers the plastic zone, are identical. Outside the singularity-dominated zone, higher order terms become significant and the stress field are different for different structures.

In contrast to crack problems, a multi-parameter description of the singular stress field occurs in other problems such as the configuration with the interface corner. In this configuration, there may be two singular terms having the same order of magnitude. Application of the similitude concept to these problems involves the evaluation of an equivalent stress intensity factor that yields identical singular stress field (Groth, 1988 b).

3.2 COMPLEX POTENTIAL METHOD

The condition at the end of a bonded CFRP plate is a bi-material wedge as shown in Fig. 3.1. In this section, the complex potential method for the analysis of a bi-material wedge under both plane strain and generalized plane stress is described.

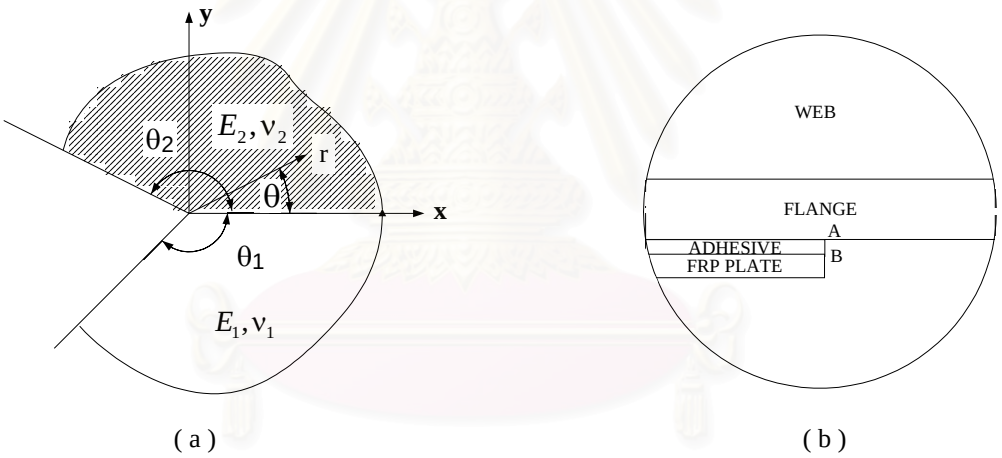

Figure 3.1 (a) A bi-material wedge configuration

(b) Stress singularities at the end of a bonded plate (singular point A and B)

In terms of the complex variable $z = x + iy = re^{i\theta}$, the basic equations of plane elasticity for equilibrium configurations in the absence of body force have solutions with the following representation in terms of two complex potentials $\Omega(z)$ and $\psi(z)$ (Green and Zirna, 1968)

$$U = u_r + iu_\theta = (2\mu)^{-1} e^{-i\theta} (\kappa\Omega(z) - z\,\overline{\Omega}'(\bar{z}) - \overline{\psi}(\bar{z}))$$

$$\tau_r = \sigma_{rr} + i\sigma_{r\theta} \quad = \Omega'(z) + \overline{\Omega}'(z) - \bar{z}\,\overline{\Omega}''(\bar{z}) - \bar{z}\,z^{-1}\overline{\psi}'(\bar{z})$$

$$\tau_\theta = \sigma_{\theta\theta} - i\sigma_{r\theta} \quad = \Omega'(z) + \overline{\Omega}'(\bar{z}) + \bar{z}\,\overline{\Omega}''(\bar{z}) + \bar{z}\,z^{-1}\overline{\psi}'(\bar{z}) \tag{3.1}$$

where

$\kappa = 3 - 4\nu$ for plane strain.

$\kappa = 3 - 4\nu/(1+\nu)$ for plane stress.

$\nu =$ Poisson's ratio.

$\mu =$ Shear modulus.

A general bi-material wedge is shown in Fig. 3.1. The wedge consists of two wedges of different materials perfectly bonded along a common edge, forming an interface. Wedge 1 and 2 has angle θ_1 and θ_2, respectively. The elastic properties of these two materials are defined by E_1, ν_1 and E_2, ν_2, respectively. Therefore, stresses and displacements near a corner of a bi-material wedge can be described by the complex potentials Ω_j and ψ_j as follows

$$\begin{aligned}
U_j &= u_{jr} + iu_{j\theta} = (2\mu_j)^{-1} e^{-i\theta}(\kappa_j \Omega_j(z) - z\overline{\Omega}'_j(\bar{z}) - \overline{\psi}_j(\bar{z})) \\
\tau_{jr} &= \sigma_{jrr} + i\sigma_{jr\theta} \quad = \Omega'_j(\bar{z}) + \overline{\Omega}'_j(\bar{z}) - \bar{z}\overline{\Omega}''_j(\bar{z}) - \bar{z}z^{-1}\overline{\psi}'_j(\bar{z}) \\
\tau_{j\theta} &= \sigma_{j\theta\theta} - i\sigma_{jr\theta} \quad = \Omega'_j(\bar{z}) + \overline{\Omega}'_j(\bar{z}) + \bar{z}\overline{\Omega}''_j(\bar{z}) + \bar{z}z^{-1}\overline{\psi}'_j(\bar{z})
\end{aligned} \tag{3.2}$$

where the subscript j refers to material j. The complex potentials are assumed to be (Carpenter and Byers, 1987)

$$\Omega_j(z) = A_j z^{\lambda_k} + a_j z^{\bar{\lambda}_k} \text{ and } \psi_j(z) = B_j z^{\lambda_k} + b_j z^{\bar{\lambda}_k} \tag{3.3}$$

Boundary conditions of the problem are the continuity condition along interface and the traction free condition along free edge as follows

a) For continuity of displacements at $\theta = 0$: $U_1(\theta = 0) = U_2(\theta = 0)$ (3.4a)

b) For continuity of stresses at $\theta = 0$: $\tau_{1\theta}(\theta = 0) = \tau_{2\theta}(\theta = 0)$ (3.4b)

c) In material 1, for stress free condition at $\theta = -\theta_1$: $\tau_{1\theta}(\theta = -\theta_1) = 0$ (3.4c)

d) In material 2, for stress free condition at $\theta = \theta_2$: $\tau_{2\theta}(\theta = \theta_2) = 0$ (3.4d)

By substituting Eq. (3.3) into Eq. (3.2) and applying the boundary conditions of Eq. (3.4a) to (3.4d), a system of equations is derived, which may be written as

$$[D]\{A_1 \quad A_2 \quad a_1 \quad a_2 \quad B_1 \quad B_2 \quad b_1 \quad b_2\} = \{0\} \tag{3.5}$$

where $D_{ij} = D_{ij}(E_1, E_2, \nu_1, \nu_2, \theta_1, \theta_2, \lambda)$

The eigenvalues of Eq. (3.5), λ_k, are related to the orders of singularities of the stress field at the bi-material wedge apex, which is a singular point. The eigenvalues were obtained from Eq. (3.5) by using the Muller's algorithm, which returned the refined eigenvalues (see Appendix B). Each eigenvalue yields an eigenvector (stresses and displacements) in terms of either a real or a complex coefficient, c_k, depending on the type of the eigenvalue. A dominant eigenvalue, λ_1, is the eigenvalue of which the real part has the lowest positive value in the open interval $0 < \mathrm{Re}(\lambda_k) < 1$. It should be noted that $-\lambda_1$ is also an eigenvalue of the problem.

For case of a real eigenvalue, Eq. (3.3) becomes

$$\Omega_j(z) = A_j z^{\lambda_k} \quad \text{and} \quad \psi_j(z) = B_j z^{\lambda_k} \tag{3.6}$$

where A and B are assumed to be complex. Substituting Eq. (3.6) into Eq. (3.2) gives

$$\begin{aligned}
2\mu_j U_j &= r^{\lambda_k}(\kappa_j A_j e^{i\theta(\lambda_k - 1)} - \overline{A}_j \lambda_k e^{i\theta(-\lambda_k + 1)} - \overline{B}_j e^{i\theta(-\lambda_k - 1)}) \\
\tau_{jr} &= r^{\lambda_k - 1}(A_j \lambda_k e^{i\theta(\lambda_k - 1)} - \overline{A}_j(\lambda_k^2 - 2\lambda_k) e^{i\theta(-\lambda_k + 1)} - \overline{B}_j \lambda_k e^{i\theta(-\lambda_k - 1)}) \\
\tau_{j\theta} &= r^{\lambda_k - 1}(A_j \lambda_k e^{i\theta(\lambda_k - 1)} + \overline{A}_j \lambda_k^2 e^{i\theta(-\lambda_k + 1)} + \overline{B}_j \lambda_k e^{i\theta(-\lambda_k - 1)})
\end{aligned} \tag{3.7}$$

a) For continuity of displacements at $\theta = 0$, $U_1(\theta = 0) = U_2(\theta = 0)$

From Eq. (3.7), $\mu_2(A_1\kappa_1 - \lambda_k \overline{A}_1 - \overline{B}_1) = \mu_1(A_2\kappa_2 - \lambda_k \overline{A}_2 - \overline{B}_2)$ (3.8)

b) For continuity of stresses at $\theta = 0$: $\tau_{1\theta}(\theta = 0) = \tau_{2\theta}(\theta = 0)$

From Eq. (3.7), $A_1 + \overline{A}_1 \lambda_k + \overline{B}_1 = A_2 + \overline{A}_2 \lambda_k + \overline{B}_2$ (3.9)

c) In material 1, for stress free condition at: $\theta = -\theta_1$: $\tau_{1\theta}(\theta = -\theta_1) = 0$

From Eq. (3.7), $\overline{B}_1 = -A_1 e^{-2i\lambda_k\theta_1} - \overline{A}_1\lambda_k e^{-2i\theta_1}$ (3.10)

d) In material 2, for stress free condition at $\theta = \theta_2$: $\tau_{2\theta}(\theta = \theta_2) = 0$

From Eq. (3.7), $\overline{B}_2 = -A_2 e^{2i\lambda_k\theta_2} - \overline{A}_2\lambda_k e^{2i\theta_2}$ (3.11)

Substituting Eq. (3.10) and (3.11) into Eq. (3.8) and (3.9) yields

$$A_1 d_1 + \overline{A}_1 d_2 + A_2 d_3 + \overline{A}_2 d_4 = 0 \quad (3.12)$$

$$A_1 d_5 + \overline{A}_1 d_6 + A_2 d_7 + \overline{A}_2 d_8 = 0 \quad (3.13)$$

where

$$d_1 = \kappa_1 + e^{-2i\lambda_k\theta_1}$$
$$d_2 = -\lambda_k + \lambda_k e^{-2i\theta_1}$$
$$d_3 = -\mu_1/\mu_2\,\kappa_2 - \mu_1/\mu_2\, e^{2i\lambda_k\theta_2}$$
$$d_4 = \mu_1/\mu_2\,\lambda_k - \mu_1/\mu_2\,\lambda_k e^{2i\theta_2}$$
$$d_5 = 1 - e^{-2i\lambda_k\theta_1}$$
$$d_6 = \lambda_k(1 - e^{-2i\theta_1})$$
$$d_7 = -1 + e^{2i\lambda_k\theta_2}$$
$$d_8 = \lambda_k(-1 + e^{2i\theta_2})$$

Solving Eq. (3.12) and (3.13) for A_2 gives

$$A_2 = \frac{d_4 d_5 - d_1 d_8}{d_3 d_8 - d_4 d_7} A_1 + \frac{d_6 d_4 - d_2 d_8}{d_3 d_8 - d_4 d_7}\overline{A}_1 = f_1 A_1 + f_2 \overline{A}_1 \quad (3.14)$$

or

$$\overline{A}_2 = \bar{f}_2 A_2 + \bar{f}_1 \overline{A}_1 \quad (3.15)$$

Solving Eq. (3.12) and (3.13) for $\overline{A}_2$ gives

$$\overline{A}_2 = \frac{d_3 d_5 - d_1 d_7}{d_4 d_7 - d_3 d_8} A_1 + \frac{d_6 d_3 - d_2 d_7}{d_4 d_7 - d_3 d_8}\overline{A}_1 = f_3 A_1 + f_4 \overline{A}_1 \quad (3.16)$$

Equating Eq. (3.15) to Eq. (3.16) yields after rearranging

$$(\bar{f}_2 - f_3)A_1 + (\bar{f}_1 - f_4)\overline{A}_1 = g_1 A_1 + g_2 \overline{A}_1 = 0 \quad (3.17)$$

Then, Eq. (3.17) can be written in the matrix as

$$\begin{bmatrix} (Rg_1 + Rg_2) & (Ig_1 - Ig_2) \\ (Ig_1 + Ig_2) & (Rg_1 - Rg_2) \end{bmatrix} \begin{bmatrix} RA_1 \\ IA_1 \end{bmatrix} = [D] \begin{bmatrix} RA_1 \\ IA_1 \end{bmatrix} = \begin{bmatrix} 0 \\ 0 \end{bmatrix} \tag{3.18}$$

Let $\begin{bmatrix} RA_1 \\ IA_1 \end{bmatrix} = \begin{bmatrix} p_{11} \\ p_{21} \end{bmatrix} c_k = [P] c_k$ (3.19)

Table 3.1 defines the coefficients c_k, p_{11}, and p_{21} that guarantee no chance of division by zero by selecting the largest term in absolute value sense for the denominator.

Table 3.1 Definition of terms in Eq. (3.19)

$L\arg est\left\|d_{ij}\right\|$	$location$	c_k	p_{11}	p_{21}
i	j			
1	1	IA_1	$-d_{12}/d_{11}$	1
1	2	RA_1	1	$-d_{11}/d_{12}$
2	1	IA_1	$-d_{22}/d_{21}$	1
2	2	RA_1	1	$-d_{21}/d_{22}$

Therefore,

$$\begin{bmatrix} A_1 \\ \overline{A}_1 \end{bmatrix} = \begin{bmatrix} 1 & i \\ 1 & -i \end{bmatrix} \begin{bmatrix} RA_1 \\ IA_1 \end{bmatrix} = [F][P] c_k \tag{3.20}$$

Then from Eq. (3.10) and Eq. (3.20)

$$\begin{bmatrix} A_1 \\ \overline{A}_1 \\ \overline{B}_1 \end{bmatrix} = \begin{bmatrix} 1 & 0 \\ 0 & 1 \\ -e^{-2i\lambda_k\theta_1} & -\lambda_k e^{-2i\theta_1} \end{bmatrix} \begin{bmatrix} A_1 \\ \overline{A}_1 \end{bmatrix} = [R_1] \begin{bmatrix} A_1 \\ \overline{A}_1 \end{bmatrix} = [R_1][F][P] c_k = [E_1] c_k \tag{3.21}$$

From Eq. (3.14) and (3.16)

$$\begin{bmatrix} A_2 \\ \overline{A}_2 \end{bmatrix} = \begin{bmatrix} f_1 & f_2 \\ f_3 & f_4 \end{bmatrix} \begin{bmatrix} A_1 \\ \overline{A}_1 \end{bmatrix} = [S] \begin{bmatrix} A_1 \\ \overline{A}_1 \end{bmatrix} = [S][F][P] c_k \tag{3.22}$$

Thus, we have from Eq. (3.11) and Eq. (3.20)

$$\begin{bmatrix} A_2 \\ \overline{A}_2 \\ \overline{B}_2 \end{bmatrix} = \begin{bmatrix} 1 & 0 \\ 0 & 1 \\ -e^{2i\lambda_k\theta_2} & -\lambda_k e^{2i\theta_2} \end{bmatrix} \begin{bmatrix} A_2 \\ \overline{A}_2 \end{bmatrix} = [R_2] \begin{bmatrix} A_2 \\ \overline{A}_2 \end{bmatrix} = [R_2][S][F][P] c_k = [E_2] c_k \tag{3.23}$$

Subsequently, the stresses and displacements can be obtained from Eq. (3.7), (3.21) and (3.23), which may be written as

$$\begin{bmatrix} 2\mu_j U_j \\ \tau_{jr} \\ \tau_{j\theta} \end{bmatrix} = [G_j] \begin{bmatrix} A_j \\ \overline{A}_j \\ \overline{B}_j \end{bmatrix} = [G_j][E_j]c_k = [J_j]c_k \tag{3.24}$$

where

$$[G_j] = \begin{bmatrix} r^{\lambda_k}\kappa_j e^{i\theta(\lambda_k-1)} & -r^{\lambda_k}\overline{A}_j\lambda_k e^{i\theta(-\lambda_k+1)} & -r^{\lambda_k}e^{i\theta(-\lambda_k-1)} \\ r^{\lambda_k-1}\lambda_k e^{i\theta(\lambda_k-1)} & -r^{\lambda_k-1}(\lambda_k^2-2\lambda_k)e^{i\theta(-\lambda_k+1)} & -r^{\lambda_k-1}\lambda_k e^{i\theta(-\lambda_k-1)} \\ r^{\lambda_k-1}\lambda_k e^{i\theta(\lambda_k-1)} & r^{\lambda_k-1}\lambda_k^2 e^{i\theta(-\lambda_k+1)} & r^{\lambda_k-1}\lambda_k e^{i\theta(-\lambda_k-1)} \end{bmatrix}$$

Finally,

$$\begin{bmatrix} u_{jr} \\ u_{j\theta} \\ \sigma_{jrr} \\ \sigma_{jr\theta} \\ \sigma_{j\theta\theta} \end{bmatrix} = \begin{bmatrix} RJ_j(1,1)/2\mu_j \\ IJ_j(1,1)/2\mu_j \\ RJ_j(2,1) \\ IJ_j(2,1) \\ RJ_j(3,1) \end{bmatrix} c_k = \{V_j(\lambda_k)\}c_k \tag{3.25}$$

From Eq. (3.25), each real eigenvalue, $\lambda = \lambda_k$, yields an eigenvector (stresses and displacements), $\{V(\lambda_k)\}$, in terms of a real coefficient, c_k. In this study, stress intensity factors, Q_{ij}, is defined in Eq. (3.26) as follows

$$\sigma_{ij} = \frac{Q_{ij}}{r^{1-\lambda_1}} \quad \text{or} \quad \sigma_{ij} = \frac{Q_{ij}}{r^{\alpha_1}} \tag{3.26}$$

where λ_1 is a dominant real eigenvalue and $\alpha_1 = 1-\lambda_1$ is a dominant order of singularity. In polar coordinates, for instance,

$$\sigma_{rr} = \frac{Q_{rr}}{r^{1-\lambda_1}}\ ,\ \sigma_{r\theta} = \frac{Q_{r\theta}}{r^{1-\lambda_1}}\ ,\ \text{and}\ \sigma_{\theta\theta} = \frac{Q_{\theta\theta}}{r^{1-\lambda_1}} \tag{3.27}$$

It can be seen from Eq. (3.25) and (3.26) that stress intensity factors associated with the dominant order of singularity are related to a real coefficient c_1. The evaluation of the unknown coefficient c_1 by the reciprocal theorem is described in the following section.

3.3 RECIPROCAL THEOREM

Consider a linear elastic structure subjected to two force systems represented by the matrix P_I and P_{II}, respectively. Displacements caused by the force system P_I alone and P_{II} alone are represented by U_I, and U_{II}, respectively. If the system P_I is applied first followed by the system P_{II}, the work done by external forces is given by

$$W_{I,II} = \tfrac{1}{2} P_I^T U_I + \tfrac{1}{2} P_{II}^T U_{II} + P_I^T U_{II} \tag{3.28}$$

where the subscript I,II with W indicates the sequence of application of these force systems. If the sequence is reversed, the work done is

$$W_{II,I} = \tfrac{1}{2} P_{II}^T U_{II} + \tfrac{1}{2} P_I^T U_I + P_{II}^T U_I \tag{3.29}$$

In both cases, work is stored as elastic strain energy, U, and the amount of energy so stored must be the same because the final deformed configuration in a linear elastic system must be independent of the sequence of load application. Therefore,

$$U = W_{I,II} = W_{II,I} \tag{3.30}$$

From which, we obtain

$$P_I^T U_{II} = P_{II}^T U_I \tag{3.31}$$

Eq. (3.31) is usually referred to as the reciprocal theorem of Betti, which states that “the work done by the system of forces P_I over the displacements U_{II} is equal to the work done by the system of forces P_{II} over the displacements U_I, where U_I and U_{II} are the displacements caused by P_I and P_{II}, respectively.”

3.4 THE RECIPROCAL WORK CONTOUR INTEGRAL METHOD

The reciprocal work contour integral method (RWCIM) was developed by Stern *et al* (1976) in order to find the values of the stress intensity factors in case of cracks, sharp corners with zero opening in homogenous materials, and cracks along

the interface of two dissimilar materials. Later, Carpenter and Byers (1987) extended this method for the case of a V-notched crack in a bi-material. The reciprocal theorem is a basis of this method.

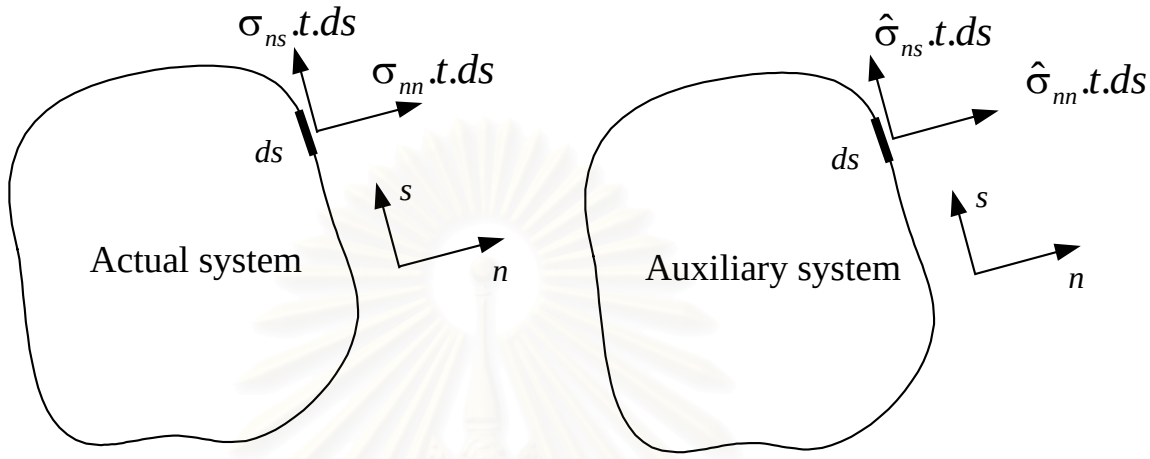

Figure 3.2 Actual and auxiliary systems

Fig. 3.2 shows a linear elastic 2-D body of thickness t in equilibrium subjected to two force systems along a closed contour. From the reciprocal theorem, we have

$$\int_C (\hat{\sigma}_{nn} u_n + \hat{\sigma}_{ns} u_s - \sigma_{nn} \hat{u}_n - \sigma_{ns} \hat{u}_s)\, ds = 0 \tag{3.32}$$

where u_n and $\hat{u}_n$ are displacements in the n-axis direction, u_s and $\hat{u}_s$ are displacements in the s-axis direction, and the integration proceeds along a closed boundary C in a counterclockwise direction corresponding to the n, s coordinate directions of Fig. 3.2.

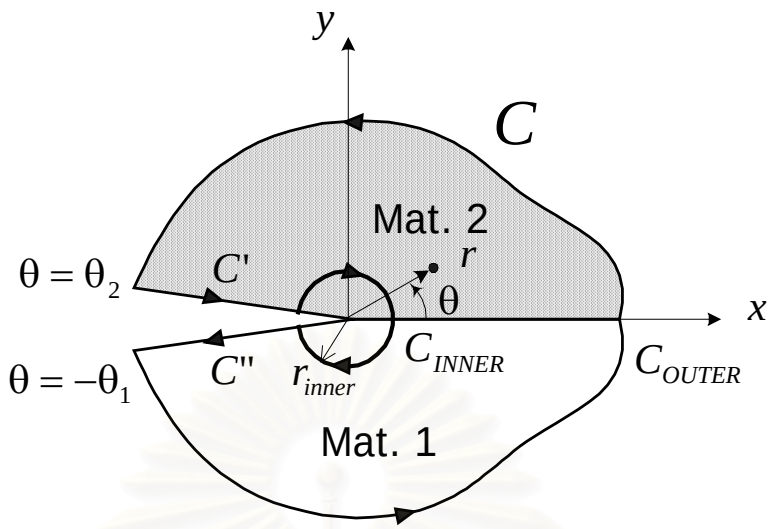

Figure 3.3 A general bimaterial wedge and a portion enclosed by a contour

In order to apply the reciprocal theorem to a bi-material wedge, a closed contour, C, was located. From Fig. 3.3, the contour C is given by

$$C = C_{OUTER} + C^{'} + C^{''} + C_{INNER} \tag{3.33}$$

Since $C^{'}$ and $C^{''}$ are the traction free surfaces, Eq. (3.32) becomes

$$\begin{aligned} &\int_{C_{OUTER}} (\hat{\sigma}_{nn} u_n + \hat{\sigma}_{ns} u_s - \sigma_{nn} \hat{u}_n - \sigma_{ns} \hat{u}_s)\, ds \\ &\quad + \int_{C_{INNER}} (\hat{\sigma}_{nn} u_n + \hat{\sigma}_{ns} u_s - \sigma_{nn} \hat{u}_n - \sigma_{ns} \hat{u}_s)\, ds = 0 \end{aligned} \tag{3.34}$$

By a suitable choice of the auxiliary system ($\hat{}$ system), Eq. (3.34) can be used to evaluate the values of stress intensity factors. In Stern *et al* (1976) and Carpenter and Byers (1987), stresses and displacements along C_{INNER} and C_{OUTER} in the auxiliary system were taken as the eigenvector corresponding to the eigenvalue $\lambda = -\lambda_1$, where λ_1 was the dominant real eigenvalue. In the real system, stresses and displacements from a finite element analysis were used along C_{OUTER}, while they were taken as the eigenvector corresponding to the eigenvalue $\lambda = \lambda_1$ along C_{INNER}.

Therefore, the inner contour integral may be written as

$$\int_{C_{INNER}} (\hat{\sigma}_{nn}\, u_n + \hat{\sigma}_{ns}\, u_s - \sigma_{nn}\, \hat{u}_n - \sigma_{ns}\, \hat{u}_s)\, ds = -\int_{\theta=-\theta_1}^{\theta=\theta_2} (\{V_j(+\lambda_1)\}^T [I_2]\, \{V_j(-\lambda_1)\})\, c_1\, c_{-1}\, r_{inner}\, d\theta \tag{3.35}$$

where c_1 and c_{-1} is an unknown coefficient associated with eigenvector $\{V_j(+\lambda_1)\}$ and $\{V_j(-\lambda_1)\}$, respectively.

$$I_1 = \begin{bmatrix} 0 & 0 & 1 & 0 \\ 0 & 0 & 0 & 1 \\ -1 & 0 & 0 & 0 \\ 0 & -1 & 0 & 0 \end{bmatrix} \qquad I_2 = \begin{bmatrix} 0 & 0 & 1 & 0 & 0 \\ 0 & 0 & 0 & 1 & 0 \\ -1 & 0 & 0 & 0 & 0 \\ 0 & -1 & 0 & 0 & 0 \\ 0 & 0 & 0 & 0 & 0 \end{bmatrix} \tag{3.36}$$

and

$$j = \begin{cases} 1 & ,if \quad \theta \le 0 \\ 2 & ,if \quad \theta > 0 \end{cases}$$

Consider the outer contour integral. Since stresses and displacements from the finite element analysis are with respect to an $x-y$ coordinate system while those of the eigenvector $\{V_j(-\lambda_1)\}$ are with respect to a $r-\theta$ coordinate system, both vectors have to be transformed to a $n-s$ coordinate system by using the transformation equation (Gibson, 1994)

$$\begin{bmatrix} u_n \\ u_s \\ \sigma_{nn} \\ \sigma_{ns} \end{bmatrix} = \begin{bmatrix} \cos(\gamma) & \sin(\gamma) & 0 & 0 & 0 \\ -\sin(\gamma) & \cos(\gamma) & 0 & 0 & 0 \\ 0 & 0 & \cos^2(\gamma) & 2\cos(\gamma)\sin(\gamma) & \sin^2(\gamma) \\ 0 & 0 & -\sin(\gamma)\cos(\gamma) & (\cos^2(\gamma)-\sin^2(\gamma)) & \sin(\gamma)\cos(\gamma) \end{bmatrix} [Y] \tag{3.37}$$

where γ is an angle between the current coordinate system ($r-\theta$ or $x-y$ system) and the $n-s$ system (positive if CCW). $[Y]$, which is a vector containing displacements and stresses in the current coordinate system, is the eigenvector $\{V_j(-\lambda_1)\}$ or the finite element solutions $[Y]_{FEM}$ defined below

$$[Y]_{FEM} = \begin{bmatrix} u_x \\ u_y \\ \sigma_{xx} \\ \sigma_{xy} \\ \sigma_{yy} \end{bmatrix} \tag{3.38}$$

Then, the outer contour integral may be written in a matrix form as

$$\int_{C_{OUTER}} (\hat{\sigma}_{nn}\, u_n + \hat{\sigma}_{ns}\, u_s - \sigma_{nn}\, \hat{u}_n - \sigma_{ns}\, \hat{u}_s)\, ds = \int_{C_{OUTER}} (\left[Y_{FEM}^{ns}\right]^T [I_1] \left[Y_{eig}^{ns}\right])\, c_{-1}\, ds \tag{3.39}$$

where $\left[Y_{FEM}^{ns}\right]$ and $\left[Y_{eig}^{ns}\right]$ are obtained from the transformation of $[Y_{FEM}]$ and $\{V_j(-\lambda_1)\}$ to the $n-s$ coordinate system, and I_1 is defined in Eq. (3.36). Therefore, from Eq. (3.34), (3.35), and (3.39)

$$GI.\, c_{-1} - QI.\, c_1.\, c_{-1} = 0 \tag{3.40}$$

which yields

$$c_1 = GI / QI \tag{3.41}$$

where

$$QI = -\int_{\theta=-\theta_1}^{\theta=\theta_2} (\{V_j(+\lambda_1)\}^T [I_2] \{V_j(-\lambda_1)\})\, r_{inner}\, d\theta$$

$$GI = \int_{C_{OUTER}} (\left[Y_{FEM}^{ns}\right]^T [I_1] \left[Y_{eig}^{ns}\right])\, ds \tag{3.42}$$

3.5 ANALYSIS FOR ADHESIVE SHEAR STRESSES, TENSILE STRESSES IN A BONDED PLATE, AND PEEL STRESSES

Analysis for adhesive shear stresses and tensile stresses in a bonded plate

A shear lag analysis, which was originally developed for evaluating the distribution of stresses in joints, can be used to evaluate the tensile stresses in a bonded plate and the shear stresses in an adhesive layer of a strengthened beam and will be described in this section.

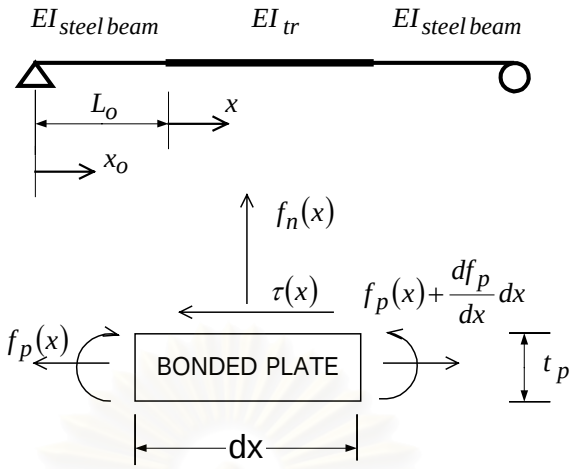

Figure 3.4 Free body diagram of a bonded plate

Fig. 3.4 shows an infinitesimal part of a plate adhesively bonded to the bottom flange of the steel beam. From equilibrium, an adhesive shear stress can be written as

$$\tau_a(x) = \frac{df_p(x)}{dx} t_p \tag{3.43}$$

where $f_p(x)$ is a tensile stress in a bonded plate and t_p is the plate thickness. Substituting $\tau_a(x) = G_a \gamma_a$ into Eq. (3.43) yields

$$\frac{df_p(x)}{dx} = \frac{G_a}{t_p} \gamma_a \tag{3.44}$$

where G_a is a shear modulus of adhesive and γ_a is a shearing strain of adhesive. Differentiating Eq. (3.44) with respect to x yields

$$\frac{d^2 f_p(x)}{dx^2} = \frac{G_a}{t_p} \frac{d\gamma_a}{dx} \tag{3.45}$$

where, $\frac{d\gamma_a}{dx} = \frac{(\varepsilon_p - \varepsilon_s)}{t_a}$ and

ε_p, ε_s = The tensile strain in a bonded plate and at bottom layer of the steel beam, respectively

t_a = The thickness of adhesive layer

The expressions for tensile strain in the plate and at the bottom flange of the beam are

$$\varepsilon_p(x)=\frac{f_p(x)}{E_p} \quad \text{and} \quad \varepsilon_s(x)=\frac{f_s(x)}{E_s}=\frac{M(x)\bar{y}}{E_s I_{tr}} \tag{3.46}$$

where E_p, E_s is elastic modulus of the plate and of the steel beam, respectively. $M(x)$ is bending moment, $\bar{y}$ is a distance from the neutral axis of a transformed section to the bottom layer of a steel beam, and I_{tr} is moment of inertia of the transformed section. By substituting Eq. (3.46) into Eq. (3.45), the governing equation is

$$f_p''(x)-\frac{G_a}{t_p t_a E_p} f_p(x)=-\frac{G_a}{t_p t_a E_s}\frac{M(x)\bar{y}}{I_{tr}} \tag{3.47}$$

If bending moment are assumed to have the form

$$M(x_o)=a_1 x_o^2+a_2 x_o+a_3 \tag{3.48}$$

where a_1, a_2, a_3 are constants and $x_o = x + L_o$. The origin of x and x_o is at the plate end and the support, respectively. Then, a general solution of the differential Eq. (3.47) is

$$f_p(x)=C_1\sinh(\sqrt{A}x)+C_2\cosh(\sqrt{A}x)+C_3x^2+C_4x+C_5 \tag{3.49}$$

where

$$A=\frac{G_a}{t_a t_p E_p}$$
$$C_3=\frac{\bar{y}a_1E_p}{I_{tr}E_s}$$
$$C_4=\frac{\bar{y}E_p}{I_{tr}E_s}(2a_1L_o+a_2)$$
$$C_5=E_p\left[\frac{\bar{y}}{I_{tr}E_s}(a_1L_o^2+a_2L_o+a_3)+2b_1\frac{t_at_p}{G_a}\right] \tag{3.50}$$

The constants of integration C_1 and C_2 are determined from the following two boundary conditions

$$f_p(x)|_{x=0} = 0 \quad \text{and} \quad \tau(L_s) = \frac{df_p[x]}{dx}|_{x=L_s} = 0 \tag{3.51}$$

where L_s is a distance from the plate end to the point of zero shear force. From Eq. (3.51), the expressions for C_1 and C_2 are found to be

$$C_1 = \frac{C_5\sqrt{A}\sinh\left(\sqrt{A}L_s\right) - 2C_3L_s - C_4}{\sqrt{A}\cosh\left(\sqrt{A}L_s\right)}$$
$$C_2 = -C_5 \tag{3.52}$$

Since $\sinh(x)$ and $\cosh(x)$ are almost equal when x becomes larger and have large values compared with other terms in the numerator, we can simplify Eq. (3.52) to $C_1 = C_5$.

Analysis for peel stresses

When consider a steel beam and a bonded plate as two isolated beams connected by the adhesive layer as shown in Fig. 3.5, the fourth order differential equation for each beam can be expressed by

$$E_sI_s\frac{d^4v_s}{dx^4} = q - b_p f_n(x) \tag{3.53}$$

$$E_pI_p\frac{d^4v_p}{dx^4} = b_p f_n(x) \tag{3.54}$$

where q = distributed load on the steel beam

b_p = width of the bonded plate

$E_sI_s, E_pI_p = EI$ of the steel beam and the plate, respectively

v_s, v_p = deflection of the steel beam and the plate, respectively

$f_n(x)$ = peel stress

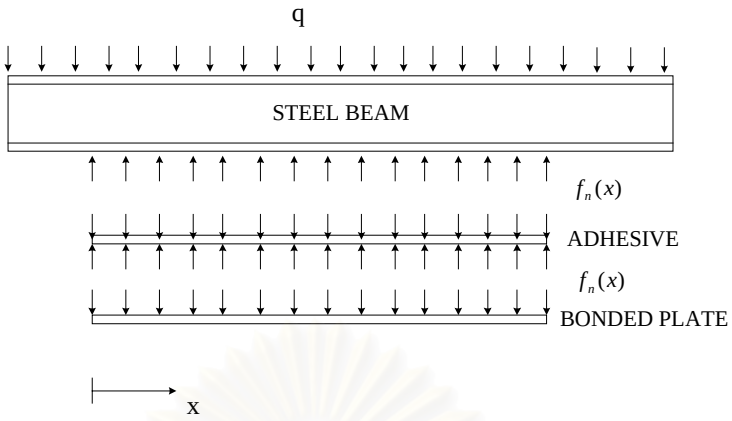

Figure 3.5 Model used to analyze for peel stresses in a strengthened beam

By considering deformation in an adhesive layer, $f_n(x)$ can be expressed as

$$f_n(x) = E_a \frac{(v_s - v_p)}{t_a} \tag{3.55}$$

where E_a, t_a = modulus of elasticity and thickness of adhesive layer, respectively. Differentiating Eq. (3.55) four times yields

$$\frac{d^4 f_n(x)}{dx^4} = \frac{E_a}{t_a}\left(\frac{d^4 v_s}{dx^4} - \frac{d^4 v_p}{dx^4}\right) \tag{3.56}$$

From Eq. (3.53) and (3.54), the governing differential equation for the peel stress is

$$\frac{d^4 f_n(x)}{dx^4} = \frac{E_a}{t_a}\left(\frac{q - b_p f_n(x)}{E_s I_s} - \frac{b_p f_n(x)}{E_p I_p}\right) \tag{3.57}$$

If $E_s I_s >> E_p I_p$, Eq. (3.57) becomes

$$\frac{d^4 f_n(x)}{dx^4} + \frac{E_a b_p f_n(x)}{t_a E_p I_p} = \frac{E_a q}{t_a E_s I_s} \tag{3.58}$$

The solution of this fourth order linear differential equation is a summation of the homogeneous and particular solution as given below

$$f_n(x) = e^{-\gamma x}[D_1 \cos(\gamma x) + D_2 \sin(\gamma x)] + e^{\gamma x}[D_3 \cos(\gamma x) + D_4 \sin(\gamma x)] + \frac{qE_p I_p}{b_p E_s I_s} \tag{3.59}$$

where $\gamma = \sqrt[4]{\frac{E_a b_p}{t_a E_p I_p}}$

At the points far from the plate end, the peel stress and its derivatives approach zero. To satisfy this condition, $D_3 = D_4 = 0$ and Eq. (3.59) reduces to

$$f_n(x) = e^{-\gamma x}[D_1 \cos(\gamma x) + D_2 \sin(\gamma x)] + \frac{qE_p I_p}{b_p E_s I_s} \tag{3.60}$$

Constants of integration D_1 and D_2 can be obtained by using the force boundary conditions. By differentiation Eq. (3.55) two times, we have

$$\frac{d^2 f_n(x)}{dx^2} = \frac{E_a}{t_a}\left(\frac{d^2 v_s}{dx^2} - \frac{d^2 v_p}{dx^2}\right) = \frac{E_a}{t_a}\left(\frac{M_p(x)}{E_p I_p} - \frac{M_s(x)}{E_s I_s}\right) \tag{3.61}$$

where $M_p(x), M_s(x)$ = bending moment in the plate and the steel beam, respectively. Differentiating Eq. (3.61) once more yields

$$\frac{d^3 f_n(x)}{dx^3} = \frac{E_a}{t_a}\left(\frac{d^3 v_s}{dx^3} - \frac{d^3 v_p}{dx^3}\right) = \frac{E_a}{t_a}\left(\frac{V_p(x)}{E_p I_p} - \frac{V_s(x)}{E_s I_s}\right) \tag{3.62}$$

where $V_p(x), V_s(x)$ = shear forces in the plate and the steel beam, respectively. When the effect of interfacial shear stress is included in the evaluation of the bending moment in the steel beam and the bonded plate, expression for the bending moment in the steel beam is

$$M_s(x) = M_s^{ext}(x) + M_s^{sf}(x) \tag{3.63}$$

where $M_s^{ext}(x)$, $M_s^{sf}(x)$ = bending moment in the steel beam due to externally applied load and due to shear flow along the interface of the steel beam and the plate, respectively. Whereas the bending moment in the bonded plate is expressed by

$$M_p(x) = M_p^{sf}(x) \tag{3.64}$$

From Fig. 3.6 and recall Eq. (3.43) and (3.49), the equations for bending moments in steel beam and bonded plate due to shear flow along the interface can be written as

$$M_s^{sf}(x) = -\bar{y}_s b_p t_p [C_5 \sinh(\sqrt{A}x) - C_5 \cosh(\sqrt{A}x) + C_3 x^2 + 2C_4 x + C_5] \quad (3.65)$$

$$M_p^{sf}(x) = -b_p \frac{t_p^2}{2} [C_5 \sinh(\sqrt{A}x) - C_5 \cosh(\sqrt{A}x) + C_3 x^2 + 2C_4 x + C_5] \quad (3.66)$$

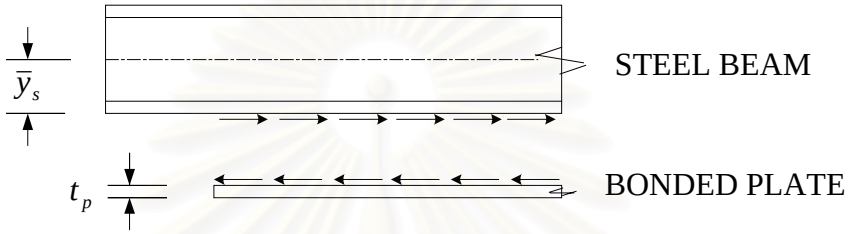

Figure 3.6 Shear flow acting on the isolated beams

Differentiation Eq. (3.65) and (3.66) results in

$$V_s^{sf}(x) = -\bar{y}_s b_p t_p [C_5 \sqrt{A} \cosh(\sqrt{A}x) - C_5 \sqrt{A} \sinh(\sqrt{A}x) + 2C_3 x + C_4] \quad (3.67)$$

$$V_p^{sf}(x) = -b_p \frac{t_p^2}{2} [C_5 \sqrt{A} \cosh(\sqrt{A}x) - C_5 \sqrt{A} \sinh(\sqrt{A}x) + 2C_3 x + C_4] \quad (3.68)$$

By substituting $x = 0$ into Eq. (3.63) to (3.68) and assuming that the steel beam alone takes full shear due to externally applied loads, the force boundary conditions at the plate end are

$$\begin{aligned} &M_s(x)|_{x=0} = M_o \text{ and } M_p(x)|_{x=0} = 0 \\ &V_s^{sf}(x)|_{x=0} = V_s = V_o - \bar{y}_s b_p t_p [C_5 \sqrt{A} + C_4] \\ &V_p^{sf}(x)|_{x=0} = V_p = -b_p \frac{t_p^2}{2} [C_5 \sqrt{A} + C_4] \end{aligned} \quad (3.69)$$

where M_o, V_o = bending moment and shear force at the plate end due to external loads, respectively. By substituting Eq. (3.69) into the right side of Eq. (3.61) and (3.62), D_1 and D_2 are obtained to be

$$D_1 = \frac{E_a}{t_a \gamma^3} \left[\frac{V_p^{sf}}{2E_p I_p} - \frac{(V_s + \gamma M_o)}{2E_s I_s} \right] \quad (3.70)$$

$$D_2 = \frac{E_a M_o}{2 t_a E_s I_s \gamma^2} \tag{3.71}$$

CHAPTER 4

DEVELOPMENT OF A DOUBLE STRAP JOINT TEST SPECIMEN

4.1 ANALYSIS OF STRESSES IN A BONDED JOINT

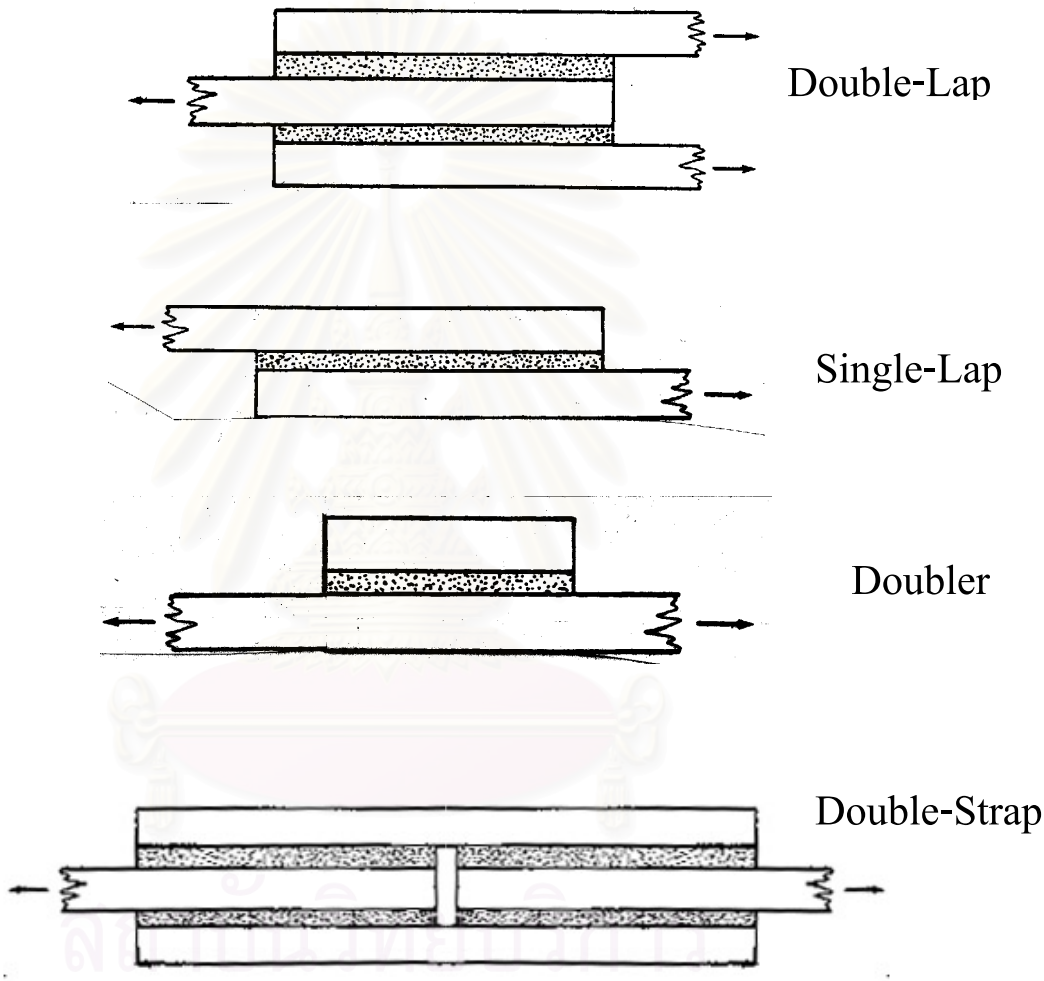

Figure 4.1 Some important bonded configurations

Fig. 4.1 shows some important types of adhesive joints. A conventional analytical study on adhesive joints is based on the classical work of Volkersen (1938). In Volkersen's analysis, which is usually referred to as a "shear-lag" analysis, adhesive is subjected to a state of pure shear, whereas adherends are under only axial stress. The analytical model for the evaluation of the adhesive shear stresses, shown in Fig. 4.2, is formulated as follows.

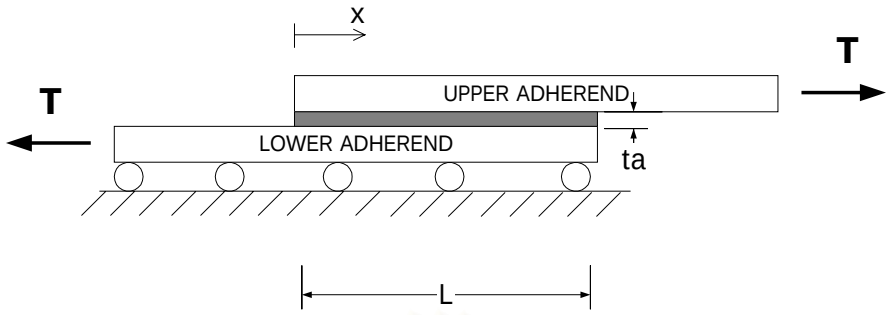

Figure 4.2 Geometry for analysis of adhesive shear stresses

Referring to Fig.4.2, the adhesive shear stresses can be written from equilibrium as

$$\tau_a = \frac{df_U}{dx} t_U \tag{4.1}$$

where τ_a = Adhesive shear stress

f_U = Tensile stress in an upper adherend

t_U and t_L = Thickness of an upper adherend and an lower adherend, respectively

Differentiating Eq. (4.1) with respect to x yields,

$$\frac{d^2 f_U}{dx^2} = \frac{G_a}{t_U} \frac{d\gamma_a}{dx} \tag{4.2}$$

where $\frac{d\gamma_a}{dx} = \frac{(\varepsilon_U(x) - \varepsilon_L(x))}{t_a} = \frac{1}{t_a}\left(\frac{f_U(x)}{E_U} - \frac{f_L(x)}{E_L}\right)$

G_a and t_a = shear modulus and thickness of adhesive layer.

E_U and E_L = Young's moduli of upper and lower adherends.

Consider a section at distance x from the joint end, from equilibrium

$$f_L(x) = \frac{1}{t_L}(T - t_U f_U(x)) \tag{4.3}$$

where f_U = Tensile stress in an upper adherend.

T = applied axial resultant (Force/length).

Therefore,

$$\frac{d^2 f_U}{dx^2} = \frac{G_a}{t_U t_a}\left(\frac{f_U(x)}{E_U} - \frac{f_L(x)}{E_L}\right) \tag{4.4}$$

After rearranging terms, we have

$$\frac{d^2 f_U}{dx^2} = \frac{G_a}{t_a}\left(\frac{1}{E_U t_U} + \frac{1}{E_L t_L}\right) f_U - \frac{G_a}{t_U t_a}\frac{T}{E_L t_L} \tag{4.5}$$

$$\frac{d^2 f_U}{dx^2} - \beta^2 f_U = -\frac{G_a}{t_U t_a}\frac{T}{E_L t_L} \tag{4.6}$$

where

$$\beta^2 = \frac{G_a}{t_a}\left(\frac{1}{E_U t_U} + \frac{1}{E_L t_L}\right) \tag{4.7}$$

Consequently, a general solution of the governing Eq. (4.6) is

$$f_U(x) = A\sinh(\beta x) + B\cosh(\beta x) + \frac{G_a}{\beta^2 t_U t_a}\frac{T}{E_L t_L} \tag{4.8}$$

Two boundary conditions for determining the constants A and B are

$$f_U(x)|_{x=0} = 0 \tag{4.9}$$

$$f_U(x)|_{x=L} = T / t_U \tag{4.10}$$

Substituting Eq. (4.8) into (4.9) and (4.10) leads to

$$B = -\frac{G_a}{\beta^2 t_U t_a}\frac{T}{E_L t_L} \tag{4.11}$$

$$A = \frac{\left(T / t_U + \frac{G_a}{\beta^2 t_U t_a}\frac{T}{E_L t_L}\left(\cosh(\beta L) - 1\right)\right)}{\sinh(\beta L)} \tag{4.12}$$

Finally, the adhesive shear stresses are obtained from Eq. (4.1) as follows

$$\tau_a(x) = t_U\,\beta\left(A\cosh(\beta x) + B\sinh(\beta x)\right) \tag{4.13}$$

For a double strap joint (with outer adherend rotation restrained at $x = L$) shown in Fig. 4.1, the effect of stiffness imbalance of adherends on shear stress distribution analyzed on the half model by the shear lag analysis is shown in Fig. 4.3.

In the figure, the adhesive shear stress is normalized by the applied stress. When the outer adherends are stiffer than the inner adherend, or, equivalently, the ratio of the stiffness of the inner to the two outer adherends is less than one, adhesive shear stress at the joint end is the highest. On the other hand, shear stress at the joint center is maximum if the stiffness ratio is more than one.

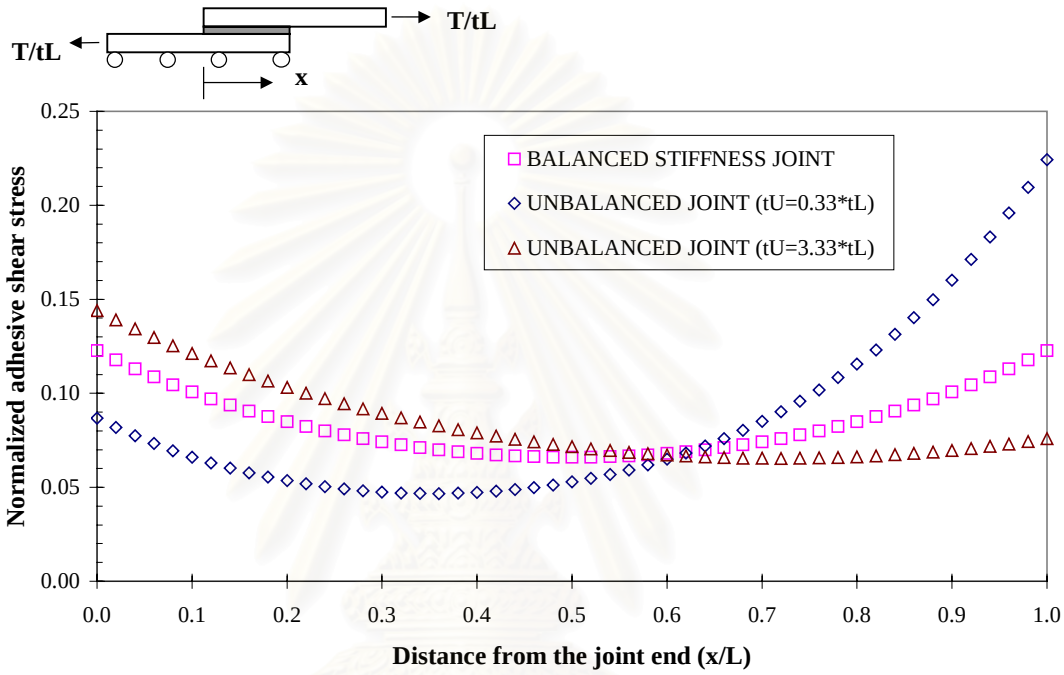

Figure 4.3 Effect of stiffness imbalance of adherends

Because the shear lag analysis is based on a one-dimensional model, it can not evaluate the stress distribution along the adhesive layer thickness. To investigate the distribution of adhesive shear stresses and the peel stresses, or transverse nominal stresses, along adhesive at various levels of the adhesive layer, a 2-D plane stress finite element analysis was conducted. A mesh of the double strap joint specimen is shown in Fig. 4.4. The mesh consisted of 8-node isoparametric quadrilaterals and 6-point isoparametric triangles. There was relatively high degree of mesh refinement around the ends of the overlap. Fig. 4.4 also shows three paths at which the stress distributions were investigated: 1) 0.01 cm above bottom interface, 2) half of adhesive layer thickness, or 0.05 cm, and 3) 0.01 cm below top interface. The mesh near the joint end is shown in Fig. 4.5. The adhesive shear stresses obtained from the shear lag analysis and those from the finite element analysis are shown in Fig. 4.6 for comparison.

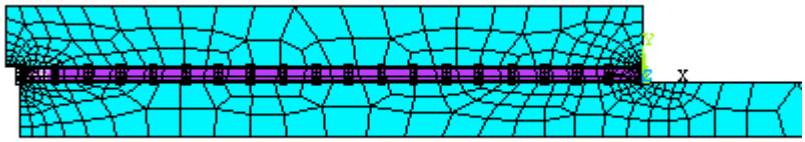

Figure 4.4 A 2-D finite element model (plane stress) showing the paths for adhesive shear stresses and peel stresses

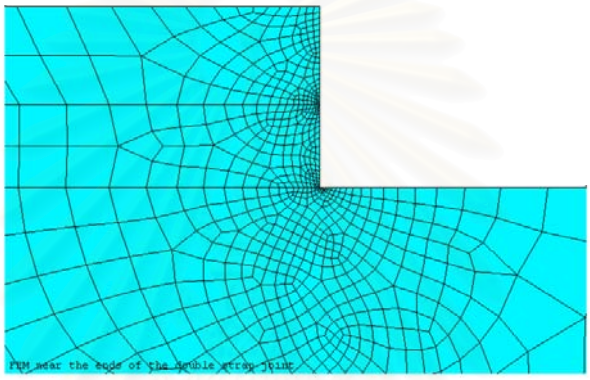

Figure 4.5 Mesh near the joint end

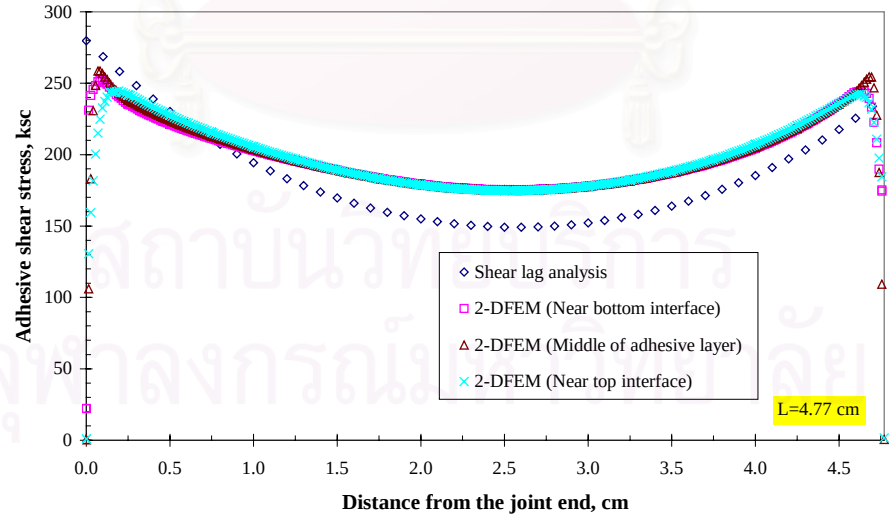

Figure 4.6 Comparison of adhesive shear stresses: shear lag analysis v.s. finite element analysis

It was found that the discrepancy of adhesive shear stresses of the three paths investigated was modest. Moreover, reasonable agreement of adhesive shear stresses from the shear lag analysis and those from the finite element analysis was observed. Although the shear stresses from this displacement-based FEM can not satisfy the exact traction free condition, as shown in Fig. 4.6, they show signs of heading to a zero value. This behavior could not be captured by the shear lag analysis.

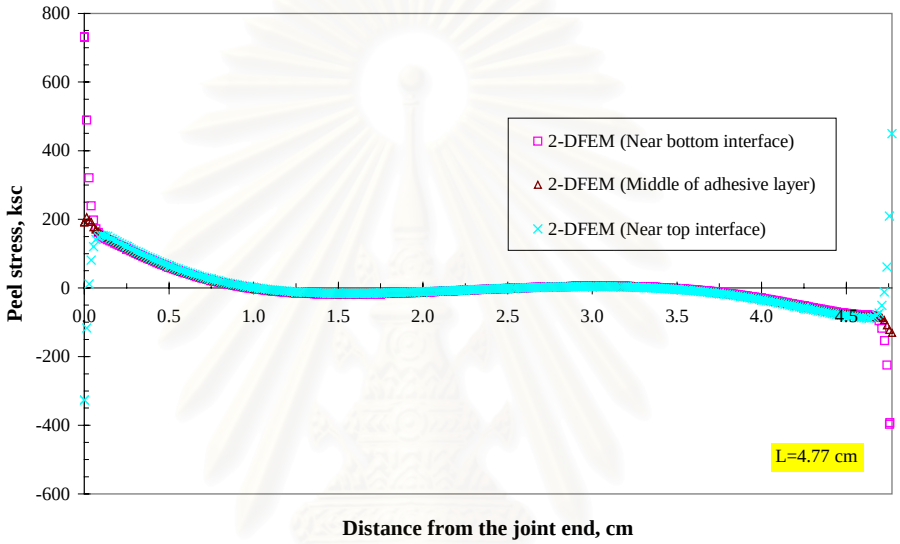

Figure 4.7 Peel stress distribution from finite element analysis

The peel stress, which is the through-thickness extensional stress in the adhesive, was also studied. From the finite element analysis, peel stress distributions in the previous three paths are shown in Fig. 4.7. Although, eccentricity of load path is not obvious as the case of single lap joints, in which the offset of two adherends leads to bending deflection, load path eccentricity is also present in double strap joints and double lap joints consisting of uniform adherend thickness. Peel stresses in these symmetric joints are needed in order to restrain the moment produced by the offset of shear force about the neutral axis of the outer adherends. In contrast to the peel stress distribution near the top interface, those near the bottom interface is tensile (positive value) at the joint end and compressive (negative value) at the joint center as illustrated in Fig. 4.7.

In the development of a test specimen, the following behaviors of double strap joints are realized:

1) Adhesive shear stresses and peel stresses are concentrated near the joint ends, while much of the joint is subjected to relatively low levels of stresses. Shear lag analysis can be used for determining the location where high stress occurs in the joint.

2) By proper design of the joint's stiffness ratio, which is the ratio of stiffness of the inner to that of the two outer adherends, the fracture critical location in the joint can be defined.

3) Unlike single lap joints, double lap joints and double strap joints are symmetrical and have lesser load path eccentricity. Therefore, they can be tested with higher degree of accuracy and consistency as reported in Swamy and Muskhopadhyaya (1995).

4.2 PRELIMINARY TEST ON CFRP-STEEL DOUBLE STRAP JOINTS

A preliminary test on double strap joints, of which the two outer adherends were CFRP laminates and the inner adherend was a steel plate, was conducted. The objective was to find the average bond strength as a preliminary value for subsequent design. The lap length was 5 cm. The thicknesses of the inner steel adherend and the outer CFRP adherend were 0.84 cm and 0.14 cm (one strip). The steel surface was sandblasted according to The Steel Structure Painting Council (1991) specification no.5 (White-Metal Blast Cleaning). Fig. 4.8 shows a specimen configuration in the preliminary test. Three specimens were tested. The adhesive thickness was controlled to be 1 mm. At the joint ends, adhesive angle was controlled to be 90^{o} perpendicular to the inner adherend, called "square end". In the test, curing time of adhesive was about two weeks. The bond strength of each specimen, calculated from the failure load of the specimen divided by the bonded area, is shown in Table 4.1.

Figure 4.8 CFRP-steel double strap joint specimen (Preliminary test)

Table 4.1 Average bond strength from a preliminary test on CFRP-Steel double strap joint specimens

Specimen no.	Average bond stength, ksc
1	154
2	162
3	164
Avg. =	160
Std. =	5

4.3 A PROPOSED TEST SPECIMEN

Specimen configuration

A double strap joint used as a test specimen is shown in Fig. 4.9. The joint consisted of only steel adherends. To prevent yielding of both inner and outer steel adherends, the average bond strength obtained from the preliminary test was used for designing the lap length. The stiffness ratio of the joint was slightly less than one, therefore controlling the highest stress location to be at the joint end. A square end condition was controlled at the joint end.

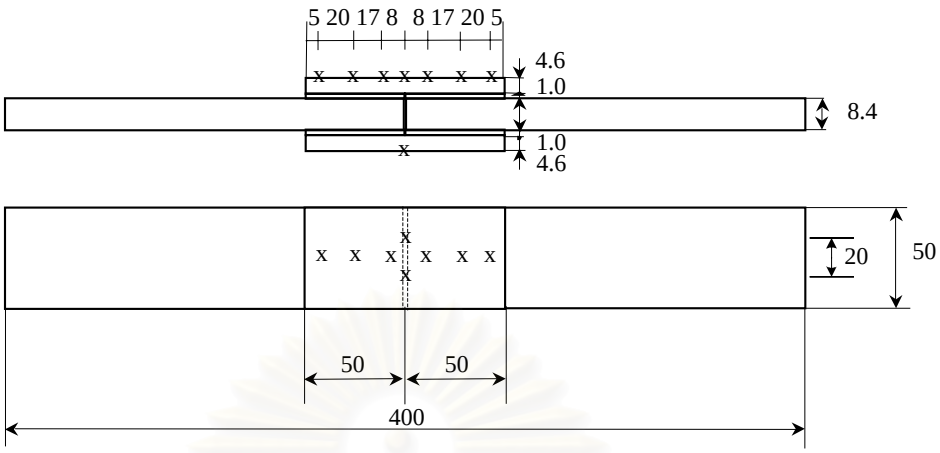

Figure 4.9 A steel only double strap joint specimen (All dimensions in mm)

In the double strap joint, there are two different bi-material wedge configurations as shown in Fig. 4.10. Since the thickness ratio of inner adherend to the two outer adherends (summed thickness) is less than one, corner A is the critical location of fracture regarding shear stresses and peel stresses.

Singular points which are corner A, B (or C, D) associated with these two bi-material wedges are also shown in the figure. Consider the dominant order of singularity at these corners, it was found that the highest one is present at the corner A (and D). For the case of bi-materials in this study where the elastic constants are $E_{steel} = 2x10^6 \quad ksc$, $E_{adh} = 27{,}500 \quad ksc$, $\nu_{steel} = 0.3$, and $\nu_{adh} = 0.35$, the dominant eigenvalues were found to be:

Corner A and D: $\lambda_1 = 0.729$ -plane stress

and $\lambda_1 = 0.674$ -plane strain

Corner B and C: $\lambda_1 = 0.752$ -plane stress

and $\lambda_1 = 0.695$ -plane strain

In practice, a spew fillet condition usually occurs at the corner D instead of a square end condition; therefore leading to a reduction of the order of singularity at this corner to be lower than the theoretical values.

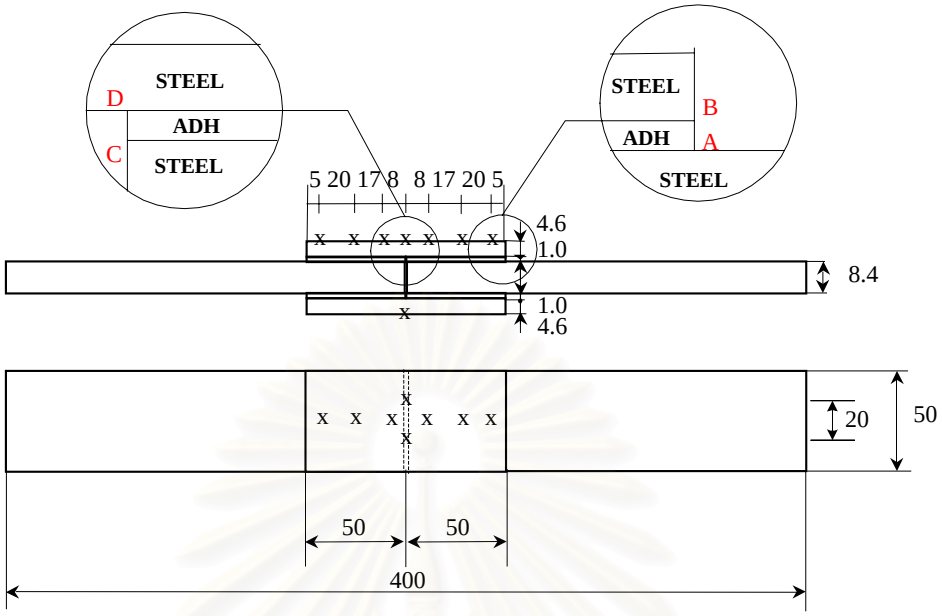

Figure 4.10 Singular points (Point A to D) in a double strap joint specimen

Specimen fabrication and testing

The steel only double-strap joint specimens had the following properties same as the strengthened steel beams: adhesive type, bi-material wedge angles and steel surface preparation. The steel surface was sandblasted according to The Steel Structure Painting Council (1991) specification no.5. The thickness of adhesive layer was controlled by putting small inserts having diameter 1 mm between inner and outer adherends. The inserts were located away from the high stress region (e.g. from the joint ends and joint center). Also, the terminus of the adhesive was made sharp perpendicular to the steel surface because the finite element model used this shape of terminus.

The test setup of the joints is shown in Fig. 4.11. All joints were tested at a crosshead speed of 1.2 mm/min. The curing time was about 2 weeks for NC-1 to NC-3, and 5 months for the rests. Strain gages were attached to the joints to check specimen alignment, to measure the strain distribution along an outer adherend, and to verify the finite element model. Fig. 4.12 compares the strain distributions along an outer adherend from the 2-D finite element analysis with the test data at various load

levels. It can be seen that the finite element analysis yields reasonable agreement with the measurement.

Figure 4.11 Test setup for double-strap joint specimens

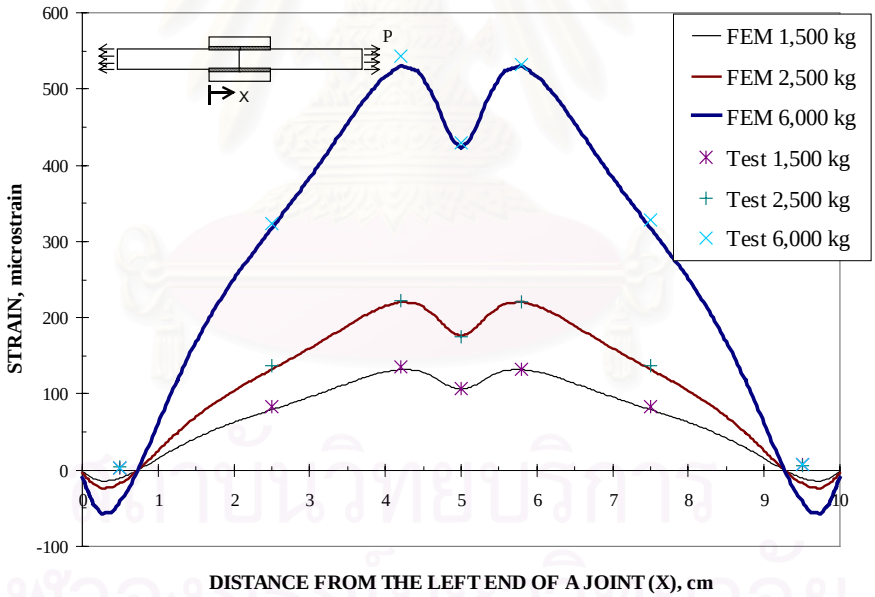

Figure 4.12 Strain distributions from the finite element analysis v.s. measurement at various load levels

4.4 A FRACTURE CRITERION

It is proposed that fracture will occur when:

$$Q = Q_{cr} \tag{4.14}$$

where Q_{cr} is the critical stress intensity factor. This value was selected to be obtained from the tests on double-strap joints. Double-strap joints were proposed since good degree of accuracy and consistency of test results can be expected compared with the unsymmetrically loaded single lap joints. The following properties of the joints must be the same as those of the strengthened steel beams: Bi-material wedge's properties and interface characteristics. From the fracture criterion, the value of Q_{cr} obtained will be then used to predict the fracture load, P_{cr}, which leads to the separation of the bonded plate from the steel beam, by using the relation

$$P_{cr} = \frac{Q_{cr}}{Q_{FEM}} P_{FEM} \tag{4.15}$$

where P_{FEM} and Q_{FEM} are the applied load in the finite element model and the Q-factor calculated from the finite element analysis.

4.5 EVALUATION OF CRITICAL STRESS INTENSITY FACTORS

Typical failure of the double-strap joint specimens is as shown in Fig. 4.13. Adhesive failure between steel and adhesive (at corner A of Fig. 4.10) can be observed from the figure. The measured failure loads of all joints are summarized in Table 4.2. Subsequently, critical stress intensity factors along interface $(\theta = 0^{\circ})$ of each specimen were calculated at the measured failure load from the Reciprocal Work Contour Integral Method. Their values corresponding to the plane strain and plane stress conditions are also shown in the table. The evaluation of stress intensity factors by RWCIM will be explained in Chapter 5. The order of singularity, α, is 0.271 and 0.326 under plane stress and plane strain condition, respectively.

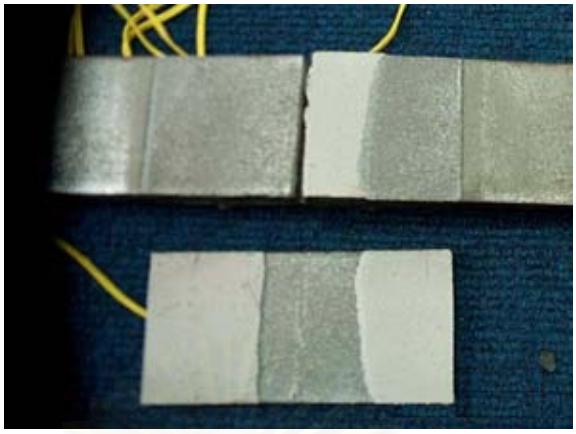

Figure 4.13 Typical failure of double-strap joint specimens (DSJ)

Table 4.2 Failure loads and stress intensity factors of all DSJ specimens

Specimen no.	Failure load, kg	$PLANE STRESS, ksc-cm^{0.271}$			$PLANE STRAIN, ksc-cm^{0.326}$		
		Q_{rr}	$Q_{r\theta}$	$Q_{\theta\theta}$	Q_{rr}	$Q_{r\theta}$	$Q_{\theta\theta}$
NC-1	9858	82.3	61.6	224.8	88.8	56.9	160.6
NC-2	7580	63.3	47.4	172.9	68.3	43.8	123.5
NC-3	8956	74.8	56.0	204.2	80.7	51.7	145.9
NC-4	9831	82.1	61.4	224.2	88.5	56.8	160.2
NC-5	10571	88.3	66.1	241.1	95.2	61.0	172.2
NC-6	10004	83.5	62.5	228.1	90.1	57.8	163.0
NC-7	9097	76.0	56.9	207.5	81.9	52.5	148.2
NC-8	9280	77.5	58.0	211.6	83.6	53.6	151.2
NC-9*	8287	69.2	51.8	189.0	74.6	47.9	135.0
NC-10*	6863	57.3	42.9	156.5	61.8	39.6	111.8
Avg. =	9397	78.5	58.7	214.3	84.6	54.3	153.1
Std. =	906	7.6	5.7	20.7	8.2	5.2	14.8

**- The width of an outer steel plate in specimen NC-9 and NC-10 was 7.5 cm. These specimens were not included in the evaluation of the average value and standard deviation.*

Average interfacial stress intensity factors with standard deviation are $Q_{rr} = 78.5 \pm 7.6$, $Q_{r\theta} = 58.7 \pm 5.7$, and $Q_{\theta\theta} = 214.3 \pm 20.7\ ksc - cm^{0.271}$ under plane stress condition. Under plane strain condition, values of stress intensity factors are $Q_{rr} = 84.6 \pm 8.2$, $Q_{r\theta} = 54.3 \pm 5.2$, and $Q_{\theta\theta} = 153.1 \pm 14.8\ ksc - cm^{0.326}$.

4.6 SMALL SCALE YIELDING

All engineering materials exhibit plasticity to some degree. At singularities, this leads to a reduction of the theoretical peak stresses as plasticity zone starts to develop. The maximum possible size of the plastic yield zone generated at the apex of the wedge can be estimated with the following expression (Lefebvre and Dillard, 1999 a: 135)

$$r_p = \gamma\left(\frac{Q_{VM}}{\sigma_Y}\right)^{1/(1-\lambda_1)} \tag{4.16}$$

where

r_p = Radius of the plastic zone

Q_{VM} = The critical stress intensity factor calculated from the von Mises stress distribution.

σ_Y = Yield strength of the adhesive

λ_1 = Dominant eigenvalue

γ = Assumption-dependent coefficient

For a lower-bound estimate based on a linear elastic solution, $\gamma = 1$. For a more conservative estimate analogous to that of a crack tip yield zone, $\gamma = 2$ (Lefebvre and Dillard, 1999 a: 136).

Small scale yielding is valid when elastic singularity governs the stresses at distances from the singularity that are large compared to the yield zone, but still small compared to typical geometrical dimensions (Groth, 1987: 22).

For crack problems, the critical stress intensity factor is only a material constant when certain conditions are met. Otherwise, this value can be geometry dependent. To achieve plane strain condition at the crack tip, plastic zone must be small compared with the specimen thickness. If the thickness is too small or the plastic zone is too large, the constraint at the crack tip relaxes. A lower degree of stress triaxiality usually results in higher toughness. Small thickness corresponds to plane stress fracture. Fracture toughness decreases with increasing thickness until

plane strain condition is reached (Anderson, 1991: 104). For adhesive joints, adhesive layer is under triaxial tension resulting from constraints imposed by the stiffer adherends (Wang and Rose, 1997: 23). Yielding and failure of adhesives are strongly influenced by hydrostatic pressure or tension, especially for adhesives that are rubber toughened to improve ductility. Experiments have shown that neither the Tresca nor the von Mises criterion adequately describes the shear-yielding behavior of polymers (Wang and Rose, 1997: 18). It is well known that measured polymer yield strength depends on mean stress levels. For example, the measured uniaxial compressive yield strength (with $\sigma_m = -\sigma_Y / 3$) is typically higher than that measured in uniaxial compression (with $\sigma_m = \sigma_Y / 3$) (Reedy and Guess, 1996: 280). Reported values of the ratio of compressive to tensile yield strength for an epoxy range from 1.1 to 1.4 (Adam and Wake, 1984). Stress relaxation test data suggested that adhesive actually displays nonlinear and stress dependent viscoelastic (Guess *et al*, 1995). The adhesive properties were often measured using strain gaged, cast dog-bone specimens tested in tension and cylindrical specimens tested in axial compression. Since tensile specimen failed prior to yield at the shrinkage induced surface flaws, the tensile yield strength was usually assumed (Reedy and Guess, 1993: 2932).

CHAPTER 5

FINITE ELEMENT EVALUATION OF STRESS INTENSITY FACTORS

In this chapter, methods for the analysis of stress intensity factors by the use of finite element analysis are presented. First, the finite element analysis using a submodeling technique with a very fine mesh near the singular point is described. Then, application of the Reciprocal Work Contour Integral Method (RWCIM) with the finite element analysis of a model with a relatively coarse mesh is discussed.

5.1 FEM ANALYSIS WITH A FINE MESH NEAR THE SINGULAR POINT

When two materials with different elastic properties are joined forming a bi-material wedge, stress singularity will be present at the apex of this bi-material wedge under mechanical or thermal loading if linear elasticity is assumed. Fig. 5.1(a) shows a general bi-material wedge and Fig. 5.1(b) shows the bi-material wedge in this study. The stress field near the singular point may be written as

$$\sigma_{ij}(r,\theta) = \sum_{k=1}^{N} \frac{K}{r^{1-\lambda_k}} . f_{ijk}(\theta) + \sigma_{ijo}(\theta) \qquad (5.1)$$

where r and θ are the polar coordinates and N is the number of r - dependent stress terms. It was shown by Bogy (1971) that λ_k are the solutions of a transcendental equation and are dependent on the elastic constants of the two materials and the angles θ_1 and θ_2. $f_{ijk}(\theta)$ is a function dependent on the angle θ. The regular term, $\sigma_{ijo}(\theta)$, and the constant K are dependent on the loading and global geometry.

For the case of N = 1, if the singular point A in Fig. 5.1(b) is approached, the stress components for small r - values will be

$$\sigma_{ij} = \frac{Q_{ij}}{r^{1-\lambda_1}} \text{ or } \sigma_{ij} = \frac{Q^*_{ij}}{(r/L)^{1-\lambda_1}} \quad , \quad (\lambda_1 > 0) \qquad (5.2)$$

where Q_{ij} and Q_{ij}^{*} is denoted as stress intensity factor in $ksc - cm^{1-\lambda_1}$ and in ksc, respectively. λ_1 is the dominant eigenvalue, and L is some characteristic length of the configuration.

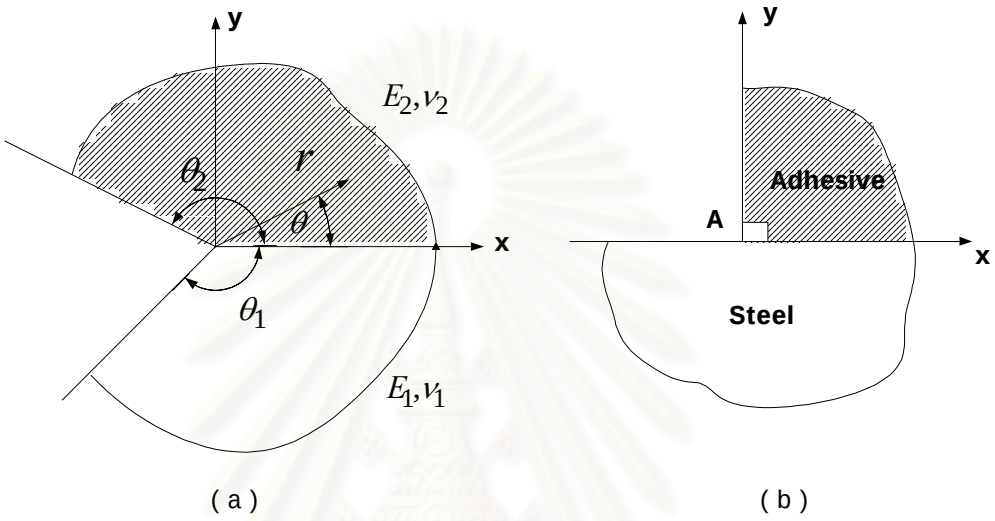

Figure 5.1 A bi-material wedge (a) general (b) This study

In this study, the finite element analysis with a fine mesh near the singular point utilized a submodeling technique. In this method, the specified boundary conditions for the submodel were obtained from displacements calculated on the cut boundary of the global model. The stress intensity factors were then calculated from the submodel. A submodel for calculating stress intensity factor is shown in Fig. 5.2 where L is half of adhesive layer thickness. The same submodel was used for both when double strap joints and the strengthened beams were the global model.

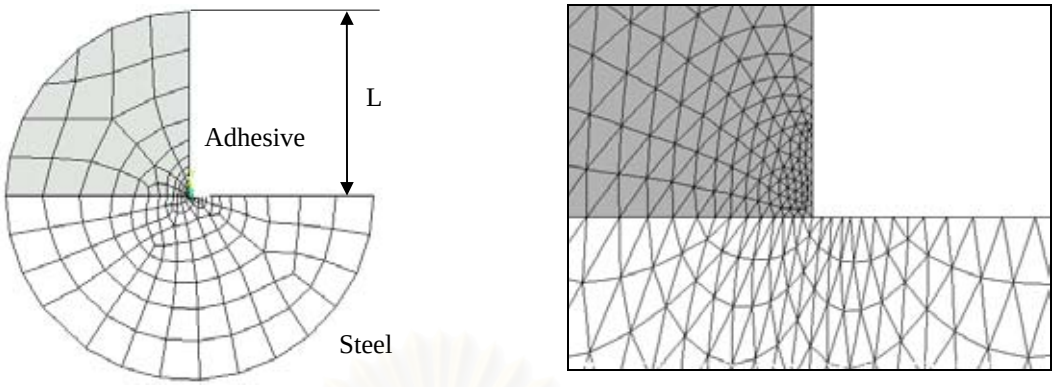

(a) (b)

Figure 5.2 A submodel (a) Typical mesh (b) Mesh near a singular point (smallest element size 1.3×10^{-6} cm)

In finite element analysis, the elements used were 8-node elements having two degrees of freedom at each node. Both plane stress and plane strain conditions were analyzed. CFRP material was assumed isotropic. Table 5.1 shows material properties used in the analysis.

Table 5.1 Material data

Steel: JIS SS400	Adhesive: SIKADUR-30	CFRP: SIKA H514
E = 200000 MPa	E = 2750 MPa	E = 300000 MPa
$\nu = 0.30$	$\nu = 0.35$	$\nu = 0.30$
Fy = 300 MPa	-	thickness = 1.4 mm.

For the case of bi-material wedge considered, λ_1 was found to be 0.624 and 0.729 for plane strain and plane stress condition, respectively. Therefore, the order of singularity was 0.326 and 0.271 for plane strain and plane stress condition, respectively. A quarter of the double strap joint was analyzed due to symmetry. Similarly, half of the strengthened beam was modeled because of symmetry. Fig. 5.3 and 5.4 shows the finite element model of the double strap joint and the strengthened beam, respectively.

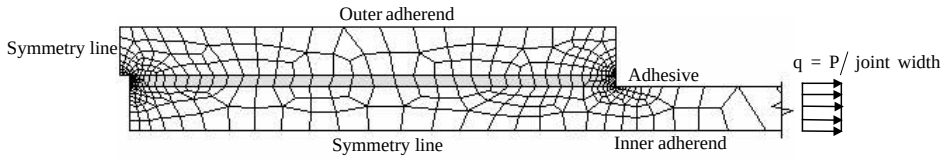

Figure 5.3 Global finite element model of a double strap joint

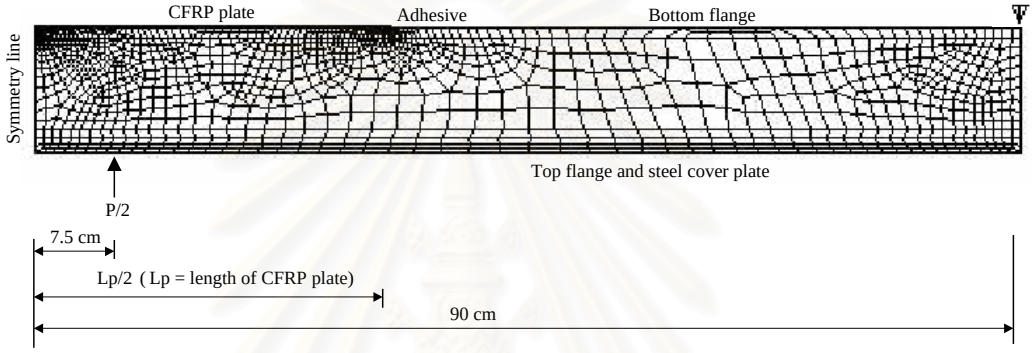

Figure 5.4 Global finite element model of a strengthened beam

The stress intensity factor and the order of singularity from each stress component were calculated from regression analysis since they were related to the interception and slope of a log-log relationship of stress values and radial distances from the singular point, respectively.

Different submodels with the smallest element size near a singular point of $5x10^{-6}$ cm, $1.3x10^{-6}$ cm, and $3.5x10^{-7}$ cm were investigated to evaluate the proper mesh fineness. It was found that further refinement from the second mesh having the smallest element near the singular point of $1.3x10^{-6}$ cm was unnecessary. Table 5.2 shows the order of the singularity calculated from each stress component along interface ($\theta = 0^{\circ}$) of each submodel under plane stress condition.

Table 5.2 Results from regression analysis of submodels with different mesh fineness

Mesh no.	α_{rr}	$\alpha_{r\theta}$	$\alpha_{\theta\theta}$
1	0.269	0.302	0.282
2	0.270	0.271	0.275
3	0.271	0.270	0.275

$\alpha_{exact} = 0.271$

5.2 FEM ANALYSIS WITH RELATIVELY COARSE MESH USING RWCIM

Evaluation of stress intensity factors using the Reciprocal Work Contour Integral Method (RWCIM), which is based on the reciprocal theorem, is described in this section. In this method, singular solutions are used near a singular point, whereas finite element solutions are used far away from a singular point. As the finite element solutions are only needed far away from the singular point, a coarse mesh is sufficient, thereby reducing computational costs and minimizing dependence on numerical accuracy of the stress intensity factors.

A finite element model of the double strap joint (DSJ), which was similar to the global model in the previous section, is shown in Fig. 5.5. The mesh near the joint end is shown in Fig. 5.6. Elements near a singular point had a side of length $t_a/8$, where t_a was adhesive layer thickness. Two rectangular outer contours, C1 and C3, selected for the evaluation of stress intensity factors using RWCIM are shown in Fig. 5.7.

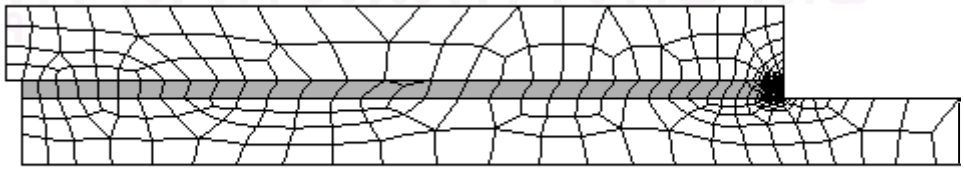

Figure 5.5 Finite element model of a joint to which RWCIM was applied (Quarter model)

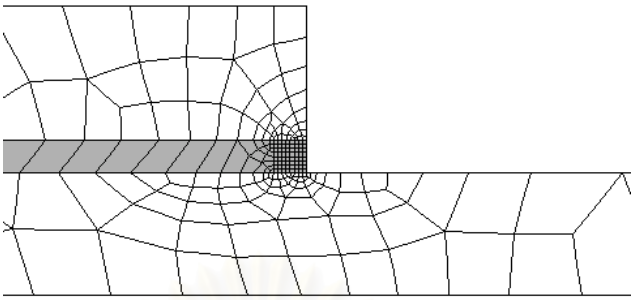

Figure 5.6 Mesh near the end of the joint

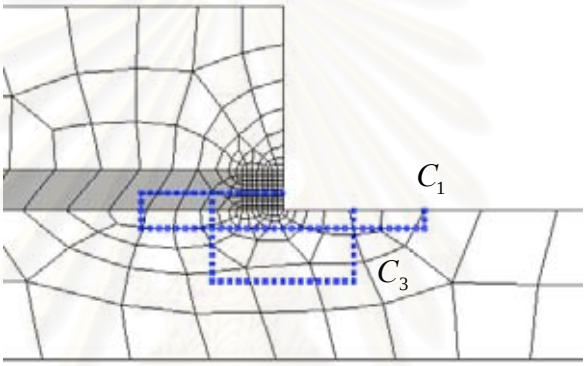

Figure 5.7 Outer contours for RWCIM (Double strap joint)

Similarly, a typical finite element model of the strengthened beam, which was similar to the global model in the previous section, is shown in Fig. 5.8. Half model was analyzed due to symmetry. Typical mesh near the plate end of all beams is shown in Fig. 5.9. Elements near a singular point had a side of length $t_a/8$. Three outer contours selected for the evaluation of stress intensity factors using RWCIM are C1, C3, and C5 as shown in Fig. 5.10.

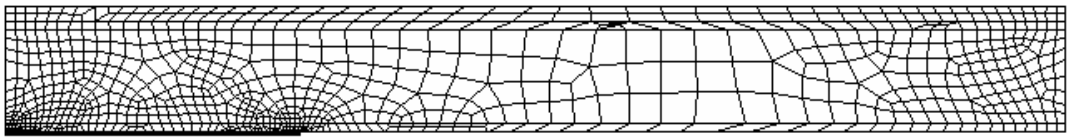

Figure 5.8 Typical finite element model of a 2-D strengthened beam to which RWCIM was applied (Half model)

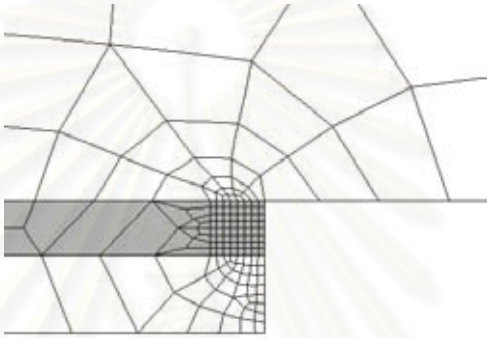

Figure 5.9 Typical mesh near the plate cut-off point

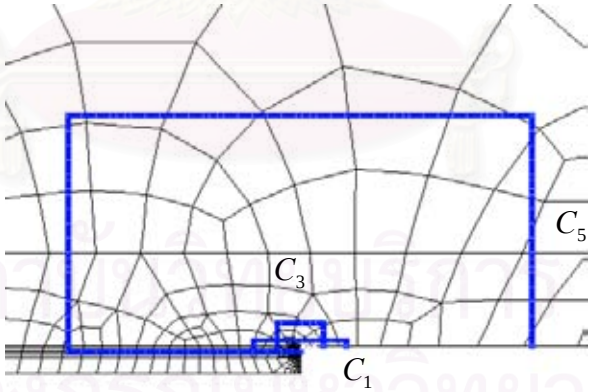

Figure 5.10 Outer contours for RWCIM (Strengthened beam)

In the calculation of stress intensity factors by RWCIM, integration of inner and outer contours were conducted by the trapezoidal integration scheme. Along the outer contour, stresses and displacements from the finite element analysis were used for system I (real system). Along the inner coutour, the eigenvector, which contains singular solutions, with an unknown coefficient c_1 corresponding to eigenvalue λ_1

were used. For system II (complementary system), stresses and displacements along the inner and the outer contours were taken as the eigenvector corresponding to eigenvalue $-\lambda_1$.

The evaluation of the integrals was carried out from the element solutions. Contour data were interpolated from the corresponding elements. The displacement components had quadratic expansions so the stresses varied linearly within elements. If the contour point was at finite element node, an average value from adjacent elements was used. Rigid body displacements were discarded in the evaluation of the contour integral. To verify the accuracy, the stresses found by this method were compared with the stress values obtained using finite element analysis with a very fine mesh near the corner of a steel-adhesive bi-material, a singular point where fracture failure was found during the static experiments.

Sufficient number of points in both inner and outer contours is necessary for the accuracy of the stress intensity factor solutions obtained using RWCIM. Therefore, a convergence study was conducted to find a proper spacing between adjacent points in the contours. Test cases were a double strap joint specimen and a strengthened beam with CFRP length of 120 cm. The stress intensity factors were calculated from different contours with different number of points (or, equivalently, different spacings between adjacent points) under plane stress condition. Effect of number of points in outer contour C1 and C3 on the stress intensity factors of the double strap joint subjected to an average failure load is shown in Fig. 5.11 and 5.12, respectively. In these figures, a circular-shaped inner contour with radius $1x10^{-4}$cm and with 100 equal-spaced points was chosen. Stress intensity factors evaluated from finite element analysis with a very fine mesh are also shown in these figures as dashed lines.

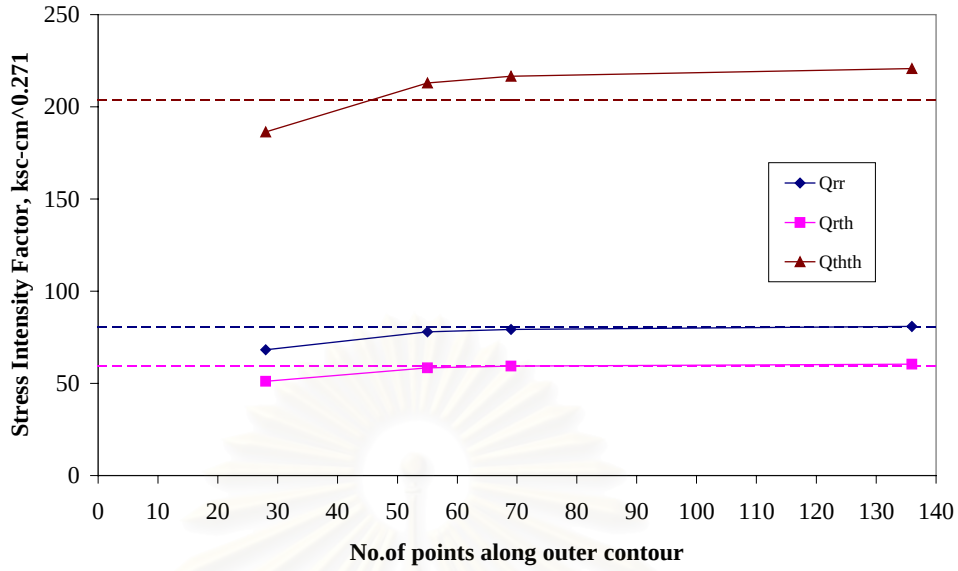

Figure 5.11 Stress intensity factors v.s. number of points along contour C1 (DSJ)

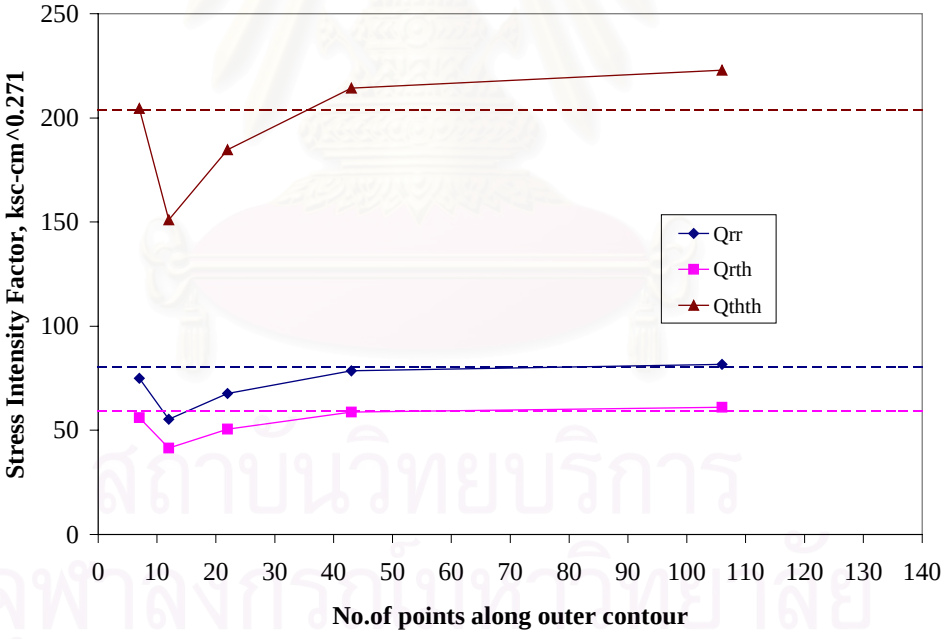

Figure 5.12 Stress intensity factors v.s. number of points along contour C3 (DSJ)

Fig. 5.13, 5.14, and 5.15 show the effect of number of points in the outer contour C1, C3, C5 on the calculated stress intensity factors under plane stress condition in a strengthened beam. The strengthened beam (Half model) was subjected to $P/2 = 7{,}290$ kg.

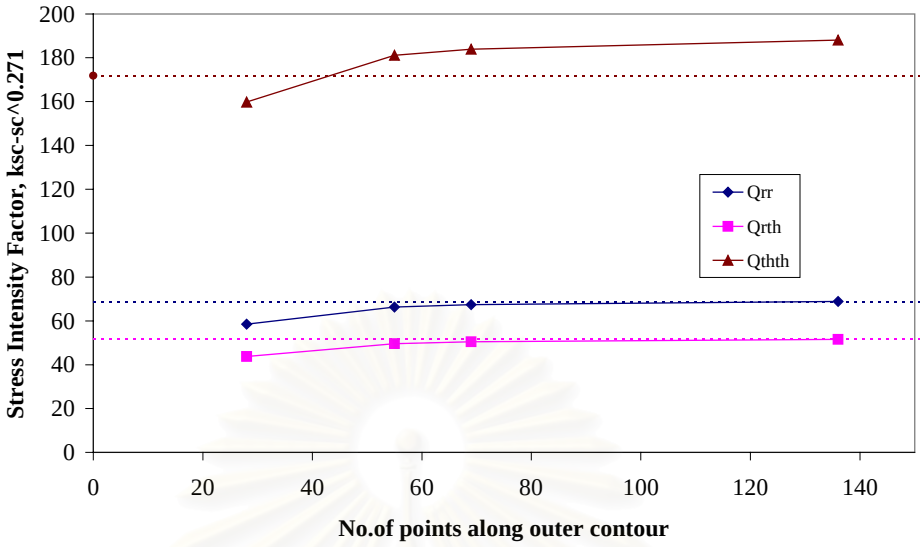

Figure 5.13 Stress intensity factors v.s. number of points along contour C1 (Strengthened beam)

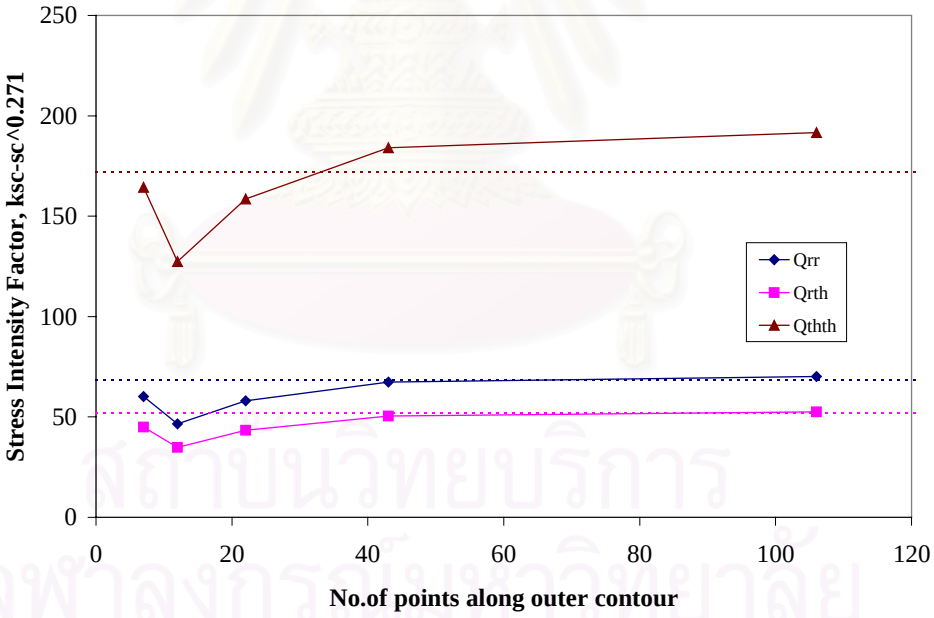

Figure 5.14 Stress intensity factors v.s. number of points along contour C3 (Strengthened beam)

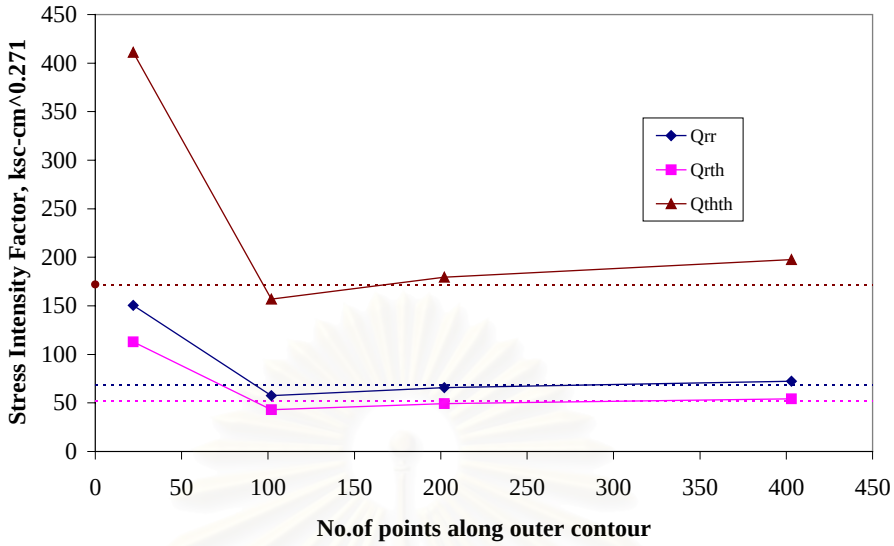

Figure 5.15 Stress intensity factors v.s. number of points along contour C5 (Strengthened beam)

From Fig. 5.11 to 5.15, the spacing of 0.025 cm between the consecutive points in all outer contours (55 points in C1, 43 points in C3, and 403 points in C5) yielded reasonable values compared with the stress intensity factors from the submodeling technique in cases of double strap joint and strengthened beam models investigated. This spacing, therefore, was selected for the evaluation of stress intensity factors in RWCIM. Table 5.3 summarizes the stress intensity factors along the interface ($\theta = 0^{\circ}$) evaluated from contour C3 at an average failure load of all double strap joint specimens under plane stress, plane strain, and pseudo plane strain conditions. In pseudo plane strain analysis, the finite element solutions for the outer contour in RWCIM were approximated using solutions from plane stress analysis. It was found that the stress intensity factor values calculated under pseudo plane strain approximated well those from actual plane strain analysis. Consequently, stress intensity factors in case of the strengthened beams under plane strain condition were approximated by the pseudo plane strain analysis.

Table 5.3 Stress intensity factor values from various analysis types

Case	Analysis type	$PLANESTRESS, ksc-cm^{0.271}$			$PLANESTRAIN, ksc-cm^{0.326}$		
		Q_{rr}	$Q_{r\theta}$	$Q_{\theta\theta}$	Q_{rr}	$Q_{r\theta}$	$Q_{\theta\theta}$
1	RWCIM-plane stress	78.5	58.7	214.3	-	-	-
2	RWCIM-plane strain	-	-	-	84.6	54.3	153.1
3	RWCIM-psuedo plane strain	-	-	-	86.1	55.2	155.7
4	Submodel-plane stress	80.5	59.6	203.7	-	-	-
5	Submodel-plane strain	-	-	-	88.2	54.8	152.8

5.3 SINGULARITY-DOMINATED ZONE

Fracture criteria based on the stress intensity factors are applicable when the singularity-dominated zone is larger than the plastic zone, in which the fracture process zone, including subcritical crack growth, is assumed to be embedded. This is similar to the similitude concept for crack problems. Similitude implies that crack tip conditions are uniquely defined by a single loading parameter such as a stress intensity factor. In the case of a stationary crack, two configurations will fail at the same critical stress intensity factor, provided an elastic singularity zone exists at the crack tip.

For the fracture criterion in section 4.4 to be useful, the asymptotic or singular stress state characterized by a stress intensity factor should dominate a region about a singular point, e.g. an adhesive-steel interface corner, that is significantly larger than the plastic zone. Also, thickness of an adhesive layer must not so thin that the fracture process zone becomes large compared with the region dominated by the stress singularity.

The singularity-dominated zone can be found by comparing results from the complex potential method and those from the linear elastic finite element analysis with a very fine mesh near the singular point. In the double strap joint specimen subjected to an average failure load, distributions of stress components in polar coordinate along the interface ($\theta = 0^{\circ}$) under plane strain condition are shown in Fig. 5.16. Good correlation of the von Mises stresses can be observed in the range

$r/L \le 0.3$, where L is half of adhesive layer thickness; suggesting the size of region along the interface dominated by stress singularity. Singularity-dominated zones from any other stress component are smaller than that from the von Mises stress.

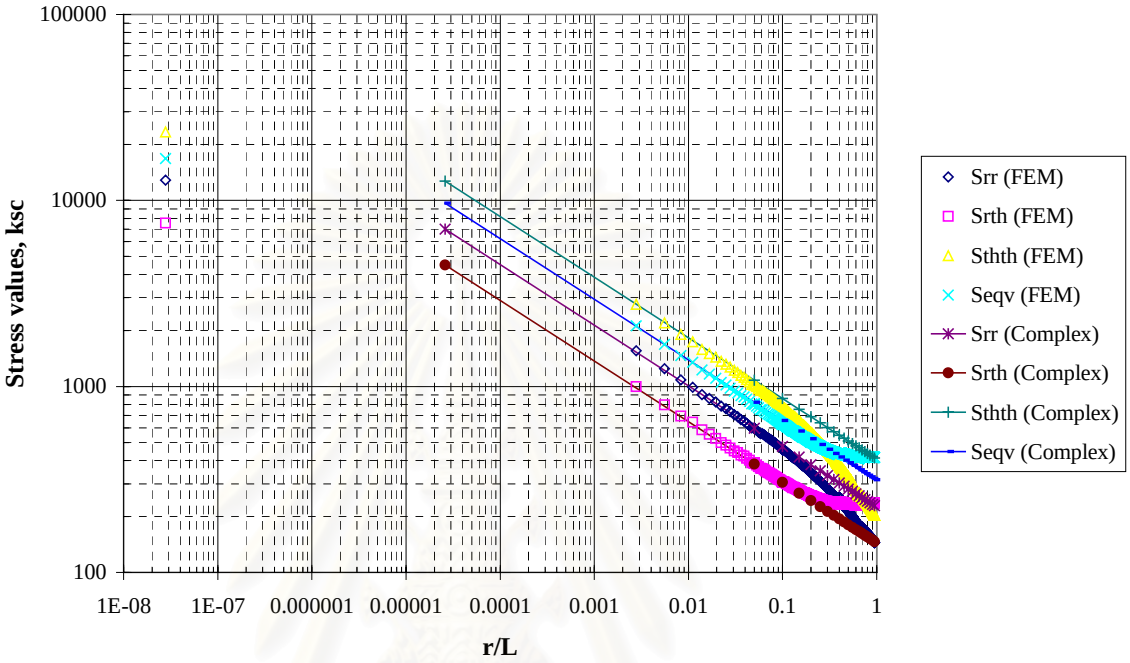

Figure 5.16 Comparison of stress distributions along interface ($\theta = 0^{\circ}$) from the complex potential method and the finite element analysis

CHAPTER 6

DESCRIPTION OF EXPERIMENTS

Static and fatigue experiments were conducted to investigate the behaviors of steel beams strengthened with partial-length, adhesive-bonded CFRP plates according to the research objectives.

6.1 STATIC TEST ON STEEL BEAMS WITH PARTIAL-LENGTH BONDED CFRP PLATES

Materials

The unidirectional CFRP laminates were Sika® Carbodur H514 made from a pultrusion process. The thickness of a laminate is 1.4 mm. A linear stress-strain relationship showed an ultimate failure strain of about 0.45%. A two-part epoxy adhesive, Sikadur® 30, with pot life of 40 minutes (at 35^{o}C) was selected. The grade of steel beams was SS400 according to TIS 1227 or JIS G3101. Properties of the materials in the study are summarized in Appendix A.

Specimen fabrication

In static test, a steel plate was manually welded to the top flange of the steel beam using the gas shielded flux core arc welding procedure. Carbon dioxide was used as the shielding gas and E71T-1 wires were used as electrodes. The bottom flange of the steel beam was sandblasted according to the Steel Structures Painting Council (1991) specification no.5. This specification was chosen since it is widely used in preparing steel surface before painting. After cleaning steel surface by isopropyl alcohol, two strips of CFRP plates (each 5 cm width) were bonded to the bottom flange of the beam. Thickness of adhesive layer was controlled to be 1 mm by placing small inserts between the steel beam and CFRP plates. Curing time of the adhesive was about 2 weeks.

Test setup

A four-point loading scheme was selected in the static test, as shown in Fig. 6.1. Three series of steel beams with different CFRP lengths were investigated. The span length was 1.80 m, while the CFRP lengths were 0.50 m, 0.65 m, and 1.20 m. Specimen details are summarized in Table 6.1. The number indicated in specimen designation is the length of CFRP plates in centimeter. For specimen B65Y-1 and B120Y-1, yielding had occurred in the bottom flange at midspan before attaching CFRP plates, which simulated severe service distress in the steel beams. The maximum preload of B65Y-1 and B120Y-1 was 129% and 172% of the calculated yield load in a bare beam section, respectively. The yield load calculated from the transformed section analysis was 8,480 kg. For each specimen, a welded steel cover plate at the top flange was designed to prevent the yielding of the compression flange at midspan, which was not the failure mode of interest.

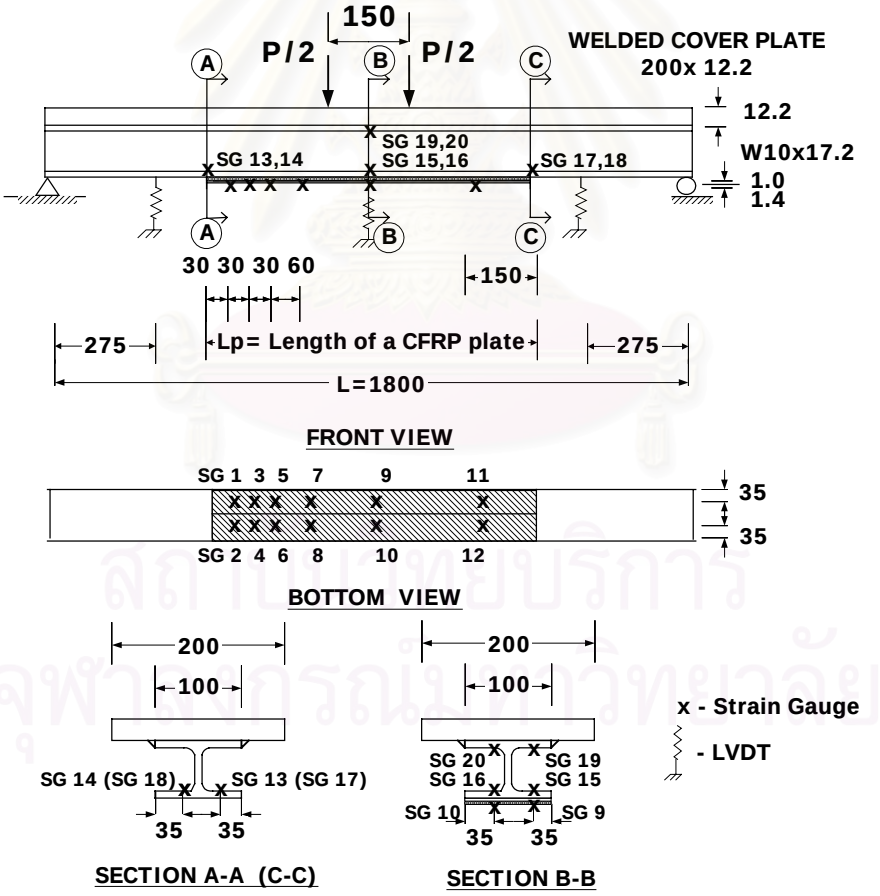

Figure 6.1 Test setup for static test on strengthened beams (All dimensions in mm)

Table 6.1 Specimen designation in static test

SPECIMEN	CFRP length, cm	Yielding before (Y/N)
B50-1	50	N
B50-2	50	N
B65-1	65	N
B65-2	65	N
B65Y-1	65	Y
B120-1	120	N
B120Y-1	120	Y

The top steel plate was designed based on the elastic-perfectly plastic section analysis. Three assumptions were 1) Strain compatibility, plane section remains plane with perfect bonding, 2) Stress-strain relationship of the steel beam is elastic-perfectly plastic with no hardening, and 3) No yielding in the compression part of the section. Fig. 6.2 illustrates parameters in the section analysis. First, an initial width and thickness of the steel plate were input in the program. From strain compatibility, both C_t and ϕ were then calculated from ε_1 and ε_3, which is the strain at top layer of the steel plate and at bottom layer of the FRP plate, respectively. At the ultimate condition, ε_1 was set to the yield strain of steel and ε_3 was set to the fiber breaking strain of CFRP. Next, equilibrium of forces was checked. If the section was in equilibrium, the third assumption that the compression part of the section is elastic was correct and the initial plate size was applicable. Otherwise, the plate size (plate width or thickness) was modified and the procedure was repeated until the equilibrium was found.

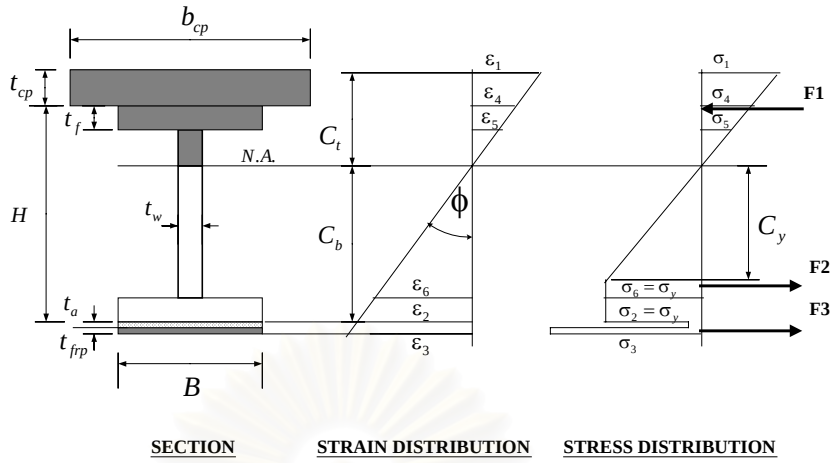

Figure 6.2 Elastic-plastic section analysis of the strengthened section

Twenty strain gages and three linear variable displacement transducers (LVDTs) were instrumented at each specimen to to measure development of tensile stress in the CFRP plate, to measure strain distribution at the mid-span section, and to investigate the onset of plate separation. Two types of strain gages with the coefficient of thermal expansion matching with steel and FRP materials were used in order to reduce the temperature-induced apparent strain. All strain gages have gage length of 5 mm and width of 1.4 mm. All data were monitored and recorded by Yokogawa® data acquisition unit. Although spew fillets are the usual conditions encountered at the plate ends, the terminus of adhesive in the test was made sharp perpendicular to the bottom flange in all specimens according to the finite element model.

6.2 FATIGUE TEST OF STEEL BEAMS WITH A BONDED PLATE END DETAIL

In fatigue test, the fabrication procedure was similar to that in the previous static test. However, no top welded steel plate was needed since the maximum loads in fatigue test were significantly less than the yield load of a beam. The width of CFRP laminates was 5 cm (1 strip).

Eight specimens were tested under constant amplitude at a stress ratio, R, of 0.2 and frequency of 2 Hz. A sine-waveform loading was generated by a servo-hydraulic actuator. There were two phases in the fatigue test as shown in Fig. 6.3.

Different levels of load ranges were applied to specimens according to the designed stress intensity factor ranges at the plate ends of the specimens. Maximum loads in the fatigue test were limited by two criteria: 1) The stress intensity factors at the plate end at maximum loads must not exceed the critical value leading to a premature plate separation mode and 2) Yielding of the steel beam at midspan must not occur. In the first phase, only data corresponding to the plate end having shorter debond initiation life was recorded. In the second phase, two data from two plate ends near midspan were recorded from each specimen. The test was stopped when no debond was detected at the plate end after 1,5000,000 cycles. In addition to a visual inspection, a technique for helping the detection of debond cracks was developed during the fatigue test. A sensor with a silver line tracing across the adhesive terminus, as shown in Fig. 6.4, was constructed at the plate end. The initiation of debond crack cuts a silver trace, causing measured voltage to be zero. Since steel and CFRP materials are both electrically conductive, it was necessary to prevent current flow between the sensors. This was achieved by placing or spraying an insulating material before tracing a silver line.

During the test, most sensors showed a zero voltage before any signs of debond could be detected by the visual inspection. At some plate ends, a sensor did not show a sign of zero voltage. Possible causes are that the debond crack did not break the silver line or that improper insulation might be present, which causes the current flows between the sensors. So, a data of each plate end was obtained by averaging the cycles at zero voltage and cycles first detected by the visual inspection. If the number of cycles detected by the sensor and by the visual inspection were much different, a data was obtained by averaging the cycles before and after the debond was observed by the visual inspection.

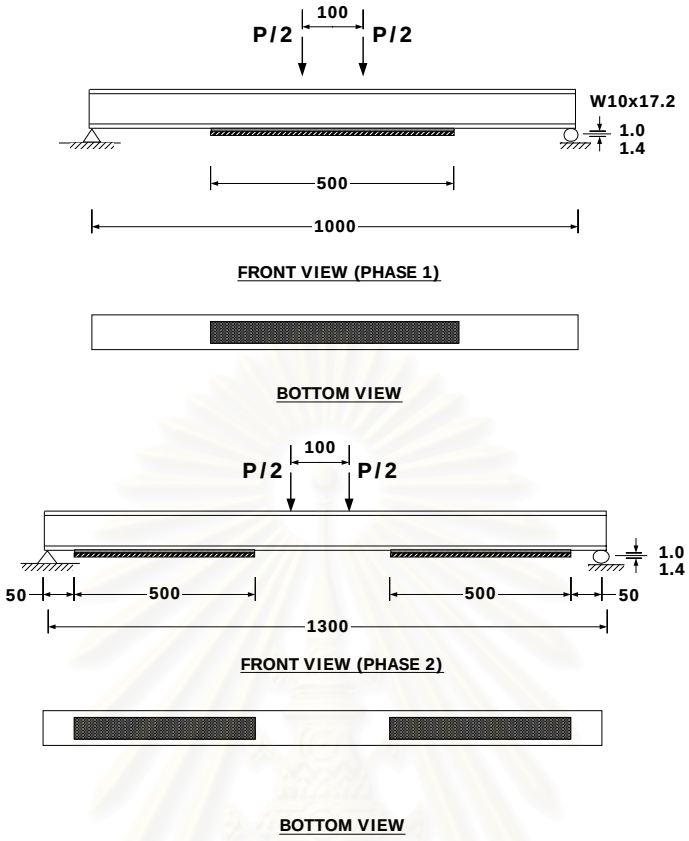

Figure 6.3 Fatigue test setup for steel beams with an adhesive-bonded CFRP plate detail (All dimensions in mm)

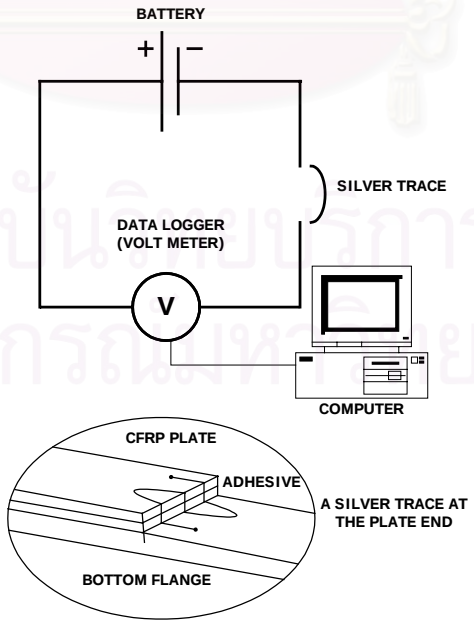

Figure 6.4 Technique for helping the detection of debond initiation at the plate end in fatigue test

CHAPTER 7

RESULTS AND EVALUATION OF EXPERIMENTAL DATA

7.1 RESULTS FROM THE STATIC TEST ON STEEL BEAMS WITH DIFFERENT CFRP LENGTHS

Two failure modes were found during the test, which were the rupture of the bonded CFRP plate at midspan and the premature separation of the bonded plate. The premature plate separation occurred in steel beams with short plate lengths, i.e. plate lengths of 0.50 m and 0.65 m. Fig. 7.1 shows the characteristic of this failure mode. For steel beams with a long plate length, rupture of the CFRP plate at midspan was observed. A typical characteristic of this failure mode is shown in Fig. 7.2.

The measured failure loads of the strengthened steel beams are summarized in Table 7.1. The predictions by the fracture criterion using $Q_{\theta\theta,cr}$ along the interface obtained from the proposed double strap joint specimens under both plane stress and plane strain conditions are also shown in the table. Methods for evaluating the stress intensity factors are described in Chapter 5.

For the premature separation mode, failure loads were detected from LVDT number 1 attached to the bonded plate at midspan, where deflection increased dramatically. These values were very close to those observed during the test. It was found that, however, the initiation of debond/separation of FRP plates from steel beams had occurred before the final fracture which led to failure or complete separation. The debond initiation loads were detected by considering the increase in the strain value from the strain gages number 13 and 14 which were attached to steel flange at the plate cut-off points in the case when left-end debond occurred or strain gages number 17 and 18 in the case when right-end debond occurred. Deviation of the strain from linear elastic trend indicated that debond had initiated. Also, the stresses transferred to FRP plates decreased as the debond cracks propagated. This debond initiation occurred at the loads lower than the failure loads at which the debond cracks propagated to the critical size. Finally, rapid crack propagation occurred due to fracture accompanying with a loud noise. A typical deviation from linear elastic trend of each specimen is depicted in Fig. 7.3. Adhesive (interface) failure at the steel-

adhesive interface was observed. Considering a dominant eigenvalue, this singular point is more severe than the CFRP-adhesive interface. The dominant eigenvalue, λ_1, at the steel-adhesive singular point is 0.729 and 0.674 under plane stress and plane strain, respectively, while that at the CFRP-adhesive singular point is 0.748 and 0.690, respectively.

A debond load of each specimen shown in Table 7.1 is a load when strain starts having the percent difference from the linear elastic trendline exceeding the maximum percent difference of data scattering used in constructing the linear line.

Figure 7.1 Premature separation of bonded CFRP plates from the steel beam

Figure 7.2 FRP plate rupture failure mode at midspan

Table 7.1 Results from the static test v.s. the predictions from a fracture criterion

SPECIMEN	FAILURE MODE	1) DEBOND LOAD, kg	2) FAILURE LOAD, kg	3) PREDICTIONS		RATIO (2)/(3)	
				1) Plane stress	2) Plane strain	1) Plane stress	2) Plane strain
B50-1	Plate separation	6,645	9,195	8,060	8,077	1.14	1.14
B50-2	Plate separation	7,675	9,550	8,060	8,077	1.18	1.18
B65-1	Plate separation	8,420	10,790	9,271	9,278	1.16	1.16
B65-2	Plate separation	8,055	10,040	9,271	9,278	1.08	1.08
B65Y-1	Plate separation	8,420	10,885	9,271	9,278	1.17	1.17
B120-1	FRP rupture	-	14,580	16,976	17,042	0.86	0.86
B120Y-1	FRP rupture	-	15,815	16,976	17,042	0.93	0.93
	Avg. of B50	7,160		-12.56	-12.81	% Different	
	Avg. of B65	8,298		-11.81	-11.81		

Table 7.2 Results from the static test v.s. the predictions from a shear lag analysis

SPECIMEN	FAILURE MODE	1) DEBOND LOAD, kg	2) FAILURE LOAD, kg	3) PREDICTIONS	RATIO (2)/(3)
B50-1	Plate separation	6,645	9,195	8,944	1.03
B50-2	Plate separation	7,675	9,550	8,944	1.07
B65-1	Plate separation	8,420	10,790	10,127	1.07
B65-2	Plate separation	8,055	10,040	10,127	0.99
B65Y-1	Plate separation	8,420	10,885	10,127	1.07
B120-1	FRP rupture	-	14,580	18,822	0.77
B120Y-1	FRP rupture	-	15,815	18,822	0.84
	Avg. of B50	7,160		-24.92	% Different
	Avg. of B65	8,298		-22.04	

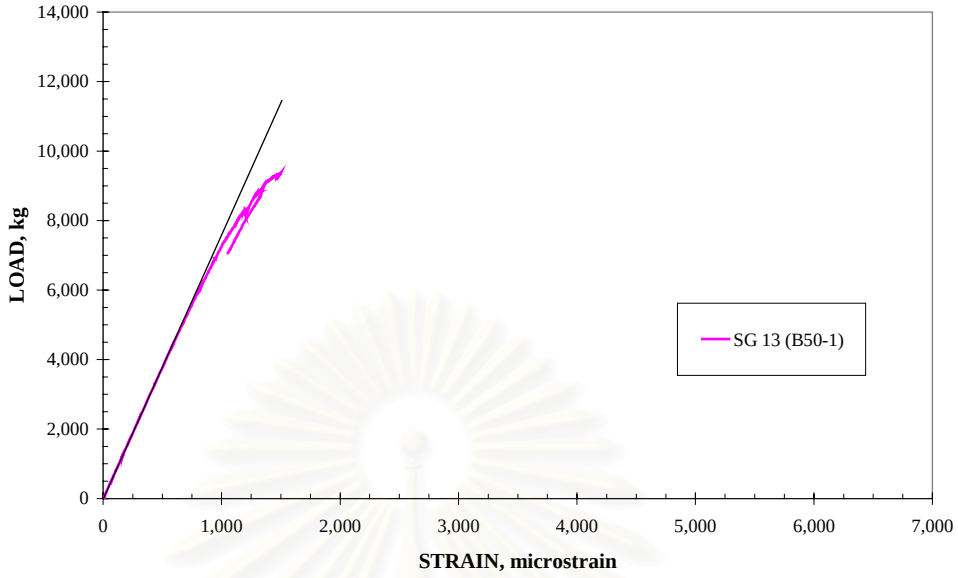

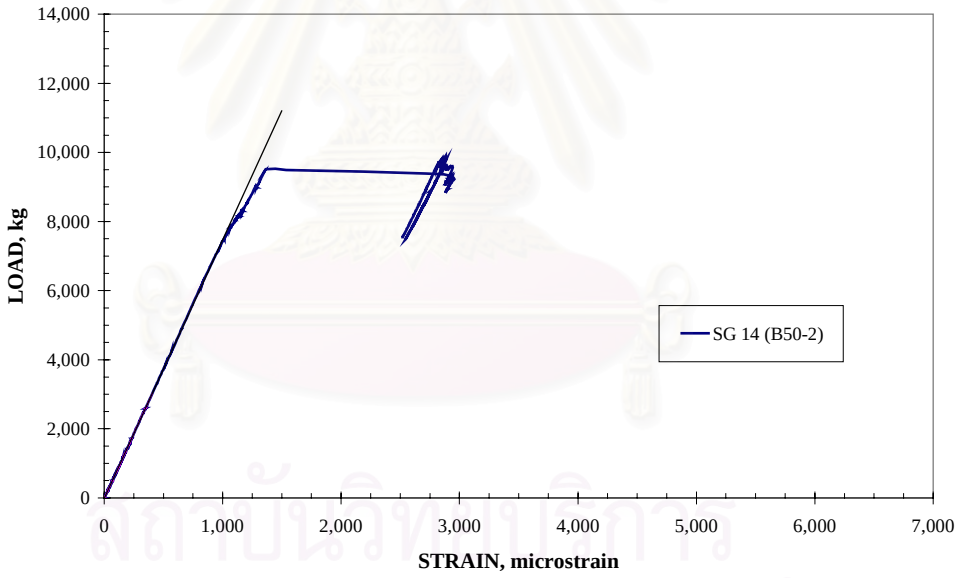

Figure 7.3 Typical deviation of the measured strain in the bottom flange at the plate ends

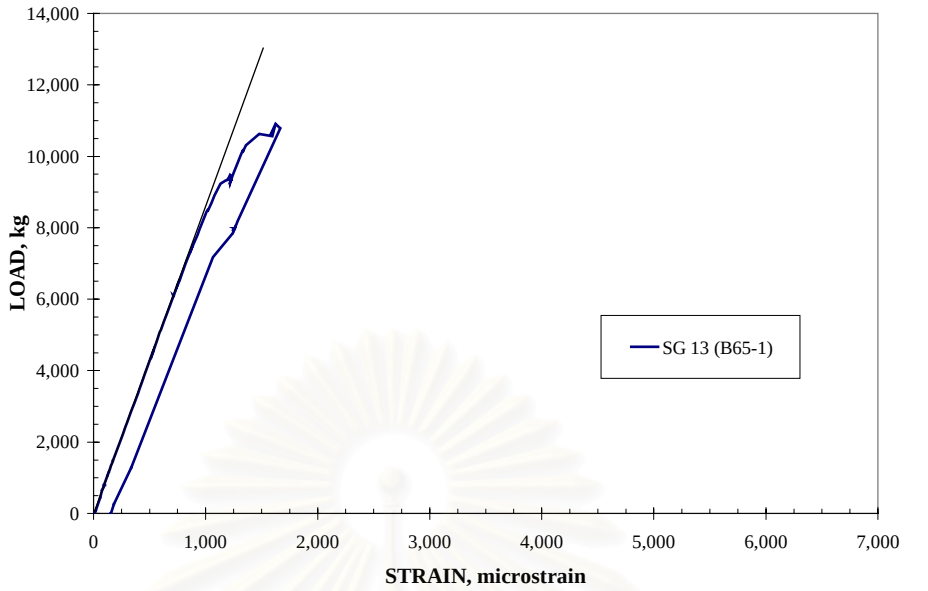

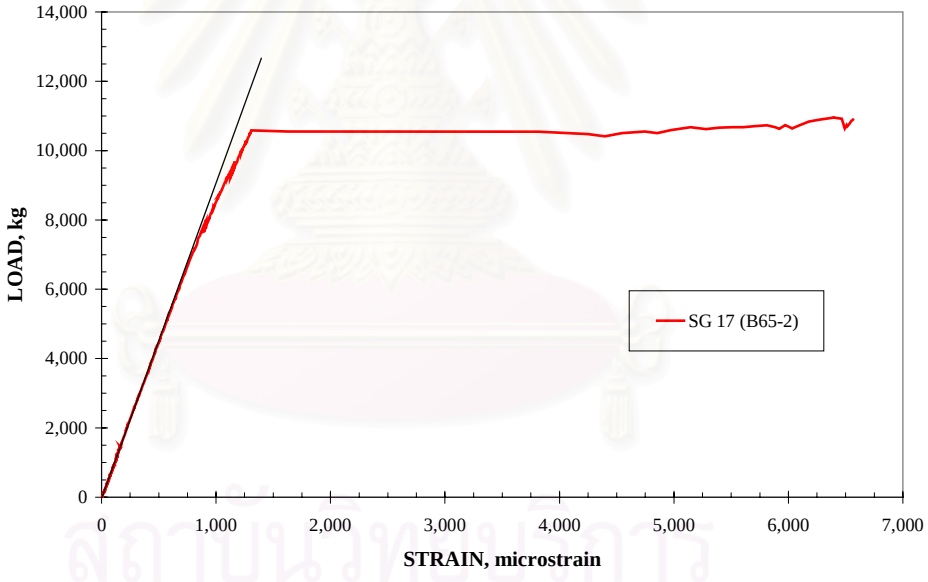

Figure 7.3 Typical deviation of the measured strain in the bottom flange at the plate ends (Continued)

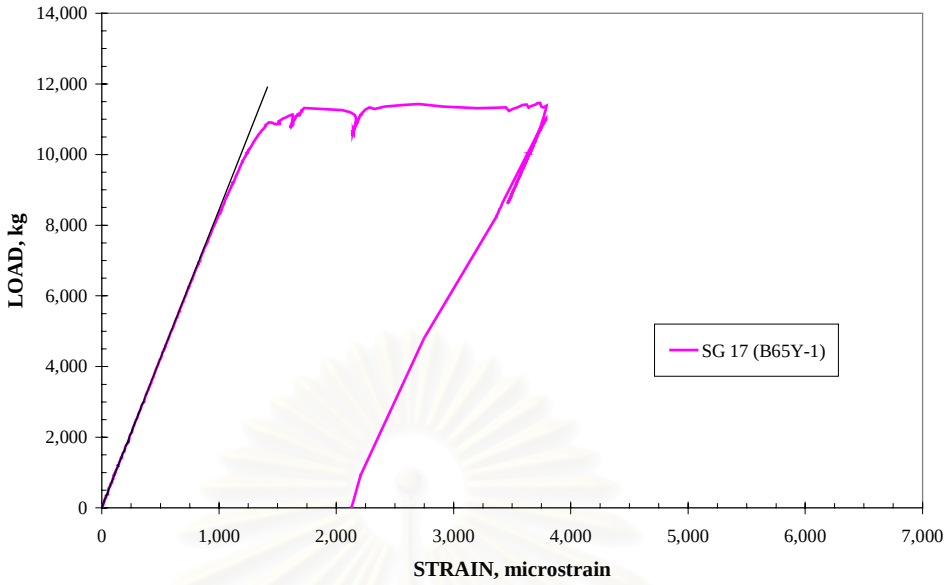

Figure 7.3 Typical deviation of the measured strain in the bottom flange at the plate ends (Continued)

Reasonable agreement is found between the predicted loads and the actual debond loads, i.e. those leading to debond initiation during the test. Difference between the debond initiation load and the prediction under plane strain condition is 12.81% and 11.81% for series B50 and B65, respectively. Moreover, from Table 7.1, the ratio of the failure load to the prediction is about 1.15. This indicates that the predictions underestimate the failure loads at which visible separation of CFRP plates from steel beams occurred.

If the shear stress at the plate end, which is maximum, obtained from the shear lag analysis is used as the failure criterion instead of the stress intensity factor, the predictions are shown in Table 7.2. The critical value of shear stress is the maximum shear stress at the end of the double strap joint calculated from the shear lag analysis at an average failure load. From table 7.2, the predicted failure loads were reasonably close to the failure loads observed during the test. However, the shear lag analysis can not capture the stress singularity and various conditions at the plate end such as a spew fillet condition. So, the failure criterion based on the shear stress obtained from the shear lag analysis may be used as a preliminary prediction of the premature plate separation. By comparing with debond initiation loads, the prediction may be used as an upper bound.

For B120-1 and B120Y-1, where the failure mode was FRP rupture at midspan, there is no deviation observed from strain gages number 13,14 and strain gages number 17,18. For strain gages number 13 and 14, as representatives, the relationship between the load and the measured strain is shown in Fig. 7.4.

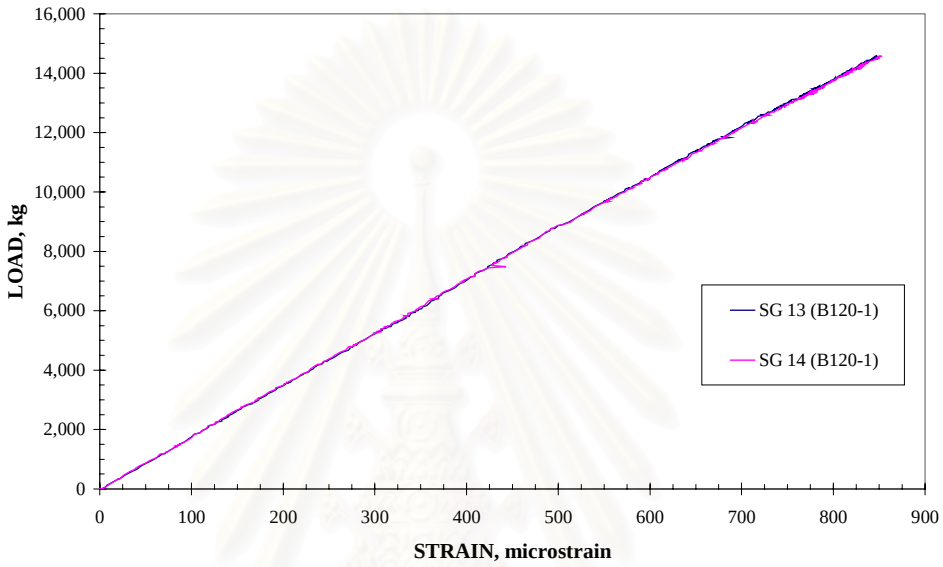

Figure 7.4 Load- strain relationship in the bottom flange of the steel beam at the plate end (B120-1)

a) Effects of CFRP length on failure modes and failure loads

Failure modes found in this investigation were: 1) FRP rupture mode, where the failure was due to rupture of the CFRP plate at midspan and 2) Premature plate separation mode, where separation of the bonded plates from steel beams occurred at relatively low loads. The first mode occurred in series B120, whereas the second mode occurred in all specimens in series B50 and B65. The premature plate separation was caused by fracture at the plate end and might be called “local” failure mode, which was unfavorable. As the plate length increased, failure load increased until the failure mode changed to FRP rupture at midspan.

In the case of crack problems, triaxial stresses significantly influence the strength of material. When the condition of plane strain is reached, the value of a stress intensity factor at fracture is minimum. Since the triaxial stresses in double

strap joints and strengthened beams are not the same, the critical stress intensity factor may be not equivalent. A fracture criterion using the critical stress intensity factors obtained from double strap joint specimens was found to be a conservative approximation of the failure loads as shown in Table 7.1. Also, the predictions were higher than the debond initiation loads. One reason might be that the critical stress intensity factors obtained from testing double strap joint specimens were evaluated at the ultimate or "failure" of the joints.

From the static test, a fracture criterion seems to be applicable for predicting the premature separation of the partial-length, bonded CFRP plates from the steel beams.

b) Development of tensile stresses in FRP plates

Development of tensile stresses in bonded CFRP plates were studied. Distributions of tensile strains in the CFRP plates measured from strain gages number 1 to 10 of all specimens are shown in Fig. 7.5 to 7.11. These figures show the tensile strains in the CFRP plate at various load levels. Also shown in the figure are the results from the shear lag analysis (see Chapter 3). It can be seen that the results from the shear lag analysis agree well with the measured data of all specimens. Consequently, it is reasonable to predict the distance that the bonded plate requires in order to develop its tensile stress to conform to conventional beam formula ($\sigma = Mc / I_{tr}$), or flexural conformance, by this one-dimensional analytical model.

Effect of yielding present in the bottom flange at midspan before attaching the CFRP plates on the development of tensile stresses was found to be minimal (e.g. specimens B65Y-1 and B120Y-1).

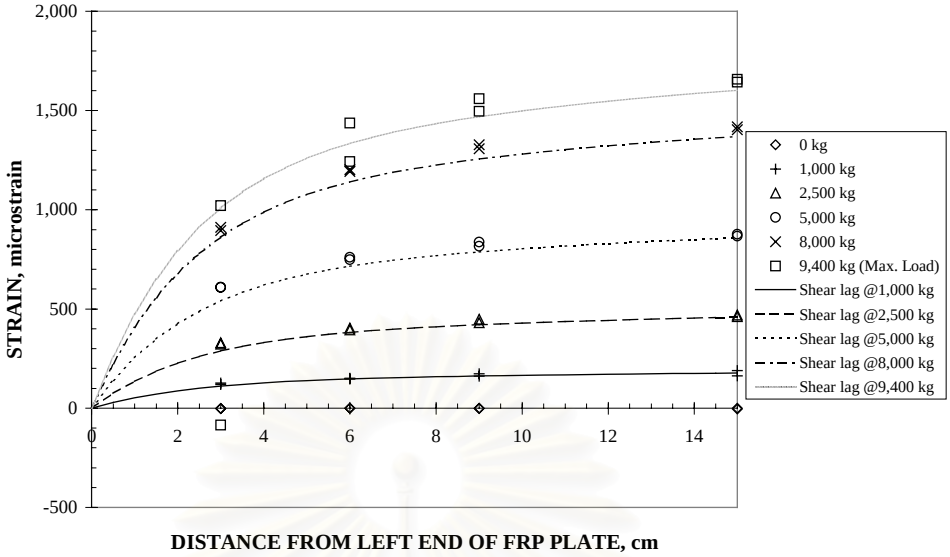

Figure 7.5. Development of tensile strains in the CFRP plate of B50-1

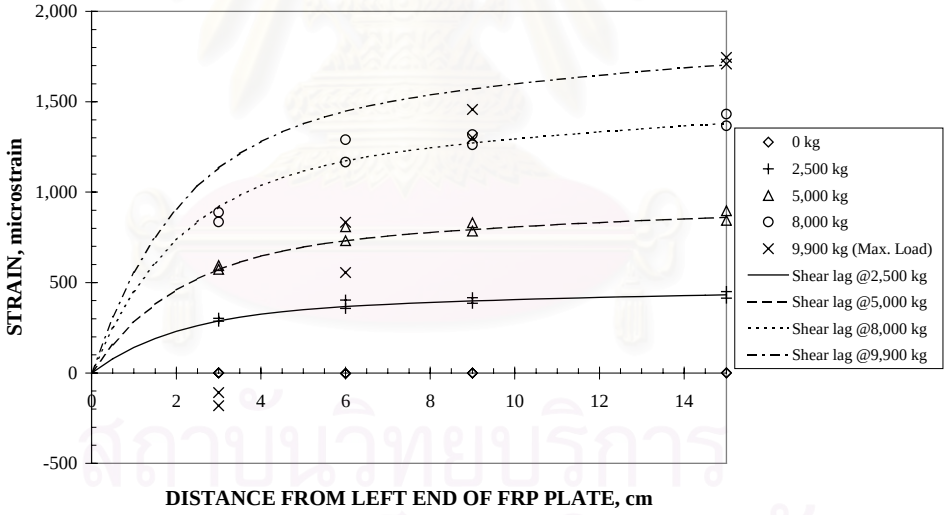

Figure 7.6 Development of tensile strains in the CFRP plate of B50-2

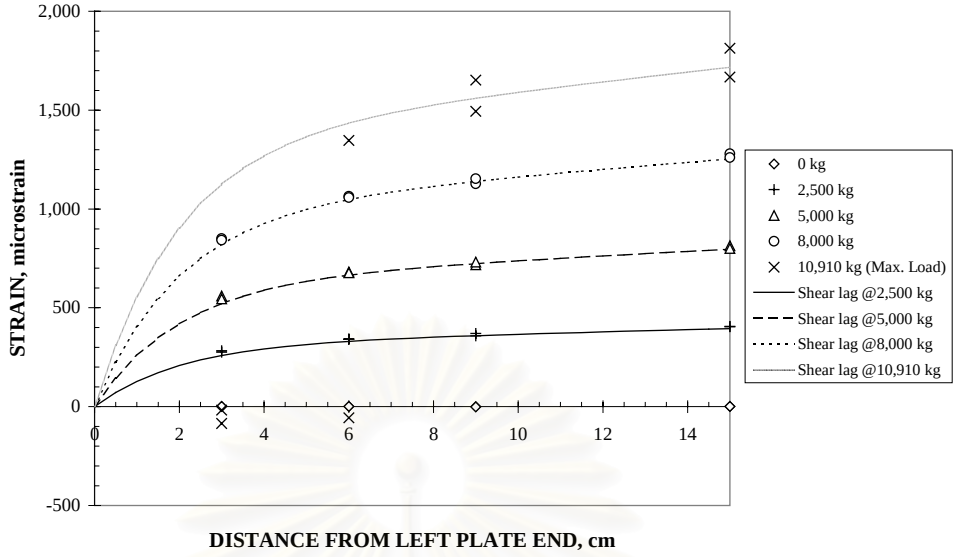

Figure 7.7 Development of tensile strains in the CFRP plate of B65-1

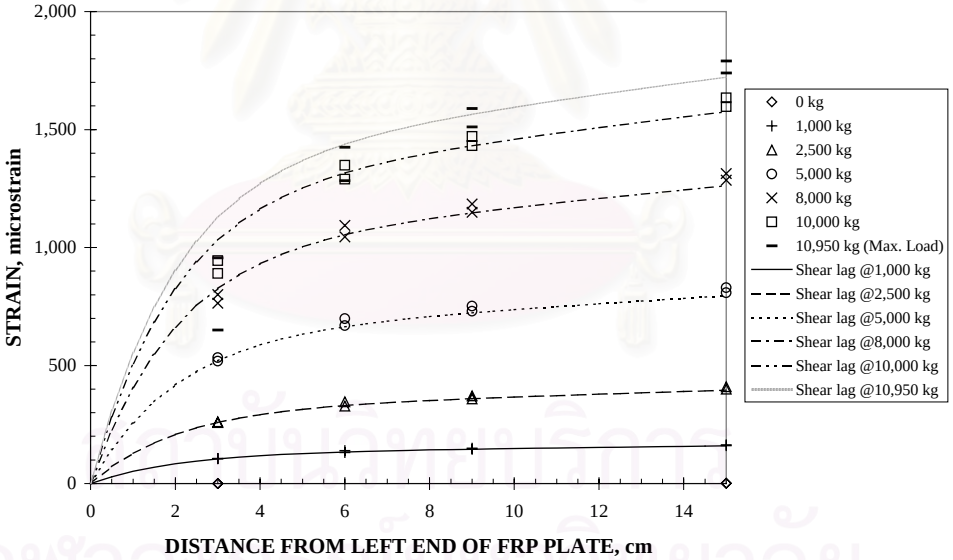

Figure 7.8 Development of tensile strains in the CFRP plate of B65-2

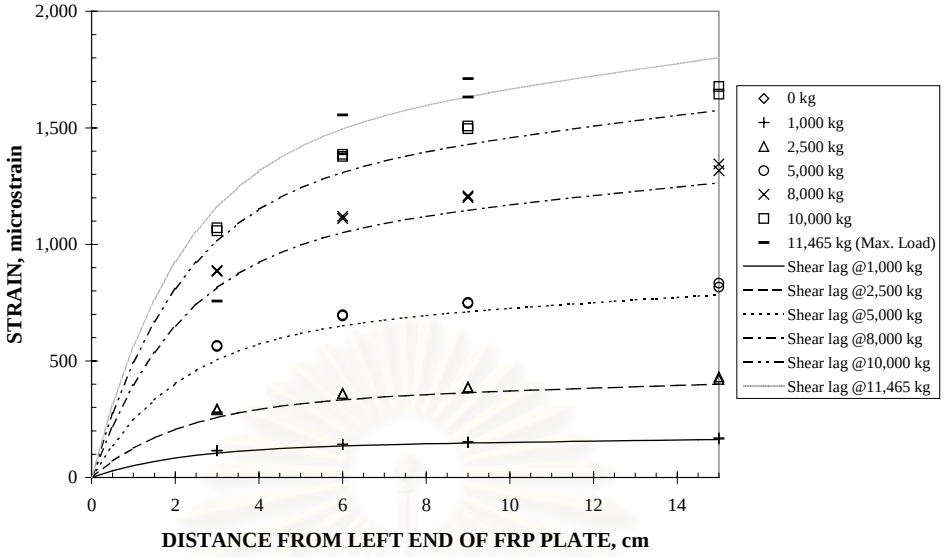

Figure 7.9 Development of tensile strains in the CFRP plate of B65Y-1

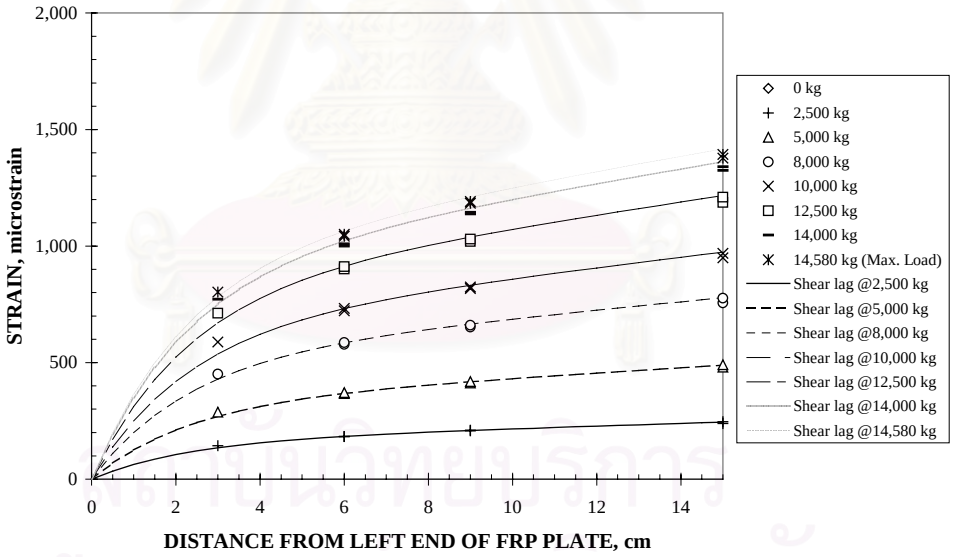

Figure 7.10 Development of tensile strains in the CFRP plate of B120-1

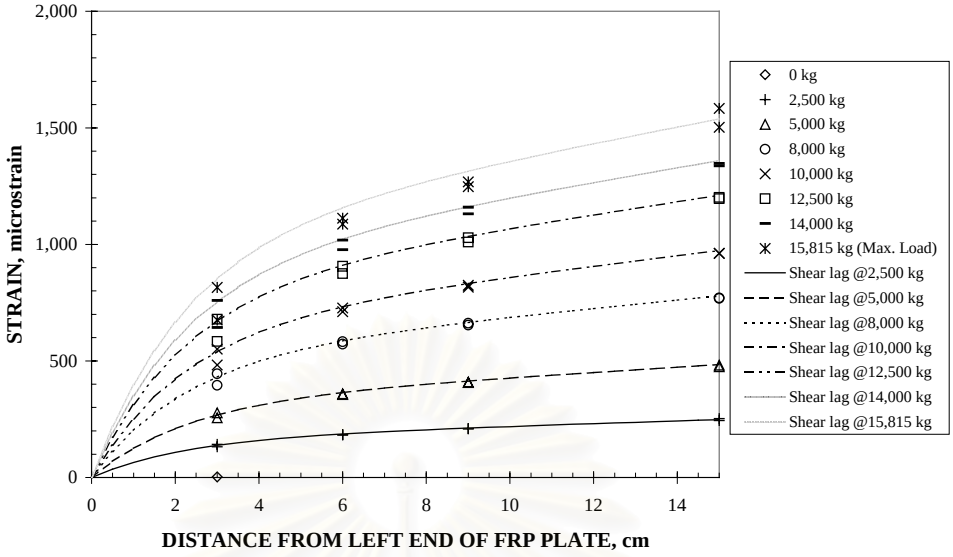

Figure 7.11 Development of tensile strains in the CFRP plate of B120Y-1

c) Strain distribution at midspan

The objective was to investigate strain distribution at the midspan section of series B120 after the occurrence of yielding in the tension flange of the steel beam. The strain distributions across midspan section from strain gages number 9,10 (at CFRP), 15,16 (at bottom flange), 19 and 20 (at top flange) in B120-1 and B120Y-1 at various load levels are shown in Fig. 7.12 and Fig. 7.13, respectively. It was found that the tensile stress in CFRP plates increased significantly after yielding had occurred in B120-1 (the yield load of the strengthened section calculated using the transformed section analysis is 8,480 kg); therefore leading to a nonlinear strain distribution. Nonlinear strain distributions were less obvious in B120Y-1.

Therefore, there were two curvatures after the occurrence of yielding if linear strain distribution was assumed as plotted in Fig. 7.14. Curvature ϕ_1 was obtained from strain gages number 15, 16, 19, and 20, while ϕ_2 was from strain gages number 9, 10, 19, and 20. The load-moment-curvature relationship obtained from an elastic-plastic section analysis is also shown in this figure. From the figure, these three curvatures deviate when the yielding occurs. Moreover, $M-\phi_2$ relationship is close to relationship from the analysis. At load 12,900 kg, the section analysis predicts the fiber stress of 13,600 ksc (about 95% of fiber breaking stress) and the stress at top

layer of the welded steel plate of 2,450 ksc (about 80% of yielded strength). Above this load level, fiber stresses obtained from the analysis exceed the fiber breaking stress. For example, fiber stress of 18,350 ksc is calculated from the analysis at load 14,600 kg.

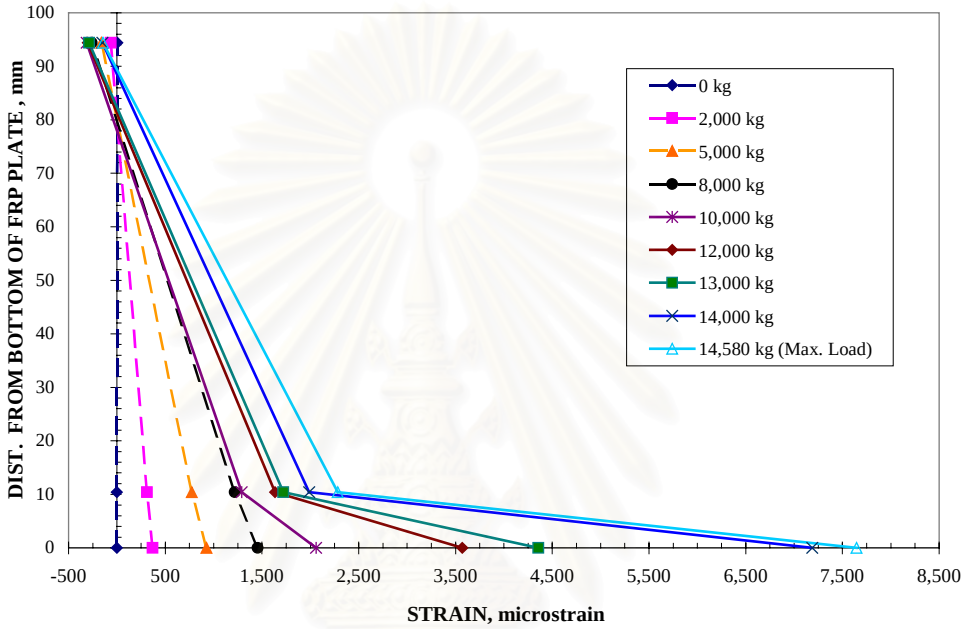

Figure 7.12 Strain distribution measured across midspan section of B120-1

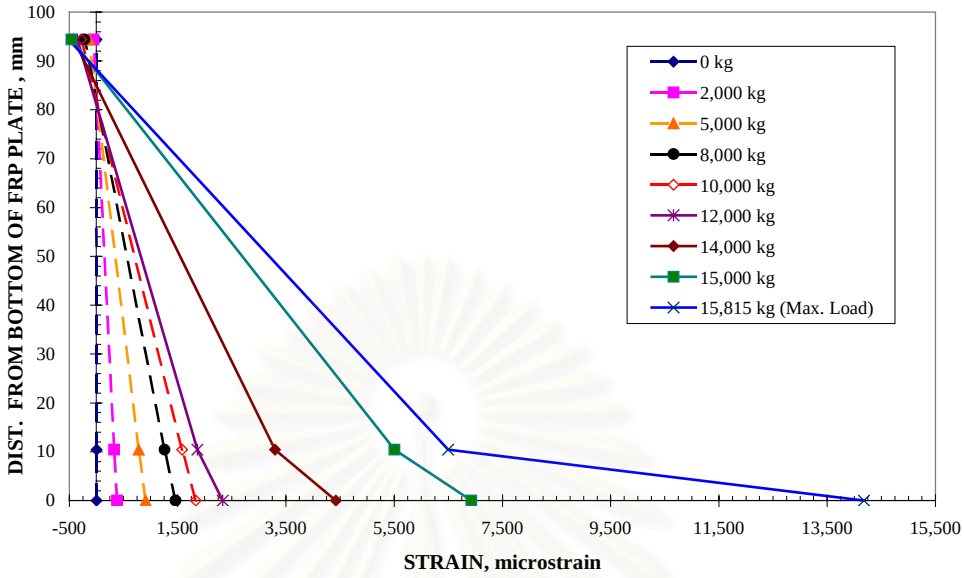

Figure 7.13 Strain distribution measured across mid-span section of B120Y-1

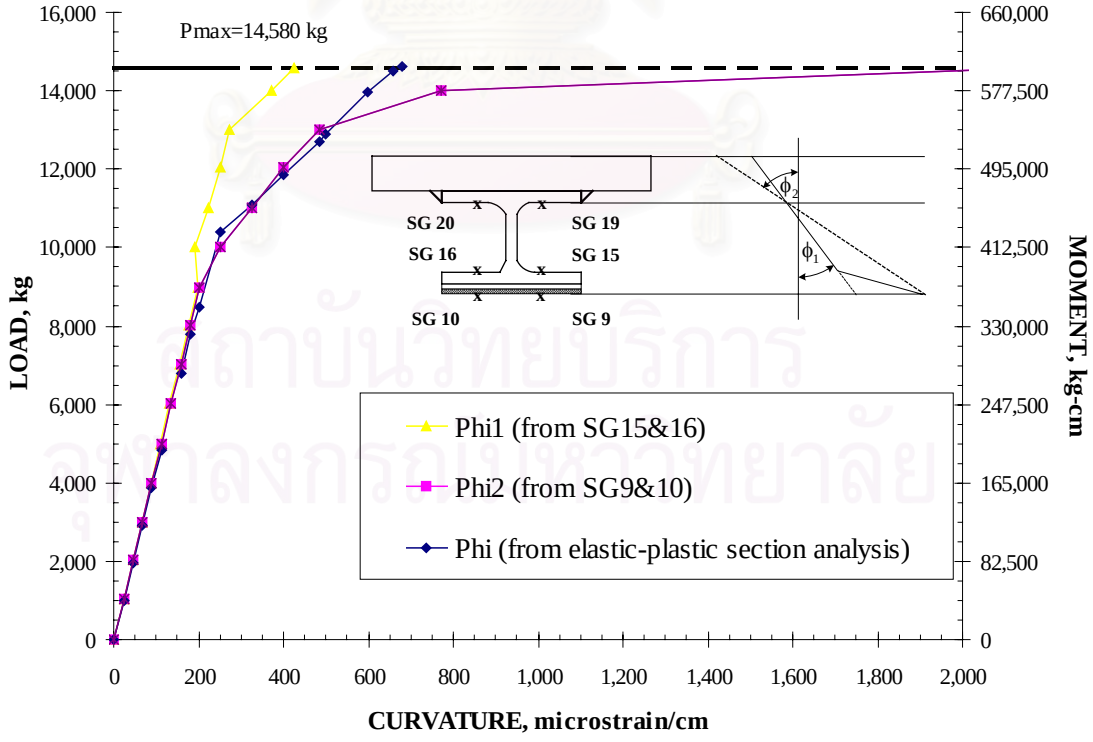

Figure 7.14 Moment-curvature relationship from elastic-plastic section analysis and from B120-1

d) Effectiveness of the strengthening scheme

Nonlinear finite element analysis was conducted to assess the response of the control, or unstrengthened, steel beam. The steel beam without CFRP plates was analyzed by 2-D nonlinear finite element analysis. Stress-strain relationship of the steel beam was assumed to be elastic-perfectly plastic with yield point of 3,000 ksc. An unconverged solution implied that the beam becomes unstable due to the presence of plastic hinge at midspan. At this stage, the midspan section was found to be almost fully yielded.

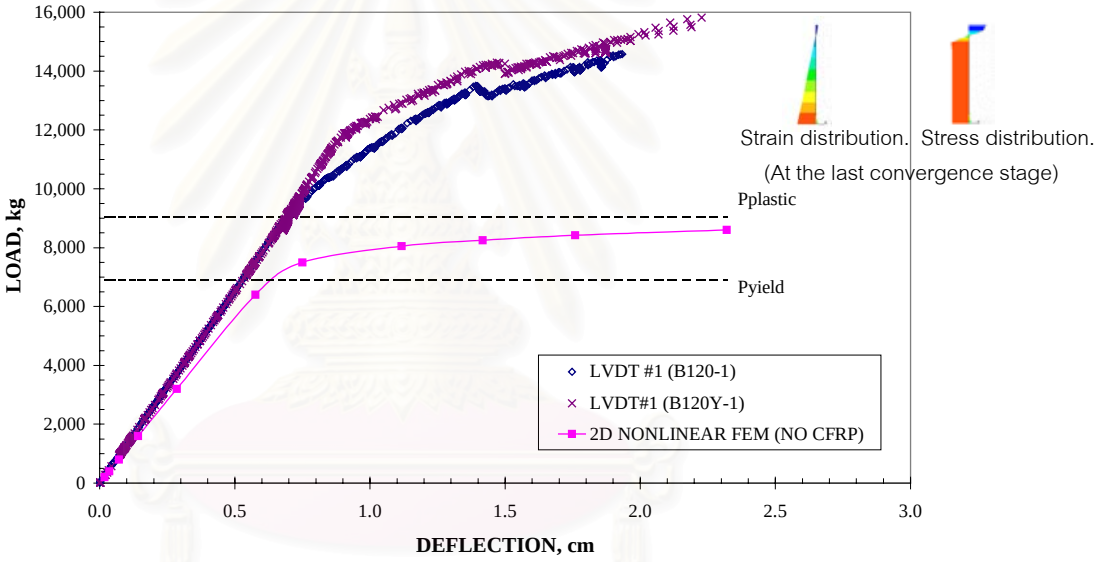

Figure 7.15 Load v.s. Deflection at midspan of B120-1 and B120Y-1

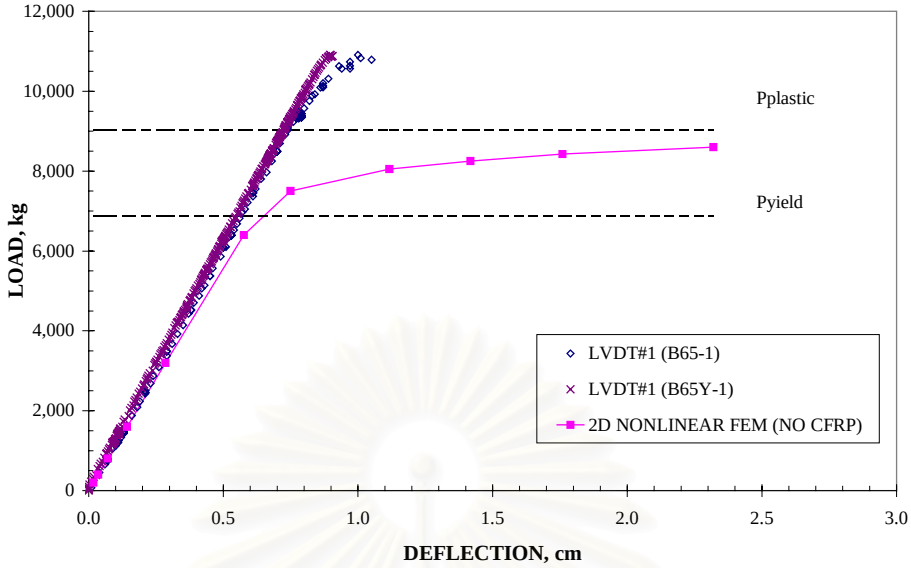

Figure 7.16 Load v.s. Deflection at midspan of B65-1 and B65Y-1

The relationships between applied load and deflection at midspan of B120-1, B120Y-1 and that from the nonlinear finite element analysis are plotted in Fig. 7.15. Plot is also made for B65-1 and B65Y-1 as shown in Fig. 7.16. Also shown in these figures are the yield load and the load at fully plastic condition of the steel beam without CFRP plate. The yield load, P_{Yield} of 6,890 kg, was calculated using the transformed section, while the load at the fully-yielded section without CFRP plate, $P_{Plastic}$, of 9,041 kg, was calculated by assuming that yielding occurred across the whole section.

It can be seen that the CFRP plate increases the ultimate strength of beam B120-1 and B120Y-1 of 161% and 175% compared with the unstrengthened beam, respectively. The stiffness gained was about 117% in the elastic range, Also, the CFRP plate significantly extended the range of elastic region. Increase in the elastic region indicates the potential for increase in service loading.

To apply the virtual work principle, the moment-curvature from elastic-plastic section analysis, and that measured from the strain gages no.9, 10, 19, 20 (M-ϕ_2) were used. In the virtual work, a section was considered having the FRP plate when the flexural conformance at the section was achieved. The distance for developing the flexural conformance was obtained from the shear lag analysis; otherwise the section

was considered without the FRP plate. The load-deflection relationships from the virtual work principle based on these two cases of moment-curvature relationships were compared with data from LVDT no.1 of B120-1, as shown in Fig. 7.17. As shown in the figure, displacements predicted by the virtual work were less than those from LVDT no.1. Also, the stiffness obtained from the analysis was 116% of that from the measurement.

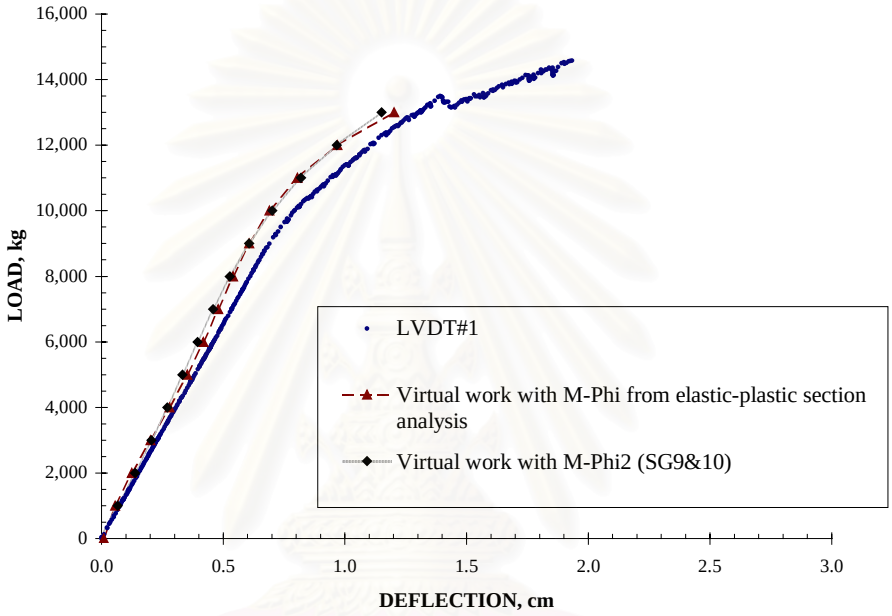

Figure 7.17 Comparison of load-deflection relationship from B120-1 and the results from virtual work

7.2 RESULTS FROM THE FATIGUE TEST

Results from the fatigue test investigating the fatigue strength of steel beams with a bonded plate end detail are discussed in this section.

During the experiments, fatigue cracks/debond occurred at the plate ends where stress singularities were present. The locus of debond initiation was near interface of the steel beam and the adhesive. After initiating, debond cracks propagated across the plate width and then expanded along the plate length. No crack was found in the bottom flanges of all steel beams tested.

The fatigue test data were plotted against a nominal stress range and a stress intensity factor range in Fig. 7.18 and Fig. 7.19, respectively. The run-out data were represented as points with arrows pointing to the right when no debond was detected at 1,500,000 cycles. The nominal stress range at the plate end in the bottom flange of the section without CFRP was calculated from the conventional beam formula. Also shown in Fig. 7.18 is the fatigue limit of AASHTO category E for nonredundant load path structures (AASHTO, 1996). It can be seen that the fatigue limit of the bonded plate detail is higher than that of the conventional welded cover plate end detail. The scatter of data was found to be lower in Fig. 7.19 than in Fig. 7.18. Thus, the stress intensity factor range is more suitable as a governing parameter in the fatigue life evaluation. The equation obtained from regression analysis was

$$\Delta Q_{\theta\theta} = -3.52 * Ln(N) + 106.8 \qquad (7.1)$$

where $\Delta Q_{\theta\theta}$ is a stress intensity factor range in $ksc - cm^{0.326}$ and N is a number of loading cycles based on the initiation of debond cracks. The relationship in Eq. (7.1) is the characteristic of the bi-material and interface investigated. The extrapolated stress intensity factor range from Eq. (7.1) was 106.8 $ksc - cm^{0.326}$. Therefore, the maximum stress intensity factor calculated according to the stress ratio, R, of 0.2 was 133.5 $ksc - cm^{0.326}$. Difference between this extrapolated value and the critical stress intensity factor, $Q_{\theta\theta,cr} = 153.1$ $ksc - cm^{0.326}$, was about 10%.

Therefore, a fatigue initiation criterion from regression analysis is proposed for the evaluation of debond initiation. This criterion is similar to S-N equation, but the range of stress intensity factor is found to be the parameter that controls the fatigue crack initiation, instead of the nominal stress range.

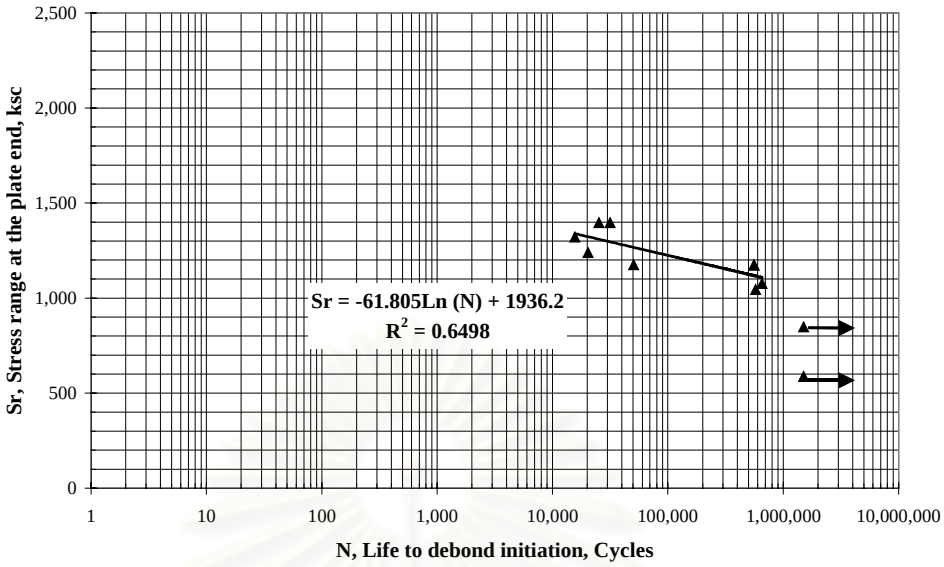

Figure 7.18 Sr-N relationship where Sr is nominal stress range, Stress ratio is 0.2

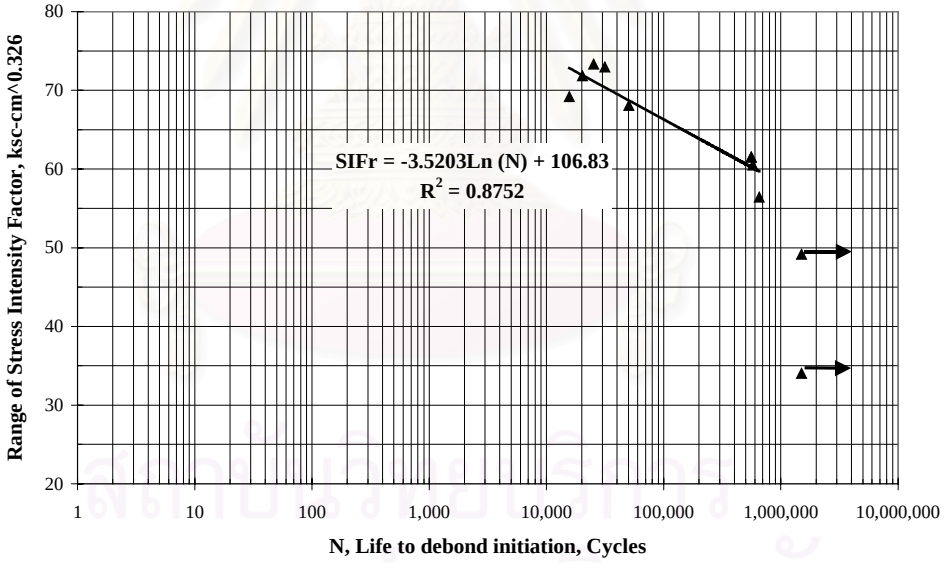

Figure 7.19 SIFr-N relationship where SIFr is $\Delta Q_{\theta\theta}$, Stress ratio is 0.2

CHAPTER 8

APPLICATION

In this chapter, the studies on the effects of some important parameters on the stress intensity factors and the distance required for the plate to develop flexural conformance are presented. The parameters investigated are: 1) Thickness of a bonded FRP plate; 2) Elastic modulus of a bonded plate; 3) Adhesive layer thickness 4) Elastic modulus of adhesive; and 5) Corner angle due to spew fillet conditions.

There are two behaviors associated with the stress intensity factors. Firstly, for the premature plate separation, high stress intensity factors can reduce the effectiveness of the strengthening scheme. Secondly, the high stress intensity factors at the plate end can shorten the service life of the strengthened beams by introducing debond cracks. A sufficient distance for the plate to develop flexural conformance has to be provided to develop its tensile stress; otherwise section compatibility can not be achieved. These three behaviors directly influence the terminal distance required for the bonded plate.

The effect of corner angle on the applicability of a fracture criterion is also studied. For the fracture criterion to work for corner angles other than one specific angle (e.g. angle 90° in this study), stress intensity factors should be able to capture the severity of the corner and should be related to the stresses in a corresponding way. For instance, if stress intensity factors decrease with increasing corner angle, the corresponding stresses near the singular point should have a similar variation. Stress intensity factors that can not represent the severity of the corner can not be used as fracture nucleation criteria in a general sense.

8.1 EFFECTS OF BI-MATERIAL'S PROPERTIES ON THE STRENGTH OF SINGULARITY

The test case is a steel beam strengthened by a 120-cm long CFRP plate, which is similar to beam B120-1 in the static test, as shown in Fig. 8.1. A singular point of the steel-adhesive bi-material wedge, where fracture is expected, is

investigated. Material properties are as follows: $E_s = 2x10^6$ ksc, $\nu_s = 0.3$, $\nu_a = 0.35$, $\theta_1 = 180^\circ$, where θ_2 and E_a are varied.

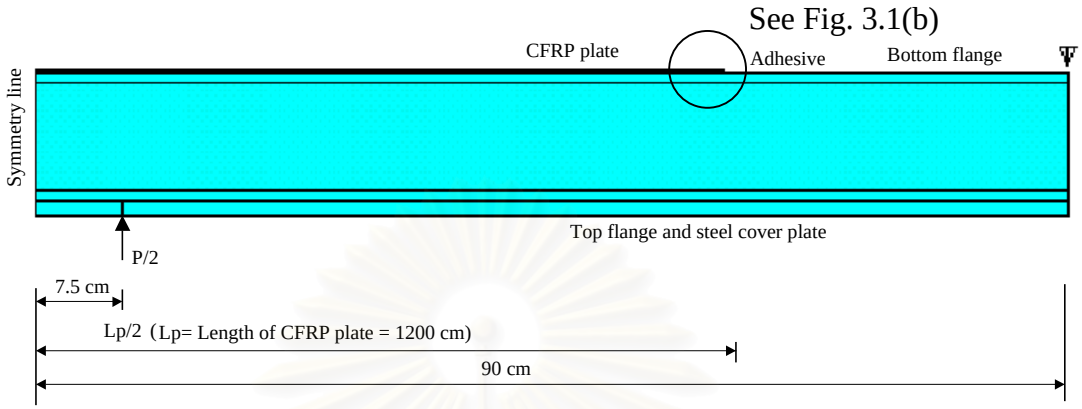

Figure 8.1 A test case (Similar to B120 specimen)

The strength or orders of singularity, $\alpha = 1 - \lambda$, where λ are eigenvalues, are obtained from the Muller's algorithm. Effect of corner angle, θ_2, and stiffness ratio, E_a / E_s on the order of singularity is shown in Fig. 8.2.

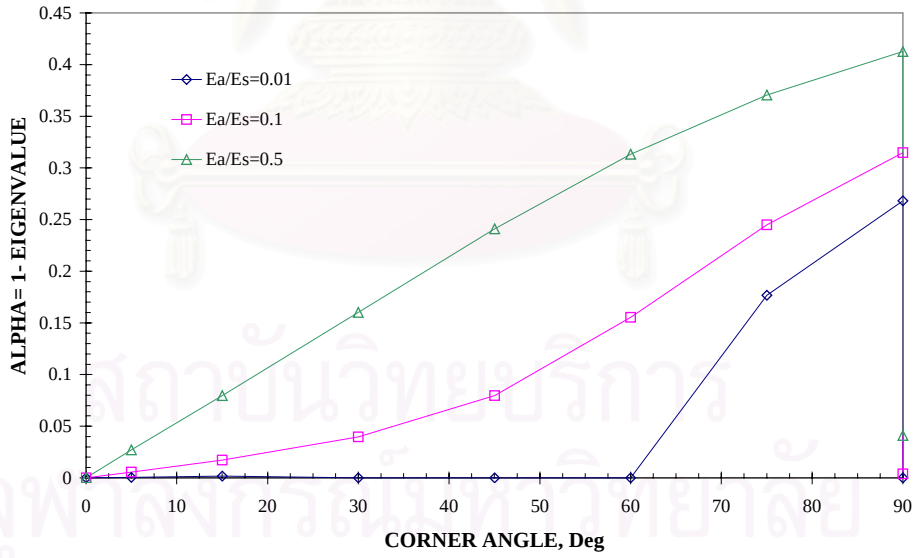

(a)

Figure 8.2 Effect of corner angle and elastic modulus mismatch on the strength of singularity: (a) plane stress condition (b) plane strain condition

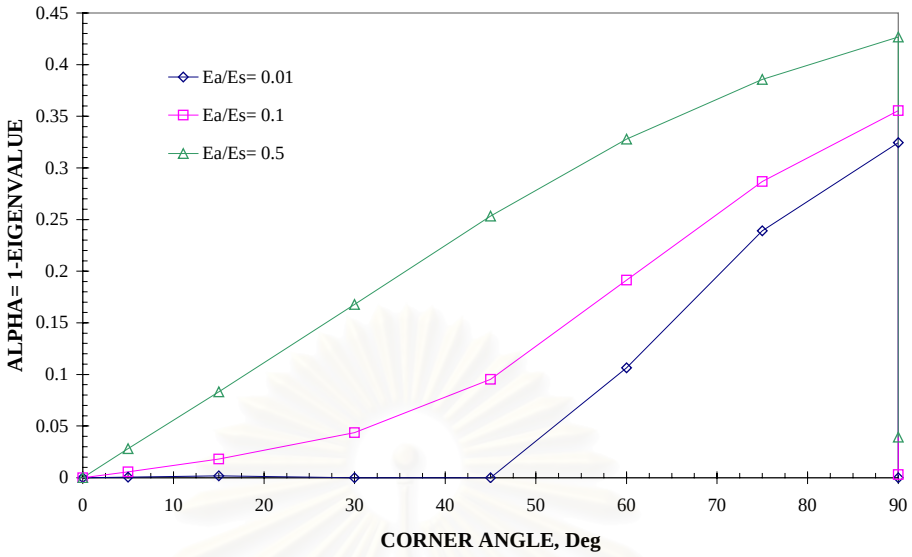

(b)

Figure 8.2 Effect of corner angle and elastic modulus mismatch on the strength of singularity: (a) plane stress condition (b) plane strain condition (Continued)

From the figures, there is only one dominant singularity (one real eigenvalue) when the corner angle, θ_2, is smaller than 90° for all stiffness ratios, E_a / E_s. Under both plane stress and plane strain conditions, two real eigenvalues occur at 90° for $E_a / E_s = 0.5$. When there is only one dominant singularity, there is a one-parameter description of a stress field. In other words, a single stress intensity factor characterizes the magnitude of the stress field in the region near the singular point. For the one-parameter description of a stress field, it seems reasonable to assume that failure occurs at a critical value of the stress intensity factor with regard to linear elasticity. Also shown in the figure, singularity generally increases with θ_2 until 90° and decreases as the stiffness ratio, E_a / E_s, decreases. For small stiffness ratios, e.g. $E_a / E_s = 0.01$, there is practically no singularity for $\theta_2 < 45^\circ$.

8.2 FACTORS AFFECTING THE STRESS INTENSITY FACTORS

A parametric study was conducted to investigate the geometrical and mechanical effects of a bonded plate and an adhesive layer on stress intensity factors.

The stress intensity factors were calculated from RWCIM under plane strain condition. In the parametric study, properties of the strengthened beam, except the value of the parameter in the investigation, are same as those of B120-1.

1) Effect of FRP thickness:

The thicknesses of bonded plates in the study are 0.14 cm (1 layer), 0.28 cm (2 layers), and 1.40 cm (10 layers). Fig. 8.3 plots the relationship between stress intensity factors and the plate thickness. From the figure, stress intensity factors increase with increasing plate thickness. When the plate thickness becomes ten times (10 layers), stress intensity factors become about twice the original values.

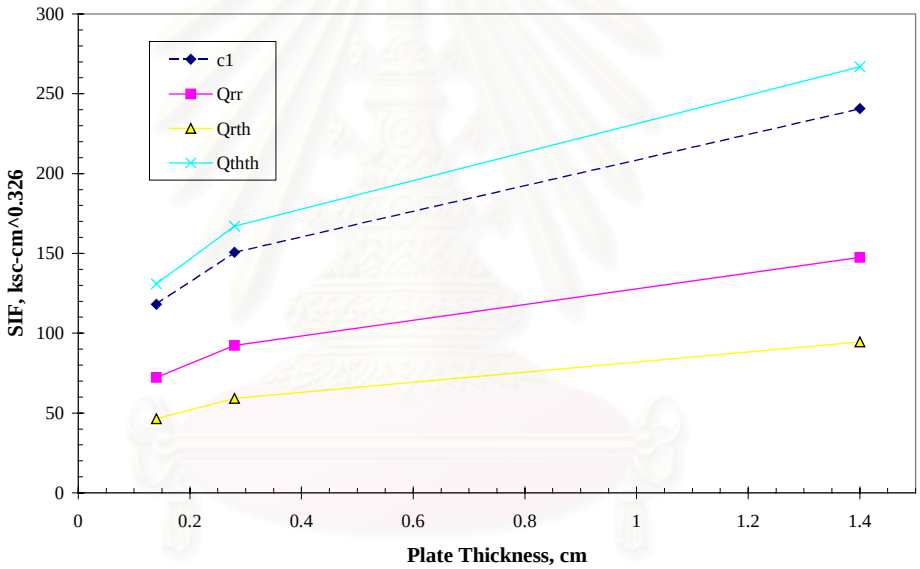

Figure 8.3 Effect of plate thickness on stress intensity factors

2) Effect of FRP modulus:

Elastic moduli of bonded plates in the study are $2x10^6$ ksc (equivalent to that of steel plate), $3x10^6$ ksc, and $6x10^6$ ksc. Fig. 8.4 plots the relationship between stress intensity factors and the plate modulus. From the figure, stress intensity factors increase with increasing plate modulus. As the modulus becomes three times, stress intensity factors increase about 50%.

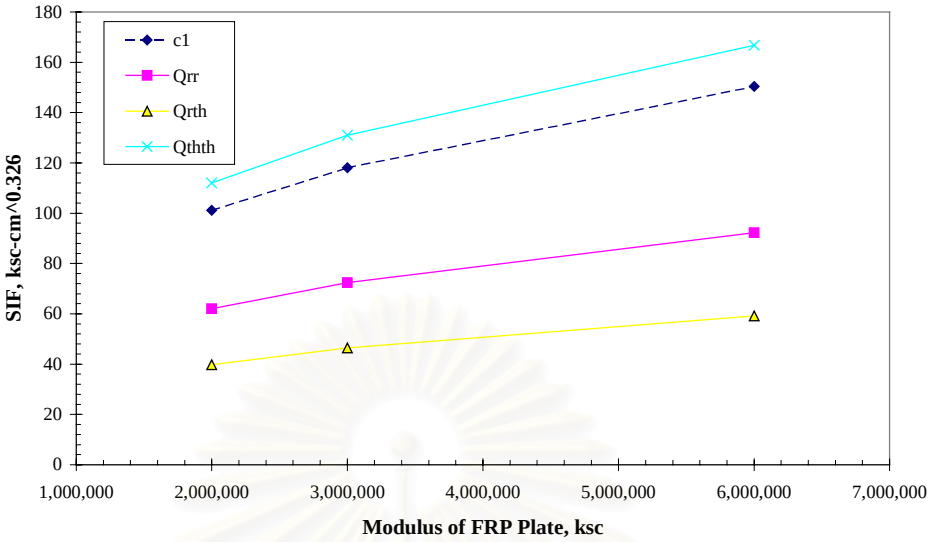

Figure 8.4 Effect of plate modulus on stress intensity factors

3) Effect of adhesive layer thickness:

The thickness of adhesive layer is varied as follows: 0.1 cm, 0.2 cm, and 1.0 cm. Fig. 8.5 plots the relationship between stress intensity factors and the adhesive layer thickness. From the figure, stress intensity factors decrease with increasing adhesive thickness in a nonlinear way. The effect of adhesive thickness becomes quite modest at relatively thick adhesive layer. Stress intensity factors decrease about 10% as the adhesive layer increases from 0.1 cm to 0.2 cm, while they decrease about 5% when the adhesive thickness increases from 0.2 to 1.0 cm.

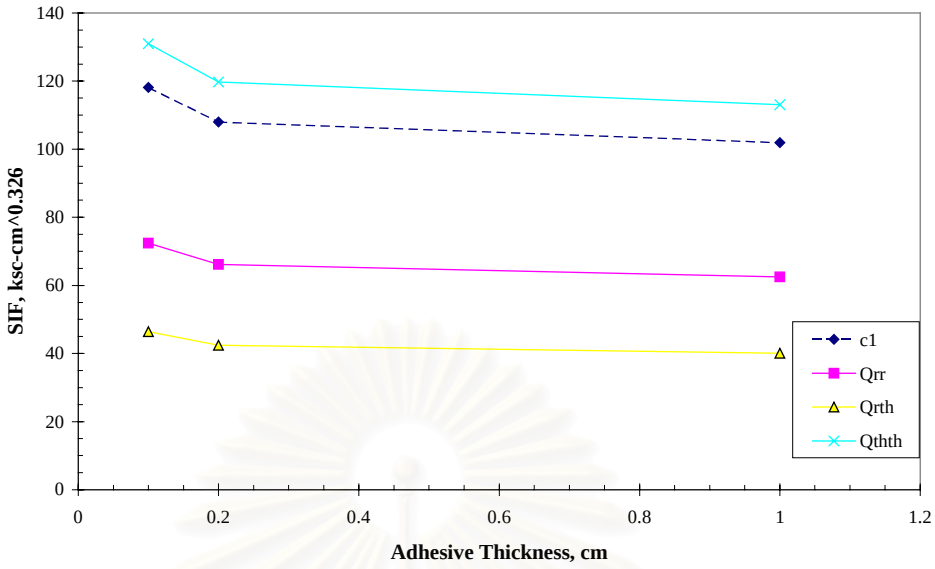

Figure 8.5 Effect of adhesive layer thickness on stress intensity factors

4) Effect of modulus of adhesive:

Elastic moduli of adhesives, E_a, in the study are $2x10^4$ ksc, $2x10^5$ ksc, and $1x10^6$ ksc. The order of singularity of a steel-adhesive bi-material wedge is 0.324, 0.355, 0.427 for each case of adhesive modulus, respectively. Since the singularities are different, stress intensity factors Q^*_{rr}, $Q^*_{r\theta}$, $Q^*_{\theta\theta}$, which are given in Eq. (5.2) and have the same unit, are plotted in Fig. 8.6. From the figure, stress intensity factors increase with increasing adhesive modulus.

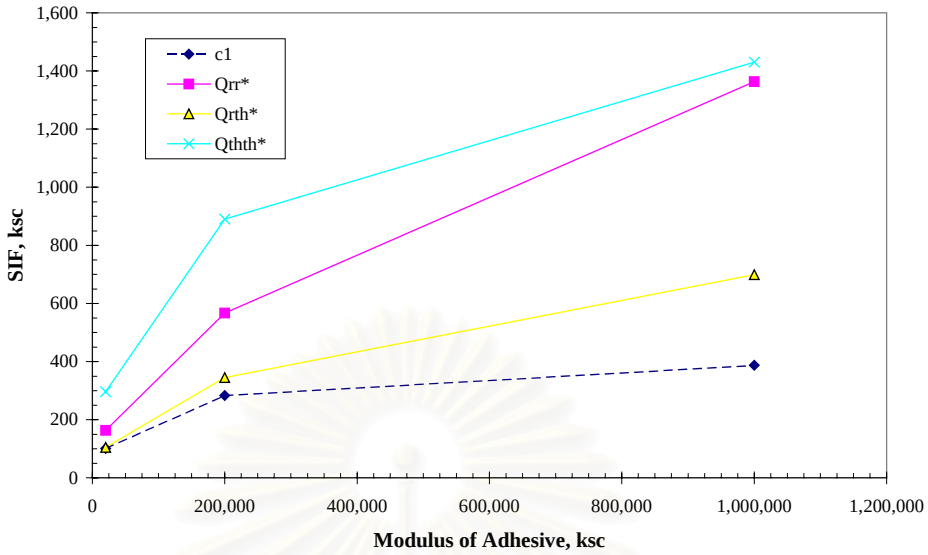

Figure 8.6 Effect of adhesive modulus on stress intensity factors

5) Effect of corner angle:

The corner angles, which simulate various conditions of spew fillet, between adhesive terminus and the flange of the steel beam are 15°, 45°, 60°, 75°, and 90°. Since there is almost no singularity for corner angles less than 45° (from the previous section), stress intensity factors are small for these angles. Singularity associated with each corner angle in the study is 0.002, 0.001, 0.106, 0.239, 0.324, respectively. Fig. 8.7 plots the relationship between stress intensity factors Q^*_{rr}, $Q^*_{r\theta}$, $Q^*_{\theta\theta}$ and the corner angle of adhesive terminus. From the figure, stress intensity factors generally increase with increasing corner angle except $Q^*_{r\theta}$.

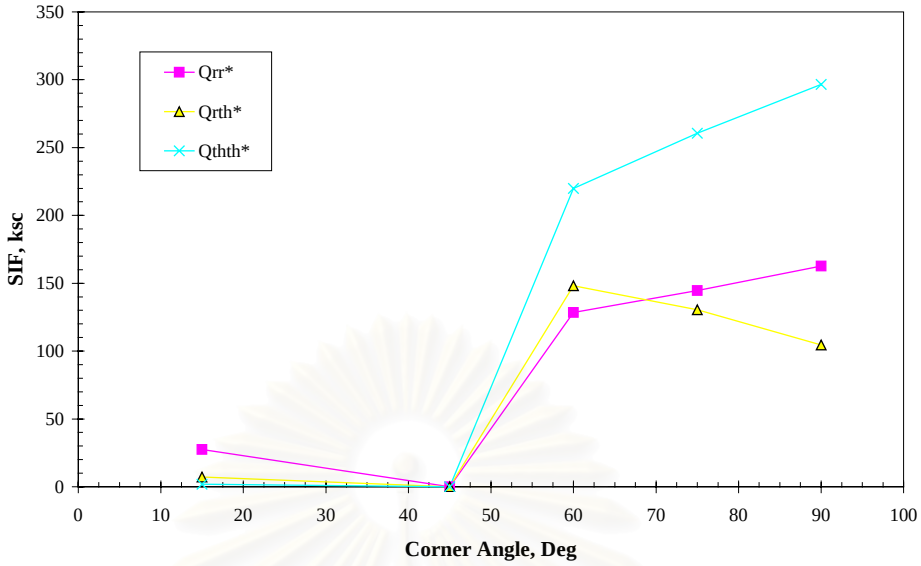

Figure 8.7 Effect of corner angle in spew fillet on stress intensity factors

Although analytical models, e.g. shear lag analysis, can not capture stress singularity, they can provide the shear stress distribution and peel stress distribution. Therefore, the influence of the previously investigated parameters on the maximum shear and peel stresses at the plate end is also studied.

Fig. 8.8 to 8.15 show the effects of the previously investigated parameters, which are 1) Thickness of a bonded plate 2) Elastic modulus of a bonded plate 3) Thickness of an adhesive layer 4) Elastic modulus of adhesive, on shear stress and peel stress distributions. The test problem is the same as that in the previous study on the stress intensity factors.

1) Effect of FRP thickness:

Fig. 8.8 illustrates the effect of thickness of a bonded plate on shear stress distribution. As shown in the figure, the maximum shear stress obtained from the shear lag analysis increases when the plate becomes thicker. Effect of the plate thickness on peel stress distribution is shown in Fig. 8.9. It can be seen that the maximum peel stress also increases with the plate thickness. When the plate thickness becomes ten times, the maximum shear stress at the plate end increases 68%, while the maximum peel stress at the plate end increases 267%.

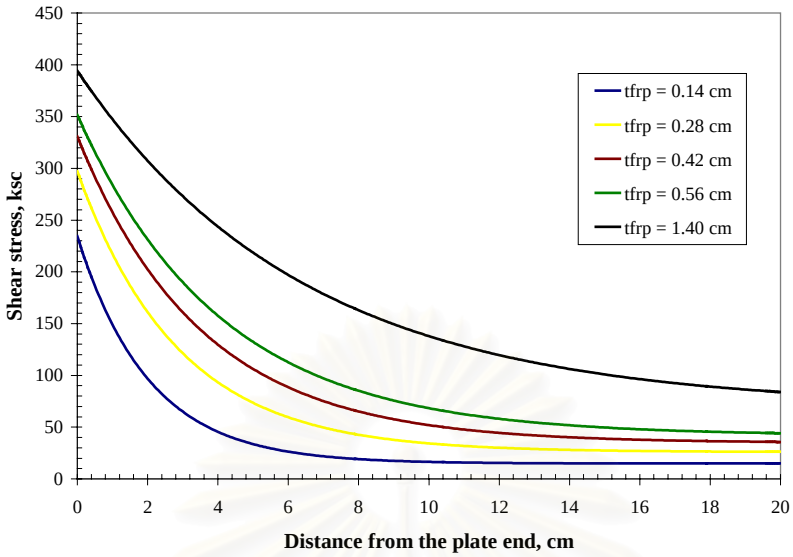

Figure 8.8 Effect of plate thickness on adhesive shear stress distribution

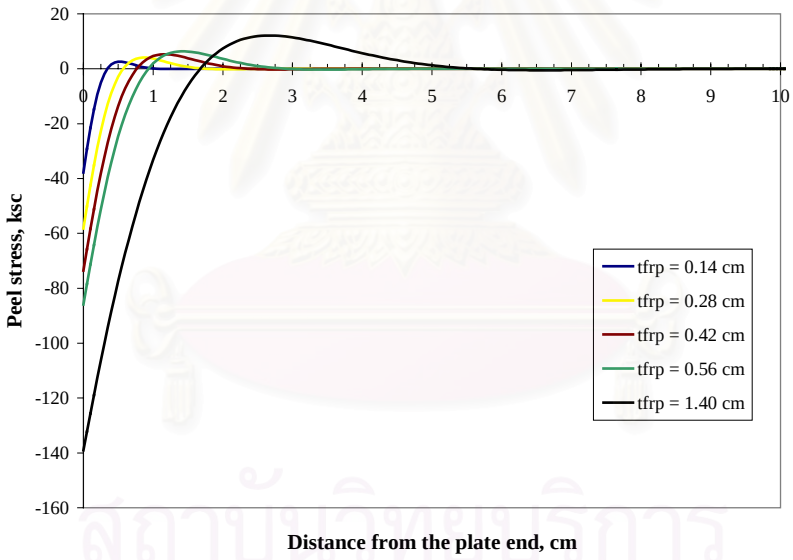

Figure 8.9 Effect of plate thickness on peel stress distribution

2) Effect of FRP modulus:

Fig. 8.10 plots the effect of plate modulus on shear stress distribution. As shown in the figure, the maximum shear stress at the plate end increases when the elastic modulus of a bonded plate increases. The value increases 104% as the plate modulus increase from $1x10^6$ ksc to $6x10^6$ ksc. Fig. 8.11 plots the effect of plate modulus on peel stress distribution. The maximum peel stress at the plate end also

increases with increasing plate modulus but in a modest way. Its value increases 32% as the plate modulus increase from $1x10^6$ ksc to $6x10^6$ ksc.

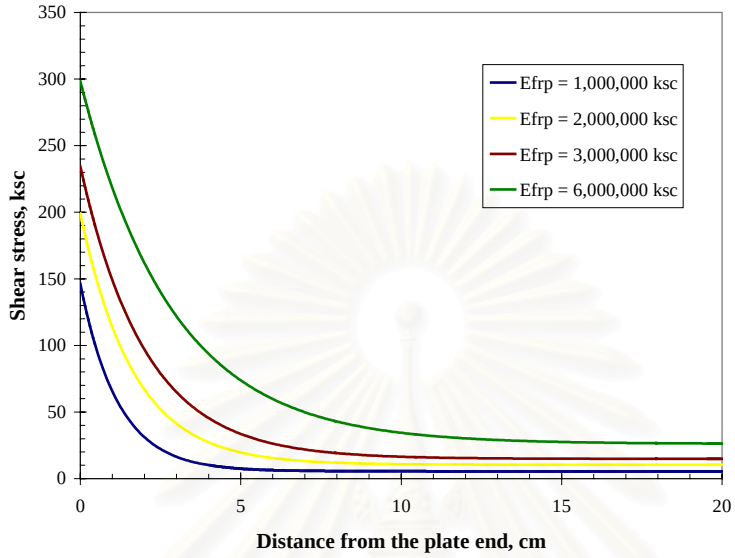

Figure 8.10 Effect of plate modulus on adhesive shear stress distribution

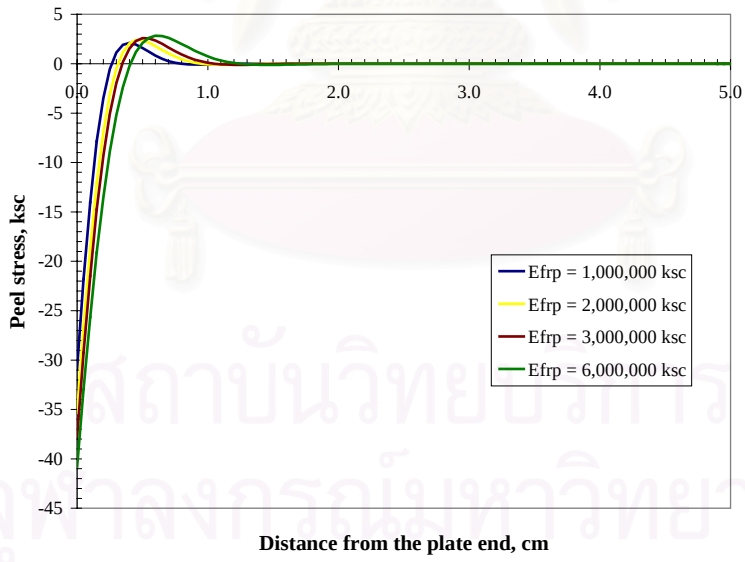

Figure 8.11 Effect of plate modulus on peel stress distribution

3) Effect of Adhesive layer thickness:

Fig. 8.12 and Fig. 8.13 shows effect of adhesive layer thickness on shear stress distribution and peel stress distribution, respectively. From the figures, the maximum

shear stress and peel stress at the plate end decrease when the adhesive layer becomes thicker. As the layer becomes 10 times thicker, the maximum shear stress and peel stress decreases 65% and 80%, respectively.

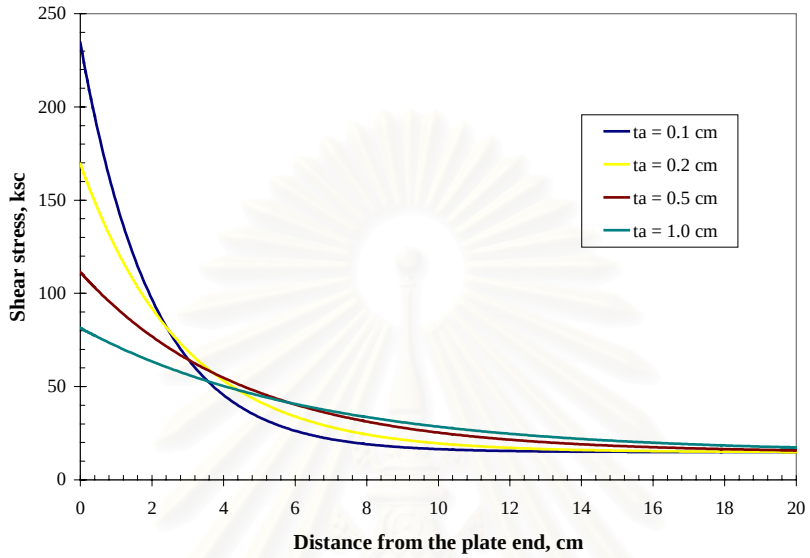

Figure 8.12 Effect of adhesive layer thickness on adhesive shear stress distribution

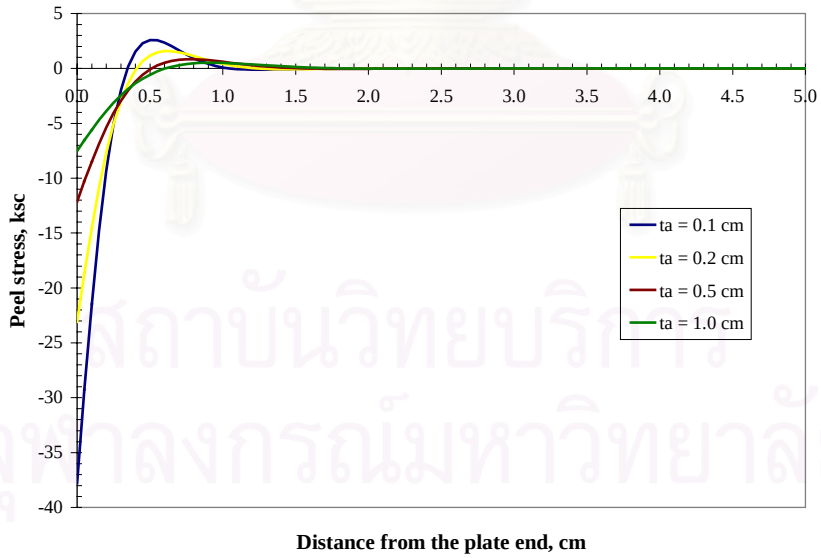

Figure 8.13 Effect of adhesive layer thickness on peel stress distribution

4) Effect of Adhesive modulus:

Fig. 8.14 and Fig. 8.15 illustrates the effect of thickness of adhesive layer on shear stress and peel stress distributions, respectively. From the figures, both the maximum shear stress and the maximum peel stress at the plate end increase with increasing adhesive modulus. As the adhesive modulus increases from $1x10^4$ ksc to $1x10^6$ ksc, the maximum shear stress and peel stress increases 810% and 27%, respectively.

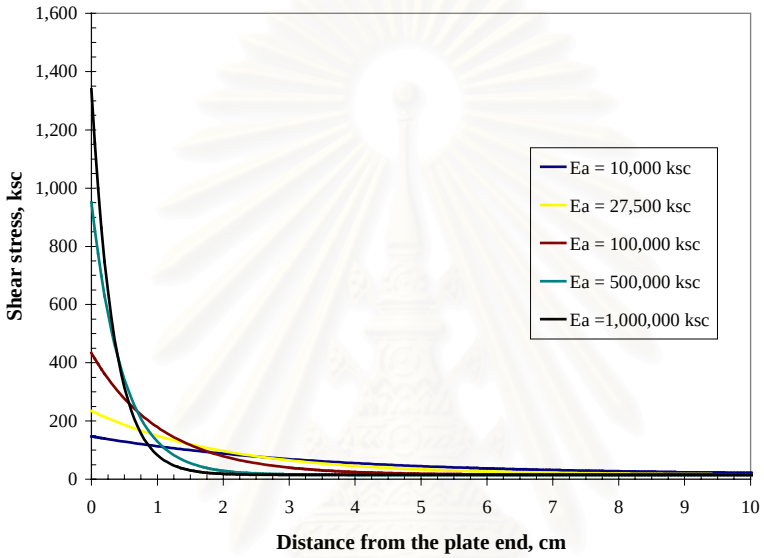

Figure 8.14 Effect of adhesive modulus on adhesive shear stress distribution

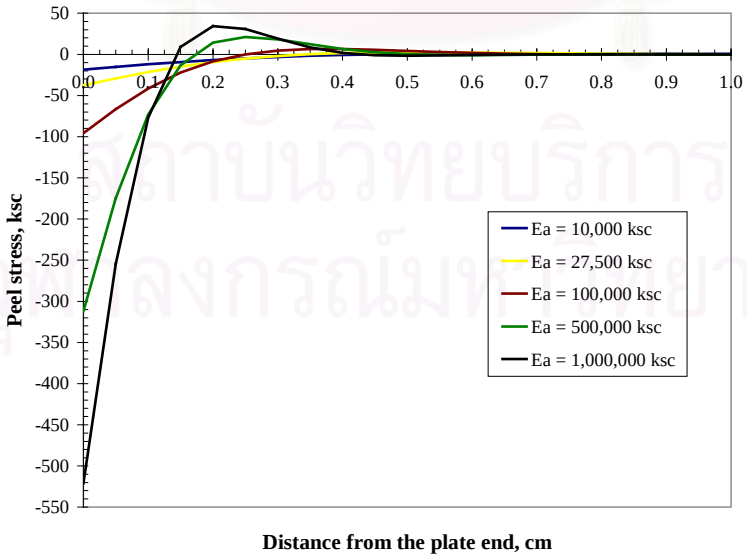

Figure 8.15 Effect of adhesive modulus on peel stress distribution

From the study, it is found that both the stress intensity factors and the maximum stresses at the plate end, which are obtained from the analytical model, show similar dependency on the parameters in the investigation. However, the maximum peel stress and shear stress, which are obtained from different models that can not capture the singular stress field at the plate end, show inconsistent dependency on the parameters investigated. Therefore, the stress intensity factors should be used for the design and analysis of the premature plate separation problem, which is an unfavorable failure mode.

8.3 FACTORS AFFECTING THE DEVELOPMENT OF TENSILE STRESSES IN A BONDED PLATE

The distance allowed for a bonded plate to develop its tensile stress to conform to a conventional beam formula ($\sigma = Mc / I_{tr}$), or flexural conformance (Task Committee on Flexural Members, 1967), is studied. A shear lag analysis is used to study the effects of some important parameters on the distance to develop the flexural conformance. The parameters investigated are the plate modulus, the plate thickness, the adhesive modulus, and the adhesive layer thickness. Fig. 8.16 to 8.19 illustrate the effects of these parameters on the development of tensile stresses in a bonded plate.

From Fig. 8.16, if the thickness of a bonded plate increases, higher distance is required to develop the flexural conformance. In contrast to the case of a welded plate, the tensile stress in the bonded plate always starts from zero at the plate end.

Fig. 8.17 plots the effect of plate modulus on the tensile stress distribution in a bonded plate. From the figure, the distance to develop the flexural conformance increases as the plate modulus increases. Fig. 8.18 shows the effect of adhesive layer thickness on the tensile stress distribution in a bonded plate. From the figure, a longer distance is needed when the adhesive layer becomes thicker. Fig. 8.19 illustrates the effect of adhesive modulus. It can be seen that the distance decreases when the adhesive modulus increases.

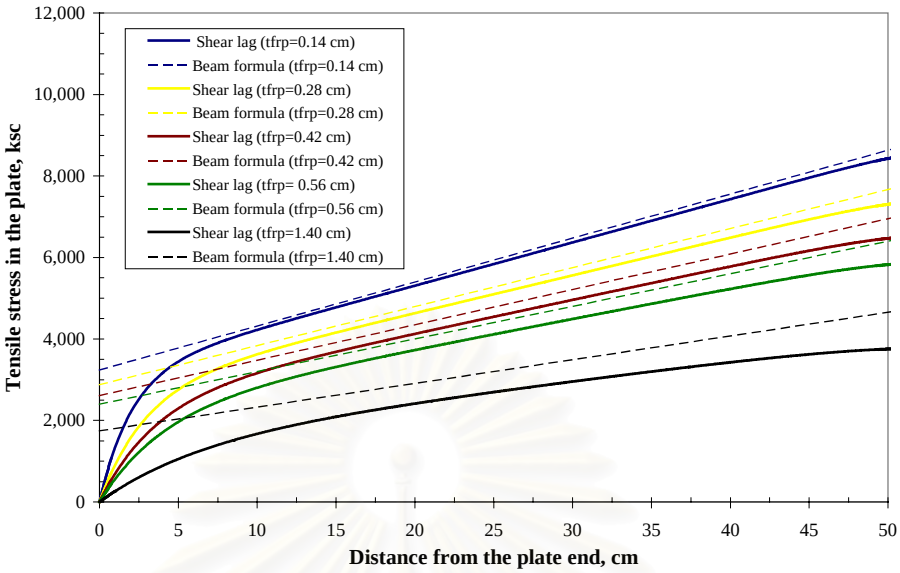

Figure 8.16 Effect of plate thickness on distance to develop the flexural conformance

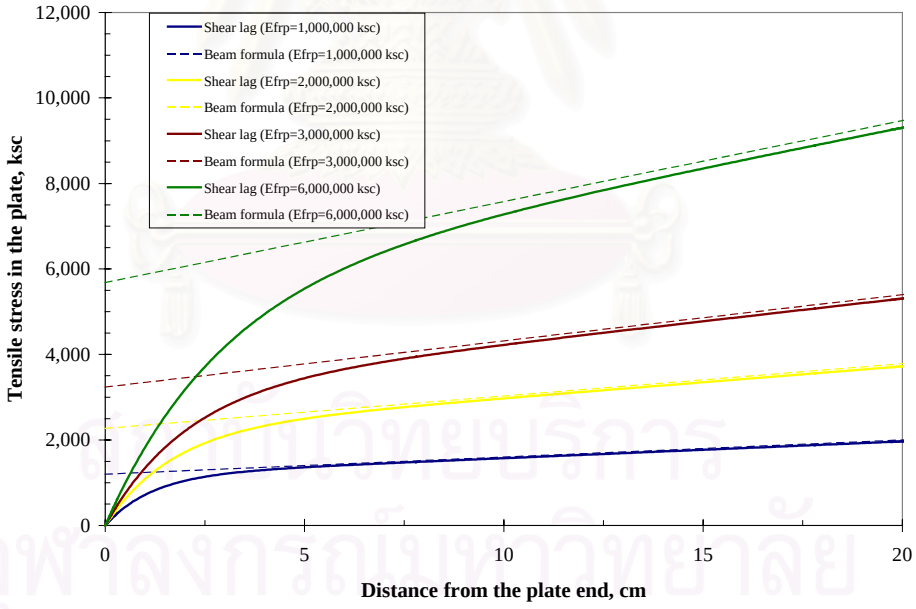

Figure 8.17 Effect of plate modulus on distance to develop the flexural conformance

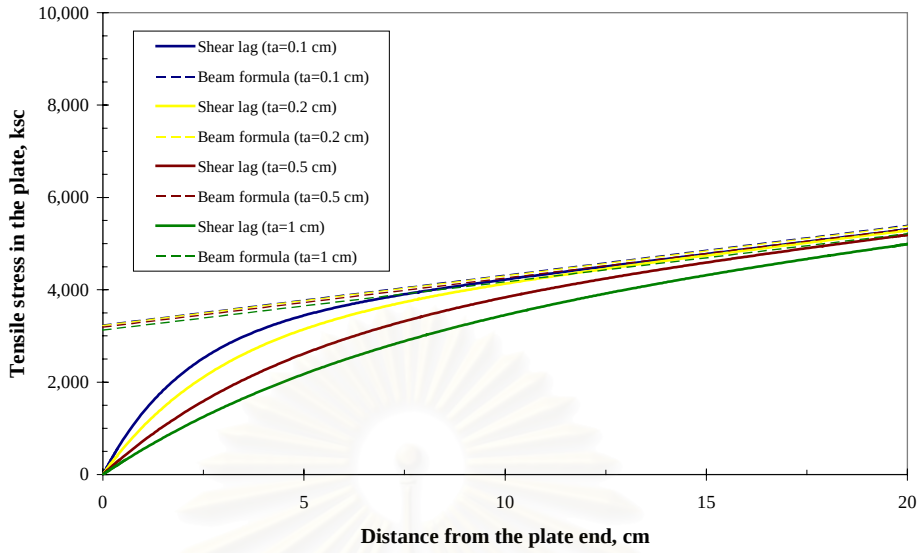

Figure 8.18 Effect of adhesive layer thickness on distance to develop the flexural conformance

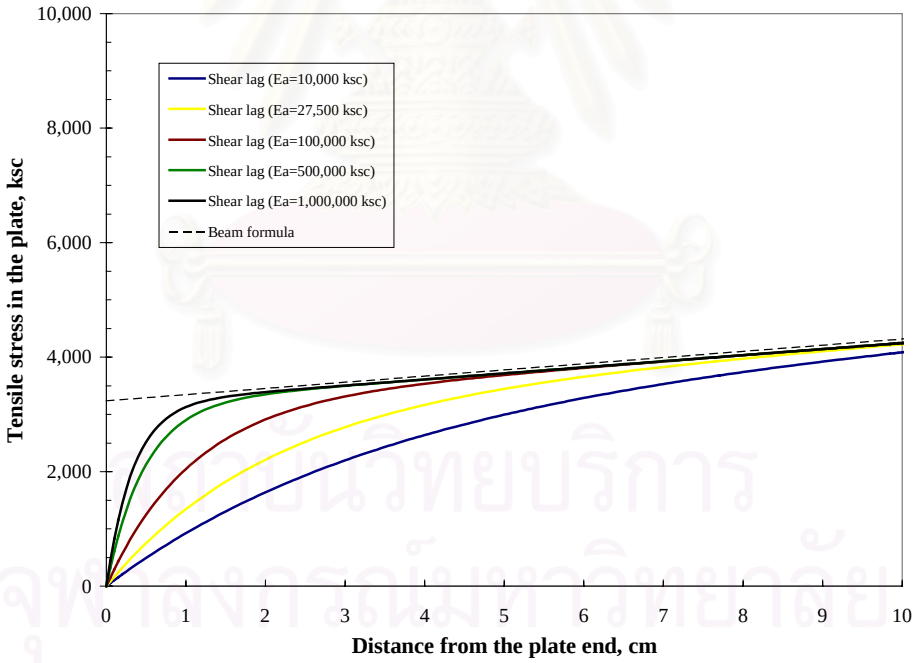

Figure 8.19 Effect of adhesive modulus on distance to develop the flexural conformance

8.4 EFFECTS OF CORNER ANGLE ON BI-MATERIAL CORNER STRESSES

Variations of both stress intensity factors and the stresses near a singular point with corner angles 60°, 75°, and 90° are investigated. Only the submodels with corner angles more than 45° are evaluated because those with corner angles less than 45° almost has no singularity. The values of stress intensity factors, $Q_{r\theta}$ and $Q_{\theta\theta}$, are first calculated using RWCIM as depicted in Fig. 8.7. Stresses near the singular point are then evaluated from the submodels subjected to boundary conditions of contour C3, a contour that is selected in RWCIM, for all cases (corner angles 60°, 75°, 90°). Subsequently, $\sigma_{r\theta}$ and $\sigma_{\theta\theta}$ corresponding to $r/L = 1x10^{-3}$, where L is half of adhesive layer thickness, are obtained from the finite element analysis of these submodels. Fig. 8.20, 8.21, and 8.22 shows the submodel for each case, respectively.

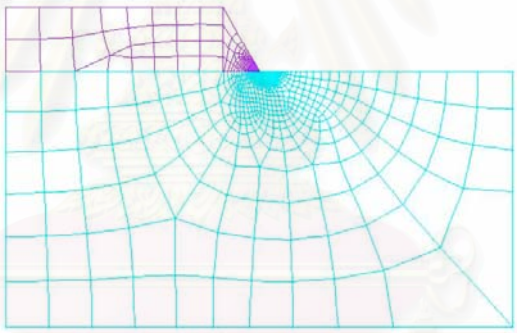

Figure 8.20 A submodel for evaluating stresses near a steel-adhesive singular point (corner angle 60°)

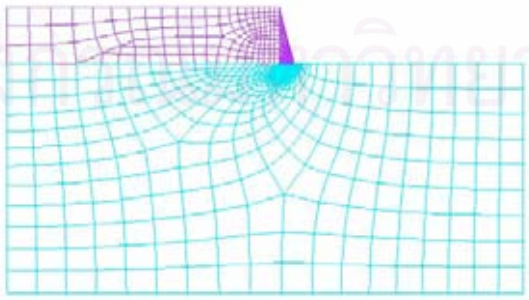

Figure 8.21 A submodel for evaluating stresses near a steel-adhesive singular point (corner angle 75°)

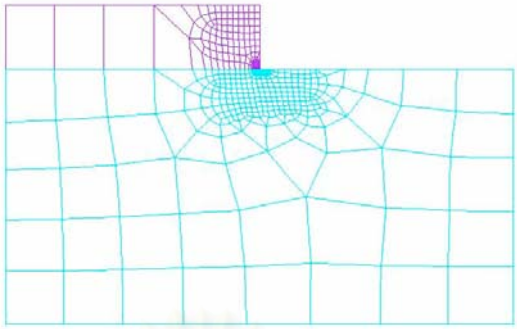

Figure 8.22 A submodel for evaluating stresses near a steel-adhesive singular point (corner angle 90°)

Stress components near the singular point from different corner angles are plotted in Fig. 8.23. It is found that all stress components increase with increasing corner angle. However, the variations of these stresses do not correspond with those of stress intensity factors from Fig. 8.7. So, stress intensity factors, by themselves, are not in correspondence with the stresses in the same way as they are for cracks.

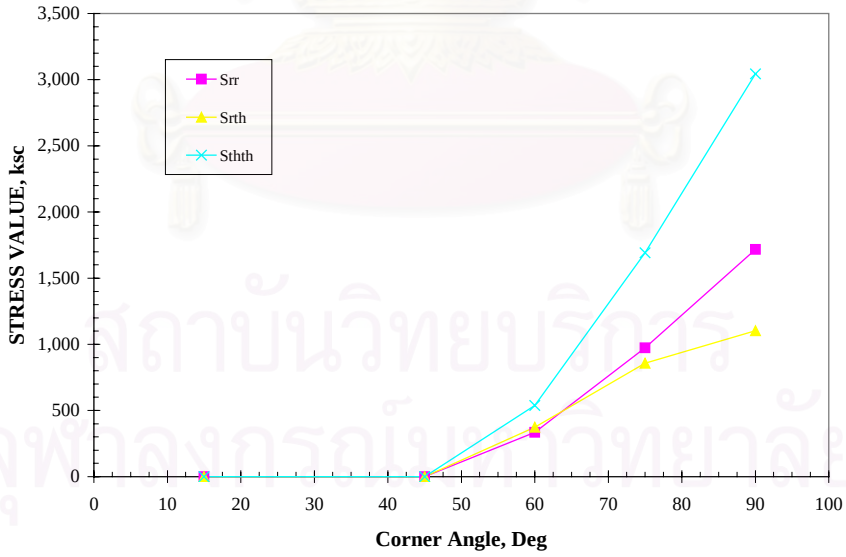

Figure 8.23 Variation of corner stresses (at $r/L = 1x10^{-3}$) with corner angle

CHAPTER 9

CONCLUSIONS AND RECOMMENDATIONS

9.1 CONCLUSIONS

Fatigue problems in steel beams with welded cover plates and the advantages of composite materials were the main motivations of this research. It was found that adhesive bonding of the unidirectional CFRP plates seems to be effective in strengthening steel beams. In developing the strengthening scheme, basic failure modes should be realized. Therefore, structural responses under both static and fatigue loadings were investigated. This research introduced a method for designing a terminal distance in order to:

1) Prevent a premature plate separation failure mode.

2) Provide a sufficient distance for a bonded plate to develop the flexural conformance.

3) Prevent plate debonding under cyclic loading during the design life of the strengthened beams.

To predict the first problem, a fracture criterion is proposed using results from the double strap joint testing. The fracture criterion is based on linear elastic fracture mechanics concepts. For the second behavior, a shear lag analysis provides reasonable agreements with the test data. So it may be used for determining a distance that the bonded plate should extend beyond the theoretical cut-off point to achieve flexural conformance.

The analytical methods for determining the fracture parameters were employed. The Reciprocal Work Contour Integral Method (RWCIM) was studied in detail including the convergence study of the contour integral where the trapezoidal rule was selected as the integration scheme. This method yielded acceptable values of the stress intensity factors without using a submodeling technique with a very fine mesh near the singular point. The method thus can save lots of computational time involved.

In the fatigue test, the debond behaviors were investigated under constant amplitude fatigue loading without environmental concerns. Steel beams with partial-length CFRP plates were tested during experimental phases. Various levels of stress intensity factor ranges were designed. Load ranges that yield the specified stress intensity factor ranges were then applied to the specimens. Test was stopped when no debond was detected at 1,500,000 cycles. The fatigue initiation criterion obtained from regression analysis of experimental data was proposed for the evaluation of the life leading to debond initiation at the end of bonded plates under fatigue loading. This criterion may be used for the evaluation of debond initiation in real structures with the bi-material's properties (steel substrate and adhesive layer) and interface characteristics (surface treatment) the same as those in this investigation. The experimental results also suggested that an endurance limit might exist, under which the plate has no chance of debonding. One advantage of adhesive bonding found from the experiment was that no fatigue crack initiated at the flanges of steel beams. A surface preparation before bonding process was necessary. This surface preparation was found to significantly influence the interfacial failures.

The terminal distance was found to depend on the elastic modulus of the bonded plate, the elastic modulus of adhesive, the thickness of a bonded plate, and the thickness of an adhesive layer. The distance required in order to develop the flexural conformance increases when the plate thickness, the adhesive layer thickness and the modulus of the plate increase. On the other hand, it decreases as the adhesive modulus increases. Based on the fracture criterion and the fatigue initiation criterion, the bonded plate has more chance of debonding (under fatigue loading) and premature separation (under static loading) when the plate thickness, the adhesive modulus and the plate modulus increase. Therefore, a longer distance is required in order to extend the plate from the high moment region, e.g. in case of a simple span.

9.2 RECOMMENDATIONS FOR FUTURE WORKS

Experimental works

1. Constant Amplitude Fatigue Loading test (CAFL) under different stress ratios and frequencies as well as Variable Amplitude Fatigue Loading test (VAFL) are suggested for further research.

2. Environmental effects (UV radiation, Galvanic corrosion etc.) and long term behaviors should be investigated.

3. Implementation and monitoring of in-situ application. A suitable surface preparation and adhesive type should be selected.

Analytical works

1. The fracture criteria when significant plasticity effects prevail, in case that the adhesive behaves highly nonlinear response.

2. Analysis the effects of clamping forces applied at the plate end on a terminal distance. The clamping forces may be beneficial in reducing the required terminal distance.

More researches are needed before the adhesive bonding of CFRP plates becomes viable for strengthening steel beams. Fatigue loading conditions different from this work should be investigated (e.g. R-ratio, frequency, and variable amplitude loading). Environmental effects and long-term behaviors should be investigated such as the durability of adhesive, the effects of UV radiation, and the galvanic corrosion phenomenon between CFRP and steel. Appropriate measures should be developed to prevent possible galvanic action due to the direct contact of the CFRP with steel in the presence of moisture. Experiments under environmental conditioning are recommended. Suitable types of adhesive materials and surface preparation should be addressed in the future. The behaviors in the field should be assessed since they may be different from those found in the laboratory. These studies will reveal the behaviors of the CFRP plates adhered to steel beams when exposed to traffic loading and environmental cycling. The factors that govern the toughness and ductility of polymers include strain rate, temperature, and molecular structure. At high strain rates or low temperatures, polymers tend to be brittle (Anderson 1991: 371).

REFERENCES

Adam, R.D. and Wake, W.C. 1984. Structural Adhesive Joints in Engineering. London and New York: Elsevier Applied Science Publishers.

Akinsanya, A.R. and Fleck, N.A. 1997. Interfacial Cracking from the Free-edge of a Long Bi-material Strip. International Journal of Solids and Structures 34 no.13: 1645-1665.

Albrecht, P. 1987. Fatigue Strength of Adhesively Bonded Cover Plates. Journal of Structural Engineering , ASCE, 113 no.6: 1236-1250.

Albrecht, P., Wattar, F., Sahli, A., and Vannoy, D.W. 1982. End-bolted Cover Plates. Report no. FHWA/MD-82/01, Department of Civil Engineering, University of Maryland, July 1982.

Albrecht, P., Wattar, F., and Sahli, A. 1983. Towards Fatigue-proofing Cover Plate Ends. Proceedings of W.H. Munse Symposium on Metal Structures, ASCE, Philadelphia, Pa., pp.24-44.

American Association of State Highway Bridges (AASHTO) 1996. Standard Specifications for Highway Bridges. 16th Edition.

Anderson, T.L. 1991. Fracture Mechanics: Fundamental and Applications. CRC Press, ISBN 0-8493-4277-5.

ASTM D3039/D3039M-95a. Standard Test Method for Tensile Properties of Polymer Matrix Composite Materials.

Bassetti, A., Liechti, P., and Nussbaumer, A. 1998. Fatigue Resistance and Repair of Bridge Riveted Members. Proceedings of the International Conference Fatigue Design Espoo, Finland, pp. 535-546. Available from: http://icomwww.epfl.ch/docs/342.pdf [2001, March]

Bassetti, A., Nussbaumer, A., and Hirt, M.A. 2000 a. Crack Repair and Fatigue Life Extension of Riveted Bridge Members Using Composite Materials. Proceedings of the International Bridge Engineering Conference, Vol I, ESE-IABSE-FIB, Sharm El Sheikh, pp. 227-238. Available from: http://icomwww.epfl.ch/docs/412.pdf [2001, March]

Bassetti, A., Colombi, P., and Nussbaumer, A. 2000 b. Finite Element Analysis of Steel Members Repaired by Prestressed Composite Patch. Proceedings of the Conference IGF 2000, XV Congresso Nazionale del Gruppo Italiano Frattura, IGF, Bari. Available from: http://icomwww.epfl.ch/docs/416.pdf [2001, March]

Bassetti, A., Nussbaumer, A., and Hirt, M.A. 2000 c. Fatigue Life Extension of Riveted Bridge Members Using Prestressed Carbon Fiber Composites. Proceedings of the International Conference Steel Structures of the 2000's, ECCS, Istanbul. Available from: http://icomwww.epfl.ch/docs/415.pdf [2001, March]

Bizindavyi, L. and Neale, K.W. 1999. Transfer Lengths and Bond Strengths for Composites Bonded to Concrete. Journal of Composites for Construction 3 no.4: 153-160.

Bogy, D.B. 1968. Edge-bonded Dissimilar Orthogonal Elastic Wedges under Normal and Shear Loading. Journal of Applied Mechanics 35: 460-466.

Bogy, D.B. 1971. Two edge-bonded Elastic Wedges of Different Materials and Wedge Angles under Surface Tractions. Journal of Applied Mechanics 35: 377-386.

Bogy, D.B. and Wang, K.C. 1971. Stress Singularities at Interface Corners in Bonded Dissimilar Isotropic Elastic Materials. International Journal of Solids and Structures 7: 993-1005.

Buyukozturk, O. and Hearing, B. 1998. Failure Behavior of Precracked Concrete Beams Retrofitted with FRP. Journal of Composites for Construction 2 no.3: 138-144.

Carpenter, W.C. 1984 a. Calculation of Fracture Mechanics Parameters for a General corner. International Journal of Fracture 24: 45-58.

Carpenter, W.C. 1984 b. Mode I and Mode II Stress Intensities for Plates with Cracks of Finite Opening. International Journal of Fracture 26: 201-214.

Carpenter, W.C. and Byers, C. 1987. A Path Independent Integral for Computing Stress Intensities for V-notched Cracks in a Bi-material. International Journal of Fracture 35: 245-268.

Chaallal, O., Nollet, M.J., and Perraton, D. 1998. Shear Strengthening of RC Beams by Externally Bonded Side CFRP Strips. Journal of Composites for Construction 2 no.2: 111-113.

Chajes, M.J., Finch Jr., W.W., Januszka, T.F., and Thomson, T.A. 1996. Bond and Force Transfer of Composite Material Plates Bonded to Concrete. ACI Structural Journal 93 no.2: 208-217.

Chen, M.C. and Sze, K.Y. 2001. A Novel Hybrid Finite Element Analysis of Bimaterial Wedge Problems Engineering Fracture Mechanics 68: 1463-1476.

Chen, Y.Z. and Nisitani, H. 1993. Singular Stress Field near the Corner of Jointed Dissimilar Materials. Journal of Applied Mechanics 60: 607-613.

Chien-Chang Lin, Ru-Chu Chu, and Yee-Shown Lin. 1993. A Finite Element Model for Single-sided Crack Patching. Engineering Fracture Mechanics 46 no.6: 1005-1021.

Demers, C.E. 1998. Axial Fatigue Strength Degradation of Carbon FRP Composites and E-glass FRP Composites. Proceedings of the Second International Conference on Composites in Infrastructure (ICCI'98), pp.86-92.

Demers, C.E. and Abdelgadir, A.A. 1999. Research in Progress: Fatigue of CFRP Composites. Proceedings of the Eight International Conference on Extending the Life of Bridges, Civil, and Building Structures (Structural Faults and Repair- 99).

Dempsey, J.P. and Sinclair, G.B. 1981. On the Singular Behavior at the Vertex of a Bi-material Wedge. Journal of Elasticity 11 no.3: 317-327.

Denney, J.J and Mall, S. 1997. Characterization of Disbond Effects on Fatigue Crack Growth Behavior in Aluminum Plate with Bonded Composite Patch. Engineering Fracture Mechanics 57 no.5: 507-525.

Dundur, J. 1969. Discussion of [Bogy 1968], Journal of Applied Mechanics 36: 650-652.

England, A.H. 1971 a. On Stress Singularities in Linear Elasticity. International Journal of Engineering Science 9: 571-585.

England, A.H. 1971 b. Complex Variable Methods in Elasticity. London: Wiley-Interscience.

Fisher, J.W., Frank, K.H., Hirt, M.A., and McNamee, B.M. 1970. Effects of Weldments on the Fatigue Strength of Steel Beams. NCHRP Report no.102, Transportation Research Board, National Research Council, Washington, D.C.

Fisher, J.W., Albrecht, P., Yen, B.T., and Klingerman, D.J. 1974. Fatigue Strength of Beams with Stiffeners and Attachments. NCHRP Rport no.147, Transportation Research Board, National Research Council, Washington, D.C.

Fisher, J.W., Mertz, D.R., and Zhong, A. 1983. Steel Bridge Members under Variable Amplitude Long Life Fatigue Loading. NCHRP Report no.267, Transportation Research Board, National Research Council, Washington, D.C.

Fisher, J.W., Yen, B.T. and Wang, D. 1987. Fatigue and Fracture Evaluation for Rating Riveted Bridges. NCHRP Report no.302, Transportation Research Board, National Research Council, Washington, D.C.

Fisher, J.W., Nussbaumer, A., Keating, P.B., and Yen, B.T. 1993. Resistance of Welded Details under Variable Amplitude Long-life Fatigue Loading. NCHRP Report no.357, Transportation Research Board, National Research Council, Washington, D.C.

Fisher, J.W. 1997. Evolution of Fatigue-resistant Steel Bridges. Transportation Research Record 1594: 5-17.

Gdoutos, E.E., Pilakoutas, K., and Rodopoulos, C.A. 2000. Failure Analysis of Industrial Composite Materials. McGraw-Hill.

Ghosh, U.K. 2000. Repair and Rehabilitation of Steel Bridges. Netherlands: A.A. Balkema Publishers.

Gibson, R.F. 1994. Principles of Composite Material Mechanics. McGraw-Hill.

Goland, M. and Reissner, E. 1944. The Stresses in Cemented Joints. Journal of Applied Mechanics 2: A17-A27.

Gradin, P.A. and Groth, H.L. 1984. A Fracture Criterion for Adhesive Joints in Terms of Material Induced Singularities. Proceedings of the Third International Conference on Numerical Methods in Fracture Mechanics. Pineridge Press, Swansea, pp. 711-720.

Green, A.E. and Zirna, W. 1968. Theoretical Elasticity. Second Edition. Oxford University Press.

Groth, H.L. 1985. A Method to Predict Fracture in an Adhesively Bonded Joint. International Journal of Adhesion and Adhesives 5 no.1: 19-22.

Groth, H.L. 1987. Analysis of Adhesive Joints. Report no. 87-17, Department of Aeronautical Structures and Materials, The Royal Institute of Technology, SWEDEN.

Groth, H.L. and Jangblad, D. 1987. Fracture Initiation at Interface Corners in Bonded Joints. Mechanical Behaviour of Adhesive Joints ©PLURALIS: 257-270.

Groth, H.L. 1988 a. Prediction of Failure Loads of Adhesive Joints Using the Singular Intensity Factor. STP 945, American Society for Testing and Materials, Philadelphia: 278-284.

Groth, H.L. 1988 b. Stress Singularities and Fracture at Interface Corners in Bonded Joints. International Journal of Adhesion and Adhesives 8 no.2: 107-113.

Guess, T.R., Reedy, E.D., and Stavig, M.E. 1995. Mechanical Properties of Hysol EA-9394 Structural Adhesive. Report SAND95-0229, Sandia National Laboratories, Albuquerque, NM.

Hassan, A.F. and Bowman, M.D. 1995. Fatigue Strength of Girders with Tapered Cover Plates. Report no. FHWA/IN/JHRP-94/13, Indiana.

Hattori, T., Sakata, S., Hatsuda, T., and Murakami, G. 1988. A Stress Singularity Parameter Approach for Evaluating Adhesive Strength. JSME International Journal Series I, 31 no.4: 718-723.

Hattori, T. 1991. A Stress-singularity-parameter Approach for Evaluating the Adhesive Strength of Single-lap Joints. JSME International Journal Series I, 34 no.3: 326-331.

Hein, V.L. and Erdogan, F. 1971. Stress Singularities in a Two-material Wedge. International Journal of Fracture Mechanics, 7 no.3: 317-330.

Hong, C.C. and Stern, M. 1978. The Computation of Stress Intensity Factors in Dissimilar Materials. Journal of Elasticity 8 no.1: 21-34.

Hoskin, B.C. and Baker, A.A. 1986. Composite Materials for Aircraft Structures. Third printing. AIAA Education Series. New York: American Institute of Aeronautics and Astronautics.

Imanaka, M., Nakayama, H., Morikawa, K., and Nakamura, M. 1995. Evaluation of Fatigue Life of Adhesively Bonded CFRP Pipe/Steel Rod Joints. Composite Structures 31: 235-241.

Imanaka, M. and Iwata, T. 1996. Effect of Adhesive Layer Thickness on Fatigue Strength of Adhesively Bonded Butt, Scarf and Butterfly Type Butt Joints. International Journal of Fracture 80: R69-R76.

Imanaka, M., Ishii, K., and Nakayama, H. 1999. Evaluation of Fatigue Strength of Adhesively Bonded Single and Single Step Double Lap Joints Based on Stress Singularity Parameters. Engineering Fracture Mechanics 62: 409-424.

Ishii, K., Imanaka, M., Nakayama, H., and Kodama, H. 1998. Fatigue Failure Criterion of Adhesively Bonded CFRP/Metal Joints under Multiaxial Stress Conditions. Composite Part A 29A: 415-422.

Ishii, K., Imanaka, M., Nakayama, H., and Kodama, H. 1999. Evaluation of the Fatigue Strength of Adhesively Bonded CFRP/Metal Single and Single-step Double-lap Joints. Composites Science and Technology 59: 1675-1683.

Japanese Society of Steel Construction (JSSC) 1995. Fatigue Design Recommendations for Steel Structures. (English version)

Jones, R., Swamy, R.N., and Charif, A. 1988. Plate Separation and Anchorage of Reinforced Concrete Beams Strengthened by Epoxy-bonded Steel Plates. The Structural Engineer 66 no.5: 85-94.

Kagawa, N., Yamada, K., Kainuma, S., and Nakamura, T. 1999. Fatigue Behavior of Improved Welded Cover Plate Detail. Proceedings of the Seventh East Asia-pacific Conference on Structural Engineering and Construction (EASEC), 1999, pp. 171-176.

Kam, T.Y., Chu, K.H., and Tsai, Y.C. 1998. Fatigue of Cracked Plates Repaired with Single-sided Composite Patches. AIAA Journal 36 no.4: 645-650.

Kinloch, A.J. 1987. Adhesion and Adhesive: Science and Technology. London: Chapman & Hall.

Lefebvre, D.R., and Dillard, D.A. 1999 a. A Stress Singularity Approach for the Prediction of Fatigue Crack Initiation in Adhesive Bonds. Part 1: Theory. J. Adhesion 70: 119-138.

Lefebvre, D.R., and Dillard, D.A. 1999 b. A Stress Singularity Approach for the Prediction of Fatigue Crack Initiation in Adhesive Bonds. Part 2: Experimental. J. Adhesion 70: 139-154.

Lenwari, A., and Thepchatri, T. 2001. Prediction of Failure Load in Steel Beams Bonded with CFRP Plates due to Fracture at Plate Ends Using Stress Singularity Parameter. Proceedings of the 14th KKNN Symposium on Civil Engineering, Kyoto, Japan, pp. 259-265.

Liu, X.H., Suo, Z., and Ma, Q. 1999. Split Singularities: Stress Field near the Edge of a Silicon Die on a Polymer Substrate. Acta mater. 47 no.1: 67-76.

Maalej, M. and Bian, Y. 2001. Interfacial Shear Stress Concentration in FRP-Strengthened Beams. Composite Structures 54: 417-426.

Maeda, T., Asano, Y., Sato, Y., Ueda, T., and Kakuta, Y. 1997. A Study on Bond Mechanism of Carbon Fiber Sheet. Non-metallic (FRP) Reinforcement for Concrete Structures, Proc., 3rd Int. Symp. (FRPRCS-3), Japan Concrete Institute, Sapporo, Japan, 1: 279-286.

Malek, A.M., Saadatmanesh, H., and Ehsani, M.R. 1998. Prediction of Failure Load of R/C Beams Strengthened with FRP Plate due to Stress Concentration at the Plate End. ACI Structural Journal 95 no.1: 142-152.

Meier, U. 1995. Strengthening of Structures Using Carbon Fibre/Epoxy Composites. Construction and Building Materials 9 no.6: 341-351.

Messick, S.C. 1996. Adhesive Selection and Evaluation for Strengthening Steel Stringer Bridges Using CFRP. Master Thesis, Department of Mechanical Engineering, West Virginia University.

Mohammed, I. and Liechti, K.M. 2000. Cohesive Zone Modeling of Crack Nucleation at Bimaterial Corners. Journal of the Mechanics and Physics of Solids 48: 735-764.

Munz, D. and Yang, Y.Y. 1992. Stress Singularities at the Interface in Bonded Dissimilar Materials under Mechanical and Thermal Loading. Journal of Applied Mechanics 59: 857-861.

Naboulsi, S. and Mall, S. 1997. Characterization of Fatigue Crack Growth in Aluminium Panels with a Bonded Composite Patch. Composite Structures 37 no.3/4: 321-334.

Oehlers, D.J. and Moran, J.P. 1990. Premature Failure of Externally Plated Reinforced Concrete Beams. Journal of Structural Engineering, ASCE, 116 no.4: 978-995.

Quantrill, R.J., Hollaway, L.C., Thorne, A.M., and Parke, G.A.R. 1995. Preliminary Research on the Strengthening of Reinforced Concrete Beams Using GFRP. Non-metallic (FRP) Reinforcement for Concrete Structures edited by L.Taerwe © RILEM, London, pp.541-550.

Reedy Jr., E.D. 1990. Intensity of the Stress Singularity at the Interface Corner between a Bonded Elastic and Rigid Layer. Engineering Fracture Mechanics 36 no.4: 575-583.

Reedy Jr., E.D. 1993. Asymptotic Interface Corner Solutions for Butt Tensile Joints. International Journal of Solids and Structures 30: 767-777.

Reedy Jr., E.D. and Guess, T.R. 1993. Comparison of Butt Tensile Strength Data with Interface Corner Stress Intensity Factor Prediction. International Journal of Solids and Structures 30 no.21: 2929-2936.

Reedy Jr., E.D. and Guess, T.R. 1996. Interface Corner Stress State: Plasticity Effects. International Journal of Fracture 81: 269-282.

Reedy Jr., E.D. and Guess, T.R. 1997. Interface Corner Failure Analysis of Joint Strength: Effect of Adherend Stiffness. International Journal of Fracture 88: 305-314.

Rice, J.R. 1988. Elastic Fracture Mechanics Concepts for Interfacial Cracks. Journal of Applied Mechanics 55: 98-103.

Ritchi, P.A., Thomas, D.A., Lu, L., and Connelly, G.M. 1991. External Reinforcement of Concrete Beams Using Fiber Reinforced Plastics. ACI Structural Journal 88 no.4: 490-500.

Rose, L.R.F. 1981. An Application of the Inclusion Analogy for Bonded Reinforcements. International Journal of Solids and Structures 17: 827-838.

Rose, L.R.F. 1982. A Cracked Plate Repaired by Bonded Reinforcements. International Journal of Fracture 18: 135-144.

Saadatmanesh, H. and Ehsani, M.R. 1991. RC Beams Strengthened with GFRP Plates I: Experimental Study. Journal of Structural Engineering, ASCE, 117 no.11: 3417-3433.

Sahli, A.H., Albrecht, P., and Vannoy, D.W. 1984. Fatigue Strength of Retrofitted Cover Plates, Journal of Structural Engineering, ASCE, 110 no.6: 1374-1388.

Schubbe, J.J and Mall, S. 1999 a. Investigation of a Cracked Thick Aluminum Panel Repaired with a Bonded Composite Patch. Engineering Fracture Mechanics 63: 305-323.

Schubbe, J.J and Mall, S. 1999 b. Modeling of Cracked Thick Metallic Structure with Bonded Composite Patch Repair Using Three-layer Technique. Composite Structures 45: 185-193.

Sen, R., Liby, L., Spillett, K., and Mullins, G. 1995. Strengthening Steel Composite Bridge Members Using CFRP Laminates. Non-metallic (FRP) Reinforcement for Concrete Structures edited by L.Taerwe © RILEM, London, pp.551-558.

Sen, R., Liby, L., and Mullins, G. 2001. Strengthening Steel Bridge Sections Using CFRP Laminates. Composite Part B: Engineering 32: 309-322.

Shahawy, M. and Beitelman, T.E. 1999. Static and Fatigue Performance of RC Beams Strengthened with CFRP Laminates. Journal of Structural Engineering, ASCE, 125 no.6: 613-621.

Sharif, A., Al-Sulaimani, G.J., Basunbul, I.A., Baluch, M.H., and Ghaleb, B.N. 1994. Strengthening of Initially Loaded Reinforced Concrete Beams Using FRP Plates. ACI Structural Journal 91 no.2: 160-168.

Spadea, G., Bencardino, F., and Swamy, R.N. 1998. Structural Behavior of Composite RC Beams with Externally Bonded CFRP. J. Composites for Construction 2 no.3: 132-137.

Steel Structures Painting Council Specification 1991. Surface Preparation. In: Vol.2: Systems and Specification 6th edition. Pittsburgh, PA.

Stern, M., Becker, E.B., and Dunham, R.S. 1976. A Contour Integral Computation of Mixed-mode Stress Intensity Factors. International Journal of Fracture 12 no.3: 359-368.

Swamy, R.N., Jones, R., and Charif, A. 1986. Shear Adhesion Properties of Epoxy Resin Adhesives. Proceedings of an International Symposium on Adhesion between Polymers and Concrete, edited by H.R. Sass ©RILEM, Paris: 741-755.

Swamy, R.N. and Muskhopadhyaya, P. 1995. Role and Effectiveness of Non-metallic Plates in Strengthening and Upgrading Concrete Structures. Non-metallic (FRP) Reinforcement for Concrete Structures edited by L.Taerwe © RILEM, London: 473-481.

Tan, M.A. and Meguid, S.A. 1997. Analysis of Bimaterial Wedges Using a New Singular Finite Element. International Journal of Fracture 88: 373-391.

Task Committee on Flexural Members. 1967. Commentary on Welded Cover-plated Beams. Journal of the Structural Division , ASCE, 93 no.ST4: 95-122.

Volkersen, O. 1938. Die Nietkraftverteilung in Zugbeanspruchten Nietverbindungen mit Konstanten Laschenquerschnitten. Luftfahrtforschung 15: 41-47 (in German).

Volnyy, V.A. and Pantelides, C.P. 1999. Bond Length of CFRP Composites Attached to Precast Concrete Walls. J. Composites for Construction 3 no.4: 168-176.

Wang, C.H. and Rose, L.R.F. 1997. Determination of Triaxial Stresses in Bonded Joints. International Journal of Adhesion and Adhesives 17: 17-25.

Wang, C.H. and Rose, L.R.F. 2000. Compact Solutions for Corner Singularity in Bonded Lap Joints. International Journal of Adhesion and Adhesives 20: 145-154.

Wang, C.H., Rose, L.R.F., and Baker, A.A. 1998. Modelling of the Fatigue Growth Behaviour of Patched Cracks. International Journal of Fracture 88: L65-L70.

Wattar, F., Albrecht, P., and Sahli, A.H. 1985. End-bolted Cover Plates. Journal of Structural Engineering, ASCE, 110 no.6: 1235-1249.

Wilkinson, J.H. 1965. The Algebraic Eigenvalue Problem. Oxford: Oxford University Press.

William, M.L. 1952. Stress Singularities Resulting from Various Boundary Conditions in Angular Corners of Plates in Extension. Journal of Applied Mechanics, 19: 526-528.

William, M.L. 1959. The Stress around a Fault or Crack in Dissimilar Media. Bulletin of the Seismological Society of America, 49: 199-204.

Yang, X.X. and Kuang, Z.B. 1996. Contour Integral Method for Stress Intensity Factors of Interfacial Crack. International Journal of Fracture 78: 299-313.

Yang, Y.Y. and Munz, D. 1997. Stress Singularities in a Dissimilar Materials Joint with Edge Tractions under Mechanical and Thermal Loadings. International Journal of Solids and Structures 34 no.10: 1199-1216.

Yang, Y.Y. 1998. Asymptotic Description of the Logarithmic Singular Stress Field and Its Application. International Journal of Solids and Structures 35 no.30: 3917-3933.

Ziraba, Y.N., Baluch, M.H., Basunbul, I.A., Sharif, A.M., Azad, A.K., and Al-Sulaimani, G.J. 1994. Guidelines toward the Design of Reinforced Concrete Beams with External Plates. ACI Structural Journal 91 no.6: 639-646.

APPENDICES

APPENDIX A

MATERIAL PROPERTIES

A.1 UNIDIRECTIONAL CFRP LAMINATES

Three specimens were tested according to ASTM D3039/D3039M-95a. The stress-strain relationships and the ultimate strengths were measured. The test setup is shown in Fig. A.1. The results from the static test are summarized in Table A.1. Typical stress-strain relationship is linear elastic as shown in Fig. A.2.

Table A.1 Tensile properties of CFRP laminates

Specimen no.	Elastic modulus (ksc)	Fiber breaking stress (ksc)	Ultimate tensile strength (ksc)
1	3,344,100	14,285	17,571
2	2,916,000	-*	-*
3	3,242,700	14,000	18,286
Average	3,167,600	14,142.5	17,928.5
Sd	182,660	142.5	357.5

*-Gripping problem

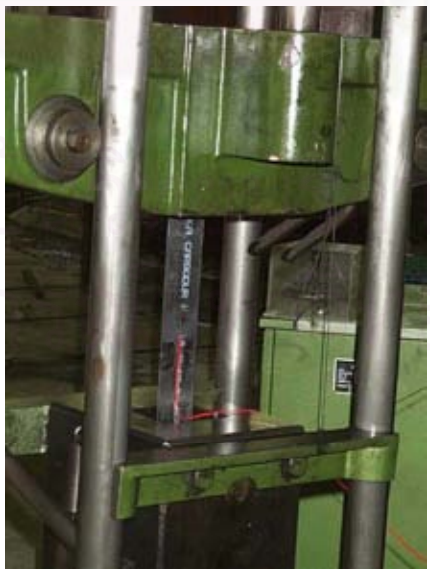

Figure A.1 Static test on CFRP laminates

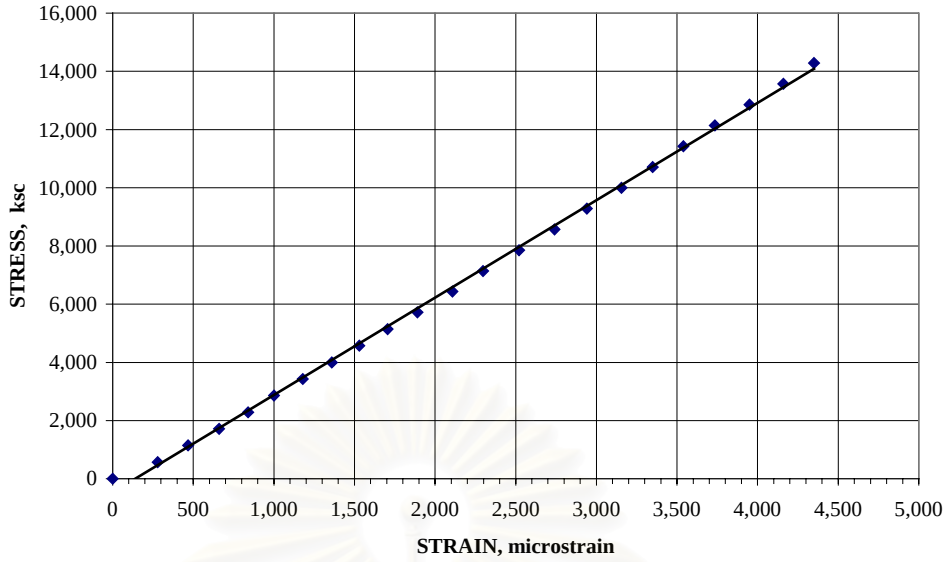

Figure A.2 Stress-strain relationship of CFRP laminate

A.2 STEEL BEAMS

The steel beams in this research were JIS SS400 according to both Thai and Japanese standard G3101. The chemical composition is shown in Table A.2. Table A.3 shows the mechanical properties of the steel from the manufacturer.

Table A.2 Chemical composition in steel (%)

C	Si	Mn	CE	Cu	SW	P	S	Nb	V	N	Sn	Ni	Cr	Mo
15	22	67	29	27	21	10	23	4	3	5	19	10	6	23

Table A.3 Mechanical properties of steel

Yield point, ksc	Tensile strength, ksc	Elongation (%)
3,000	4,400	29.75

A.3 ADHESIVE

Adhesive in this study was Sikadur® 30. It was a two-part, high-modulus structural epoxy resin. Its mechanical properties in flexure, tension, and compression were summarized in Table A.4, A.5, and A.6, respectively. Each test was conducted according to the relevant ASTM standard.

Table A.4 Flexural strength test (ASTM C348): specimen's size is 4x4x16 cm

Specimen no.	Width of sample, B (cm)	Thickness of sample, D (cm)	Length of sample, L (cm)	Flexural strength, ksc		
				24 hours	7 days	10 days
1	4.05,4.02, 4.02	4.06,4.05, 4.02	16.10,16. 20,16.20	399.59	440.87	493.19
2	4.11,4.00, 4.05	4.01,4.05, 4.04	16.20,16. 30,16.20	451.30	467.76	490.96
3	4.03,4.03, 4.05	4.10,4.02, 4.02	16.10,16. 10,16.20	403.61	431.16	453.78
Average				418.18	446.60	479.31

Table A.5 Tensile strength test (ASTM C190): specimen's size is 2.5x2.5x6.5 cm

Specimen no.	Tensile strength, ksc		
	24 hours	7 days	10 days
1	188.85	216.31	216.86
2	189.52	193.80	240.46
3	196.77	220.49	233.09
Average	190.77	210.20	230.14

Table A.6 Compression test (ASTM C109): specimen's size is 5x5x5 cm

Specimen no.	Compressive strength, ksc	
	24 hours	7 days
1	656	696
2	635	696
3	643	700
Average	645	698

APPENDIX B

NUMERICAL ALGORITHM FOR AN EIGENVALUE

B.1 MULLER'S ALGORITHM

In order to determine the values of the eigenvalues of Eq. (3.5) (Chapter 3), the Muller's algorithm was selected. This algorithm is based on the method of successive interpolation (Wilkinson, 1965). The objective is to locate zeros, $z = \xi + \eta i$, of $f(z)$. In this algorithm, the next approximation z_{k+1} to zero is determined from the $r+1$ previous approximations z_k, z_{k-1},..., z_{k-r} as a zero of the polynomial of degree r passing through the points $(z_k, f(z_k))$,..., $(z_{k-r}, f(z_{k-r}))$. If we take r to be 1 or 2 then the corresponding polynomial are linear and quadratic. It is convenient to write

$$f(z_i) = f_i \tag{B.1}$$

For the case $r = 1$ we have

$$z_{k+1} = z_k + \frac{f_k(z_k - z_{k-1})}{f_{k-1} - f_k} = \frac{z_k f_{k-1} - z_{k-1} f_k}{f_{k-1} - f_k} \tag{B.2}$$

For the case $r = 2$, Muller's method is followed. We write

$$h_i = z_i - z_{i-1}, \quad \lambda_i = h_i / h_{i-1}, \quad \delta_i = 1 + \lambda_i \tag{B.3}$$

and with this notation it can be verified that the required λ_{k+1} satisfies the quadratic equation

$$\lambda_{k+1}^2 \lambda_k \delta_k^{-1}(f_{k-2}\lambda_k - f_{k-1}\delta_k + f_k) + \lambda_{k+1}\delta_k^{-1} g_k + f_k = 0 \tag{B.4}$$

where $g_k = f_{k-2}\lambda_k^2 - f_{k-1}\delta_k^2 + f_k(\lambda_k + \delta_k)$ (B.5)

From this we obtain

$$\lambda_{k+1} = -2 f_k \delta_k / \{g_k \pm [g_k^2 - 4 f_k \delta_k \lambda_k (f_{k-2}\lambda_k - f_{k-1}\delta_k + f_k)]^{\frac{1}{2}}\} \tag{B.6}$$

The sign in the denominator of Eq. (B.6) is chosen so as to give the corresponding λ_{k+1} (and hence h_{k+1}) the smaller absolute magnitude. With successive quadratic interpolation we can move out into the complex plane although the initial three input values are real.

If we take r to be greater than two, each step of the iteration needs the solution of a polynomial equation of degree three or higher. Therefore, the use of cubic or higher interpolation could merely be justified unless it had better convergence properties.

APPENDIX C

RECOMMENDATION FOR DETERMINING A TERMINAL DISTANCE

Recommendation for designing a bonded plate for strengthening a steel girder is outlined below. Three criteria for determining a terminal distance, which will be used for designing the length of a bonded plate, are suggested.

C.1 DESIGN STEP

1. Determine dead load and live load envelopes.
2. Design the thickness and the width of a bonded plate (e.g. a CFRP plate) based on static analysis with a proper safety factor and locate the theoretical cut-off point.
3. Determine the length of the CFRP plate to be extended beyond theoretical cut-off points according to the maximum distance of the following three criteria:

    3.1 Prevent the premature plate separation failure mode (Section 4.4, a fracture criterion, is proposed).

    3.2 Provide sufficient distance for a bonded plate to develop the flexural conformance (Section 3.5, a shear lag analysis, is found to be applicable).

    3.3 Prevent the debond initiation under fatigue loading during the design life of the strengthened beams under expected traffic volume (Section 7.2, a fatigue initiation criterion based on stress intensity factor range, is suggested).

C.2 DETERMINATION OF A THEORETICAL CUT-OFF POINT

According to AASHTO (1996) section 10.13, the theoretical end of the cover plate, when using service load design methods, is the section at which the stress in the

flange equals the allowable service load stress, exclusive of fatigue considerations. When using strength design methods, the theoretical end of the cover plate is the section at which the flange strength without that cover plate equals the required strength for the design loads, exclusive of fatigue requirements.

Example :

Determine the theoretical cut-off point for a design static load of 12,900 kg, which is the failure load of the FRP rupture mode calculated from an elastic-plastic section analysis. The configuration is shown in Fig. 6.1.

Solution

From a section analysis, P_{Yield} = 6,890 kg (M_{Yield} = 284,213 kg-cm) and

$$P_{Plastic} = 9{,}041 \text{ kg} \quad (P_{Plastic} = 372{,}941 \text{ kg-cm})$$

At 12,900 kg, the bending moment diagram is illustrated in Fig. C.1.

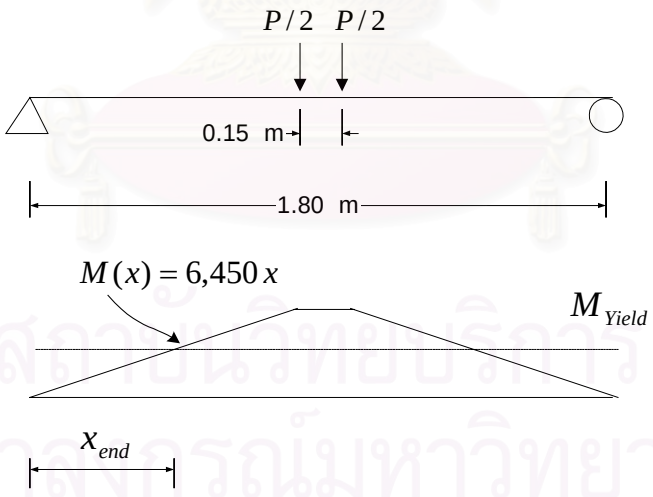

Figure C.1 Bending moment for determining the theoretical end

Calculate x_{end} based on M_{Yield} :

$$6{,}450\, x_{end} = 284{,}213$$

x_{end} = 44.1 cm

Consequently, the required length of a CFRP plate extending between the theoretical ends is 91.8 cm.

VITA

Akhrawat Lenwari

Akhrawat Lenwari was born on January 12, 1978 in Ratchaburi, Thailand. He is the last of three children of Mr. Ubol and Mrs. Wilai Lenwari. He graduated with the Bachelor of Engineering in Civil Engineering (Honors) from Chulalongkorn University, Thailand in April 1998. Then, he started his Ph.D. study at Chulalongkorn University in May 1998. During the study, he received a research assistant scholarship (Royal Golden Jubilee) from the Thailand Research Fund (TRF).